Sensing of Diclofenac by a Porphyrin-based Artificial Receptor

Journal:	*New Journal of Chemistry*
Manuscript ID	NJ-ART-06-2018-002737.R2
Article Type:	Paper
Date Submitted by the Author:	07-Aug-2018

Complete List of Authors:	Gallo, Emma; University of Milan, of Chemistry Intrieri, Daniela; università, Damiano, Caterina; università, Department of Chemistry Rizzato, Silvia; Università di Milano, Deparment of Chemistry Paolesse, Roberto; Universita degli Studi di Roma Tor Vergata, Chemical Science and Technologies Venanzi, M.; Universita degli Studi di Roma La Sapienza Facolta di Scienze Matematiche Fisiche e Naturali, Monti, Donato; Universita degli Studi di Roma Tor Vergata, Department of Chemical Science and Technologies Savioli, Marco; Universita degli Studi di Roma Tor Vergata, Science and Chemical Technologies Stefanelli, Manuela; University of Rome , Chemical Science and Technology

NJC
A journal for new directions in chemistry
New Journal of Chemistry

ISI impact Factor (published in 2016): **3.277**

NJC is a **general** chemistry journal. We solicit innovative and cutting-edge reports of high quality and broad appeal that have the potential to open new directions in chemistry or other scientific disciplines. Both experimental and theoretical works are welcome.

The following manuscript has been submitted for consideration as a

PAPER

Papers report a complete study that leads to new understanding or gives new insight into the subject under investigation. If preliminary results have been published in a communication, a subsequent full paper should include additional results that justify another publication.

The Editors and Editorial Board ask you as a reviewer to keep the criteria in mind when making your recommendation for publication in *NJC*. **Routine or incremental work**, however competently researched and reported, should not be recommended for publication in *NJC* as it does not meet our expectations with regard to novelty and impact.

Thank you for your help with the evaluation of this submission. The editors rely on experts such as yourself to **improve the scientific quality** of the journal. Please support your answers to the questions with **appropriate comments** to allow the editors to make the best decision and the authors to properly revise their manuscript.

If you recommend **Major Revision** or **Reject and Resubmit** then we would appreciate it if you would indicate your willingness to re-evaluate the manuscript after revision.

We very much appreciate it if you can respect the deadline for filing your report. If you should need additional time to complete your report, please contact the editors at NJC@rsc.org.

Professor Mir Wais Hosseini
Editor-in-Chief of *NJC*

We also invite you to consider *NJC* for one of your upcoming manuscripts. Submissions can be made on the Scholar One website: http://mc.manuscriptcentral.com/njc or follow the 'submit an article' link on the *NJC* homepage given below.

ROYAL SOCIETY OF CHEMISTRY
cnrs
www.rsc.org/njc

Journal Name

ARTICLE

Sensing of Diclofenac by a Porphyrin-based Artificial Receptor

Daniela Intrieri,[a] Caterina Damiano,[a] Silvia Rizzato,[a] Roberto Paolesse,[b] Mariano Venanzi,[b] Donato Monti,*[b] Marco Savioli,[b] Manuela Stefanelli[b] and Emma Gallo.*[a]

Received 00th January 20xx,
Accepted 00th January 20xx

DOI: 10.1039/x0xx00000x

www.rsc.org/

The reported studies deals with the synthesis of porphyrin chemosensor **2**, designed for the detection of the emerging pollutant Diclofenac. Owing to the peculiar structure of its molecular frame, which is composed by a tetrapyrrolic platform linked to a Rhodamine B residue, receptor **2** reversibly interacts with Diclofenac sodium salt (DCF)Na. The resulting **2@DCF** adduct was detected by UV-Vis spectroscopy in a large pH range (5.5-9.0) as well as in the presence of competitive analytes. Both static and time-resolved Fluorescence, Resonance Light Scattering (RLS) and UV-Vis spectroscopies allowed for the evaluation of the binding behaviour, in terms of association constant and structural features of formed **2@DCF**. In particular, the host-guest recognition event occurs with the growth of large porphyrin aggregates, as stated by the quenching of the fluorescence emission as well as the enhancement of RLS intensities, and with an overall 1:1 binding constant of about $10^5 M^{-1}$.

Introduction

Water management has become an urgent worldwide policy issue for the 21st century, consequently the development of efficient and selective procedures for the detection of water pollutants is a topic of global interest and concern. In the last few years a special attention has been given to the identification of *Contaminants of Emerging Concern* (CECs) in surface water, wastewater as well as groundwater. This class of compounds includes those chemicals that are widely spread in the environment for their abundant use and consequentially they are potentially dangerous for human health.[1] Examples of CECs are pharmaceuticals and chemicals for personal care and their increasing use can have dramatic outcomes for the ecosystem sustainability.[2]

Among all the emerging contaminants, Diclofenac (Figure 1), an anti-inflammatory drug that was recently inserted into the priority emerging pollutants list by the EU,[3,4] does not exhibit immediate toxic effects towards living organisms, although a continuing exposure may be responsible for serious environmental damage. Diclofenac is usually detected by employing time-consuming, expensive and off-site classical analytic procedures, mainly chromatographic methods.[5-10] Although analytical instrumentation cannot be overtaken in terms of sensitivity and selectivity, it cannot allow the on-site continuous monitoring, which is an essential requisite for providing prompt remediation procedures. Chemical sensors represent a viable solution to these requirements and sensitive, rapid, cost-effective and real-time analyses are now feasible by employing electrochemical,[11-13] supramolecular[14,15] and biomolecular[16,17] user-friendly sensors. A key component of these devices is the sensing material which is responsible for the molecular recognition (interaction with Diclofenac) and triggering the transduction event (optical, photophysical, electrical, etc.) for sensor signalling.

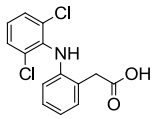

Figure 1. Structure of Diclofenac.

The advancement of the supramolecular chemistry concepts has allowed the rational design of molecular receptors, able to satisfy the sensitivity and selectivity requirements for the binding of target analytes.

Among the different materials that have been exploited as recognising layers, porphyrins have assumed a role of ever-growing importance as responsive materials due to their physico-chemical properties,[18-20] which allow a significant number of potential transductions to detect even low amounts of the target analyte. The interaction of Diclofenac with the metal (e.g. iron[21] or manganese[22]), coordinated into the porphyrin core, often represents the key-point of the sensing mechanism of metal porphyrin-based chemosensors.

We here report the synthesis, characterisation and study of the sensing ability of a porphyrin chemosensor containing Rhodamine B, which interacts with Diclofenac without forming covalent bonds, therefore favouring the recycling and reuse of

[a] Department of Chemistry, University of Milan, Via C. Golgi 19, 20133 Milan (Italy). E-mail: emma.gallo@unimi.it.
[b] Department of Chemical Science and Technologies, University of Roma Tor Vergata, Via della Ricerca Scientifica, 00133 Rome (Italy) E-mail: dmonti@uniroma2.it.

†Electronic supplementary information (ESI) available: experimental details, characterization data, crystallographic data in CIF, supporting tables and crystal data CCDC 1843312. See DOI: 10.1039/x0xx00000x.

the device. Reported data represent the first step for the development of a chemical sensor, which is currently ongoing in our laboratories and will be reported in the due course.

Results and discussion

Knowing that i) Rhodamine B (RhB) presents a very good affinity for Diclofenac,[23,24] ii) RhB[25] and porphyrin[26] molecules are very active fluorescent probes and iii) porphyrin-RhB conjugated systems are efficient dyads for electron transfer mechanisms,[27-29] we synthesised porphyrin **2** by using a slight modification of a reported procedure.[30] Porphyrin **2** was obtained by reacting porphyrin **1** with RhB in the presence of KI, which triggered the formation of porphyrin/RhB species as an iodine salt (Scheme 1). The sensing capacity of **2** was tested by analysing UV-Vis and Fluorescence spectral patterns in the presence of the target analyte (see below).

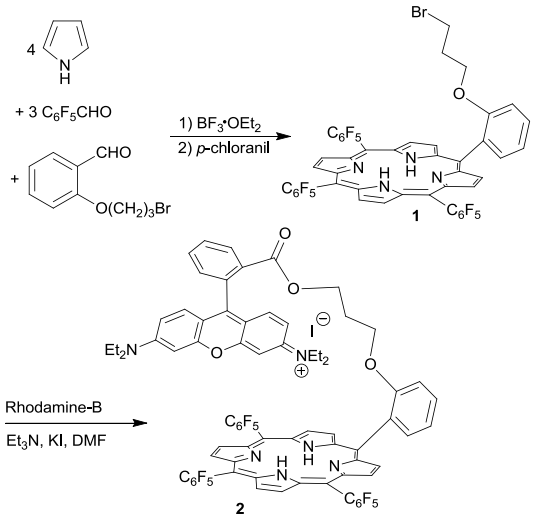

Scheme 1. Synthesis of porphyrin **2**.

Porphyrin **2** was fully characterised, the ^{1}H NMR analysis confirmed the proposed structure and the UV-Vis spectrum showed an intense Soret band at 412 nm (log εM = 5.67). It should be noted that Q porphyrinic bands are partially superimposed to the intense band at 559 nm (log εM = 5.24) of the RhB moiety, linked to the porphyrin platform. Indeed, the free RhB in methanol shows an intense absorption around 551 nm.

It is to note that the *meso*-pentafluorophenyl substituents of the porphyrin ring were chosen to strengthen the hydrophobic character that, together with the polar hydrophilic iminium salt of RhB, assures the amphiphilic nature of **2**. This feature will be fundamental for anchoring the molecule onto the solid surface by non-covalent interactions,[31,32] needed for the future sensor development, and for the interaction with the polar analyte in the water medium, respectively.

Before testing the reactivity of **2** towards Diclofenac, its chemical stability was studied in order to evaluate the strength of the RhB/porphyrin linkage. It should be noted that RhB leaching not only would hamper the recyclability of the device but could also be responsible for contamination events.[33]

Although promoting a future anchorage of the device onto the surface, the low hydrophilic character of **2** prevented the execution of stability tests in pure water. Thus, to obtain a homogeneous solution, a H_2O/CH_3OH = 1:1 (v:v) mixture was employed as the solvent. In this polar mixture porphyrin **2** was stable for at least 72 h, as revealed by UV-Vis spectroscopic analyses. Good stability was also maintained by changing the pH of the medium. Several UV-Vis spectra were performed in the 6.5-9.5 pH range and collected data indicated that **2** decomposed only when stirred under strong basic conditions (pH > 9) for more than 24 hours. It is important to underline that in a real-time analysis, the sensor is exposed to the polluted water only for a short period of time, during which the chemical stability in both acidic and basic media is assured.

In view of positive stability tests, the chemical interaction between **2** and the sodium salt of Diclofenac, (DCF)Na, which is the active principle of Diclofenac-based pharmaceuticals, was investigated in H_2O/CH_3OH = 1:1 (v:v) mixture (Figure 2).

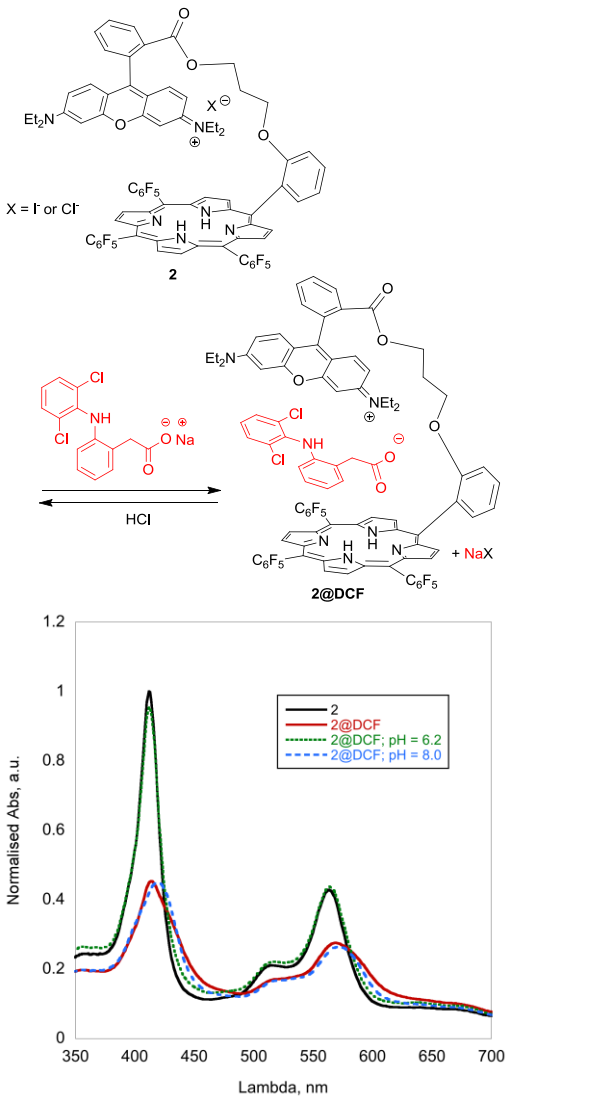

Figure 2. UV-Vis spectra showing the reversible formation of **2@DCF** adduct.

The treatment of porphyrin **2** with (DCF)Na resulted in evident UV-Vis spectral changes, indicating the formation of **2@DCF** adduct. The UV-Vis spectrum of **2** (1.25×10^{-5} M) (black line) dropped in intensity and showed a bathochromic effect (red line) after the addition of (DCF)Na in a 3:1 ratio with respect to **2** (Figure 2). It should be noted that the successive addition of HCl (1,0 mL, 1.3×10^{-2} M) to reach pH = 6.2 was responsible for the regeneration of **2** (dotted green line) as chloride salt and Diclofenac as a neutral species by protonation of the carboxylate group. It is worthwhile to note that, on changing the pH of the mixture from 6.2 to 8.0 by adding a NaOH solution, **2@DCF** adduct was restored (dotted blue line) indicating a complete reversibility of the sensing mechanism (see ESI for experimental details).

Even if the formation of **2@DCF** was easily observed by UV-Vis spectroscopy, all the attempts to isolate the adduct as a pure solid failed to suggest the onset of weak interactions between **2** and Diclofenac. This result was in agreement with the good reversibility of the sensing process which is an important feature in preventing the chemosensor deactivation and assuring the reversibility needed for the development of a sensors device.

Then, in order to confirm the essential role of RhB in the sensing process, we synthesised porphyrin **3** (Scheme 2), which displays an ammonium salt in place of Rhodamine salt, and its sensing ability towards Diclofenac was investigated. Porphyrin **3** was fully characterised and the UV-Vis spectrum in methanol of **3** showed an intense Soret band at 409 nm (log εM = 5.49) and four weaker Q bands at 505 nm (4.27), 535 nm (3.39), 580 nm (3.76) and 635 nm (2.96) (ESI).

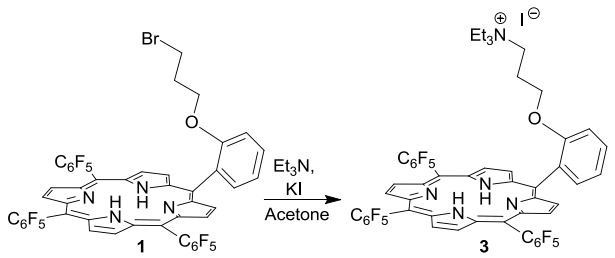

Scheme 2. Synthesis of porphyrin **3**.

The molecular structure of **3**, determined by single crystal X-ray diffraction, showed a "close" conformation (Figure 3). The amino-alkyl side arm is folded toward the core of the macrocycle with the terminal methyl groups of the pendant triethylammonium moiety pointing toward the pyrrole rings. Despite the asymmetric arrangement of the substituents, all the conformational data (see ESI for crystallographic details) seem indicating very small distortions of the macrocycle and a square-like inner cavity shape. This three-dimensional arrangement is very interesting in view of the desired synergic activity of the tetrapyrrolic core with the recognition *antenna* in forming a 'binding pocket' for the analyte.

Porphyrin **3** was treated with (DCF)Na by using the same experimental conditions that were employed for the reaction between porphyrin **2** and (DCF)Na. The UV-Vis analysis did not reveal any interaction between **3** and the analyte, confirming that RhB was crucial for the sensing recognition and the sole presence of the ammonium salt was not sufficient to interact with the sodium salt of Diclofenac by a metathesis reaction.

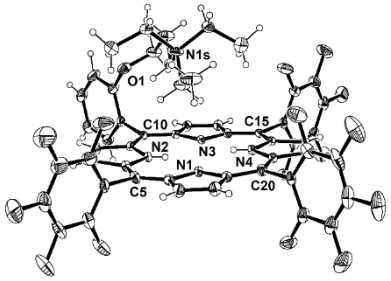

Figure 3. ORTEP diagram of the porphyrin **3**. Thermal ellipsoids are shown at 30% probability levels. The iodine counterion and hexane solvent molecules are omitted for clarity.

Then, in order to evaluate a possible recognition role of NH functionalities of the tetrapyrrolic core, which could interact with the carboxylate group of Diclofenac by forming hydrogen bonds, the free porphyrin **2** was reacted with $Zn(OAc)_2 \cdot (H_2O)_2$ to yield **Zn(2)** complex. The latter complex was fully characterised and showed the same chemical stability of its precursor **2** in a polar medium at different pH values (see above). The study of the sensing activity of **Zn(2)** was evaluated and compared with that of the free base porphyrin **2**. Collected data indicated that the two compounds showed similar sensing capabilities, suggesting that neither the inner NH functionalities nor the coordinated Zn(II) ion are directly involved in the molecular recognition event.

This hypothesis was confirmed by the inertness toward (DCF)Na of the analogue Zn(TPP) (TPP = dianion of tetraphenyl porphyrin), which does not present any functional group on the molecular skeleton. In fact, the UV-Vis analysis of the reaction of Zn(TPP) with a stoichiometric excess of (DCF)Na (Zn(TPP)/(DCF)Na = 1:5) did not reveal any change in the spectrum of the macrocycle indicating that either Zn(TPP) did not interact with the analyte or, if an interaction exists, this is below the detection limits of UV-Vis spectroscopy. This study suggested that the Diclofenac detection by **2** is dictated by the presence of Rhodamine group in the chemosensor periphery. Thus, in order to better assess the role of the porphyrin fragment in the sensing mechanism, the reaction between free Rhodamine B and (DCF)Na was analysed by UV-Vis spectroscopy. No change of the spectral pattern of the substrates was observed suggesting that the sensing performance of **2** must be assigned to the entire molecule and not only to the Rhodamine unit. All data reported up to now indicate that the recognition process seems to occur by *a lock and key* mechanism due to a specific three-dimensional arrangement which is driven by a combination of electrostatic and $\pi-\pi$ interactions between the analyte and receptor.

The evaluation of the binding constant value for the formation of **2@DCF** molecular complex was carried out by UV-Vis spectroscopy (Figure 4). In order to keep the concentration of the receptor at a constant value throughout the titration, the (DCF)Na solution was prepared by dissolving the required

amount of salt into a 10.0 μM porphyrin solution itself. Experimental data were conveniently fitted by an overall 1:1 binding equilibrium; a Langmuir type equation revealed a good efficiency of the binding with the experimental K_{bind} value of 9.3 (± 0.8) x 10^4 M^{-1}. Experiments were performed twice and the obtained results showed a very good reproducibility (see ESI for experimental details).

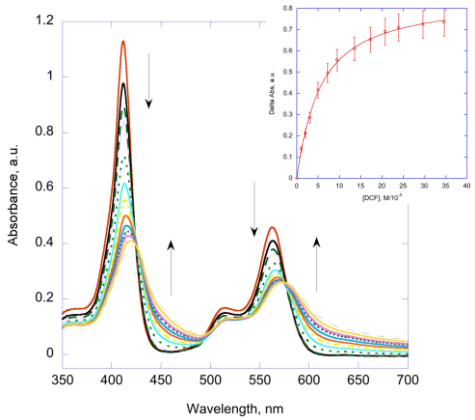

Figure 4. Spectral pattern variation of **2** (5.0 μM; MeOH/H_2O = 1:1). Inset: evaluation of the binding constant value for the **2@DCF** formation by a Langmuir type equation.

It should be noted that when **2** was left standing in a solid state for a prolonged time (some weeks), some extent of aggregation occurred, as stated by the typical UV-Vis spectral changes (hypochromicity and broadening of the porphyrin Soret B band). However, this process did not affect the binding properties of **2**, as supported by the reproducibility of K_{bind} values (within the experimental errors) which were calculated by using samples of **2** after different periods of storage.

Importantly, similar K_{bind} values were obtained by analysing the formation of **Zn(2)@DCF** adduct to definitely rule out an active role of the central zinc metal during the molecular recognition event.

A closer inspection of the spectroscopic variations, due to the chemosensor/analyte interaction, gave more insights on the intimate sensing mechanism. The molecular binding occurred with the concomitant formation of aggregated structures, which is driven by the saturation of the electronic positive charges of **2**. The aggregation process was revealed by the strong hypochromic and bathochromic shift of the **2@DCF** spectral features upon the Diclofenac addition (Figure 4) and by the concomitant increase of the Resonance Light Scattering (RLS) signal of the adduct (Figure 5). It is worth noting that RLS, i.e. the enhancement of the scattered light close to the absorption wavelength, is shown to be a sensitive and selective method for studying electronically coupled chromophore arrays, such as porphyrins and related macrocycles, due to the great dependence of the signal intensity upon the extent of arrays.[37]

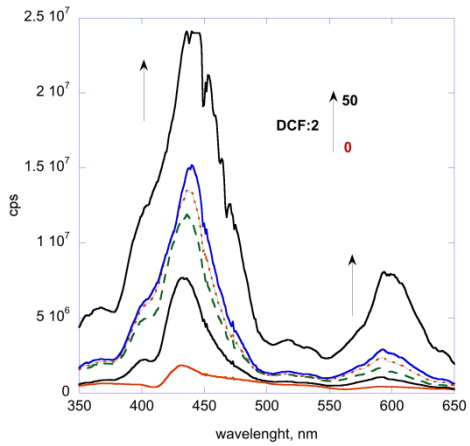

Figure 5. Resonance Light Scattering spectral variation of **2** (5.0 μM) upon the (DCF)Na addition.

The inspection of Figure 5 revealed a strong increase of the scattered signal upon the (DCF)Na addition. This, jointly with the corresponding variation observed in the UV-Vis spectra, strongly indicated the formation of large arrays of porphyrin aggregates, up to a micrometric scale.

Analogous studies were also being carried out by using Fluorescence Spectroscopy. Fluorescence emission spectra of **2** were measured in a H_2O/CH_3OH = 1:1 (v:v) solvent mixture by exciting the dyad compound at λ_{exc} = 412 nm. Three emission peaks were detected at λ_{em} = 590, 641 and 705 nm, which were attributed to Rhodamine B and porphyrin moieties, respectively. These values shifted to longer wavelengths with respect to the emission maxima of **3** (λ_{em} = 637 and 699 nm) and Rhodamine B alone (λ_{em} = 569 nm) suggesting an electronic coupling of the fluorophores in the dyad compound. Interestingly, the collection of the excitation spectra of **2** at λ_{em} = 590 nm (RhB emission) showed a distinct contribution from the porphyrin absorption spectrum. Analogously, a relevant contribution from the RhB absorption spectrum was detected by collecting the excitation spectra of **2** at λ_{em} = 705 (porphyrin emission) (See ESI). These findings clearly indicated that excited state Energy Transfer (ET) processes took place from the Rhodamine excited state to the tetrapyrrolic moiety and *vice versa* from the porphyrin excited state to the Rhodamine group. Due to the observed ground state electronic coupling between the two fluorophores, ET can be safely ascribed to a Dexter mechanism, which requires a short-range interaction between the electronic distributions of the two components of the dyad. These results confirmed that the receptor **2** preferentially attains a molecular conformation in which the two chromophores are located at short distances apart.

The DCF/**2** binding interactions were also investigated by measuring the emission spectra of **2** at different (DCF)Na concentrations by using the same experimental conditions which were employed for UV-Vis absorption experiments.

Achieved data indicated a strong quenching of the **2** emission for both the excitation wavelengths related to Rhodamine and porphyrin groups. This effect can be ascribed to either i) a

direct quenching of Diclofenac on both the chromophores or ii) the breaking of the Rhodamine-porphyrin excited state interaction due to a decrease of the electronic coupling between the two chromophores. However, both mechanisms require that Diclofenac should be placed at very short distances with respect to the two chromophores, likely intercalated between the porphyrin and Rhodamine moieties (Figure 2).

The **2@DCF** binding isotherm, obtained by measuring the fluorescence intensities of the porphyrin moiety at different (DCF)Na concentrations, displayed the K_{bind} of 2.7 (± 0.3) x 10^4 M^{-1} (ESI) which is in fair agreement with the *K* value calculated by using UV-Vis spectroscopy. The small discrepancy between the two *K* values (9.3 (± 0.8) x 10^4 M^{-1} by UV-Vis absorption *versus* 2.7 (± 0.3) x 10^4 M^{-1} by fluorescence emission) could be ascribed to the fact that UV-Vis spectroscopy only depends on ground-state interactions while fluorescence is affected by the extent of both ground- and excited state interactions. Time-resolved fluorescence experiments, carried out on the porphyrin emission at different (DCF)Na concentrations, clearly demonstrated the onset of excited state interactions between the porphyrin moiety and DCF. In particular, the analysis showed, upon the DCF binding, a marked quenching of all the three lifetimes accounting for the time decay of the porphyrin moiety. This finding indicates that DCF binding affected both monomeric (τ = 11 ns), and aggregated (τ = 2-1 ns) forms of **2**, with the last species becoming the most abundant in the presence of a (DCF)Na excess (ESI).

In order to verify the sensor selectivity, the reactivity of both **2** and **Zn(2)** species towards sodium salt of Diclofenac was investigated in the presence of Pb^{2+} or Cd^{2+} metal pollutants as well as ammonia (1.28 x 10^{-4} M, in a 1:1 molar ratio with respect to Diclofenac). UV-Vis spectroscopic studies revealed that the sensing ability of both porphyrin chemosensors was not affected by the presence of the above listed species, underlining the good selectivity of these receptors towards the target analyte. Quantitative binding experiments have been carried out in the presence of possible interfering carboxylate drugs such as sodium phenylacetate, sodium salicylate, L-tyrosine sodium salt, sodium sarcosinate and L-alanine sodium salt. The results obtained showed that the binding ability of receptor **2** was very slightly affected by the presence of the above contaminants at both 1:1 and 1:5 molar ratio, with respect to the DCF concentration (Figure 6, see ESI for experimental details).

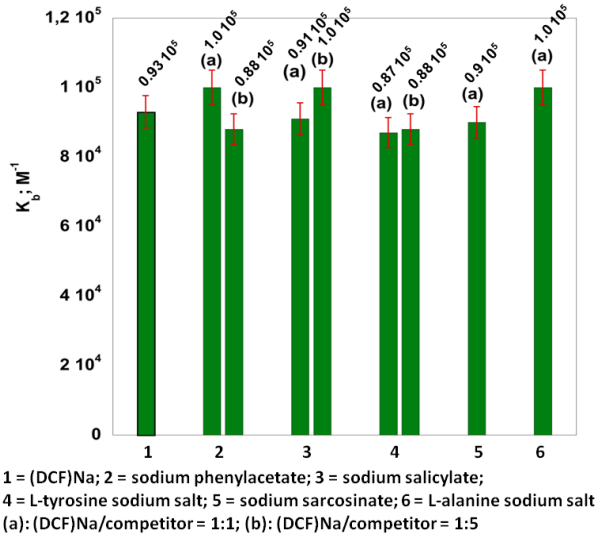

Figure 6. Binding constant values for the formation of **2@DCF** adduct in the presence of interfering sodium salts. (a): 1:1 molar ratio, (b): 1:5 molar ratio (error bars 5%).

Conclusions

In conclusion, we reported the synthesis and full characterisation of the porphyrin/Rhodamine B molecular chemosensor **2** and its zinc complex **Zn(2)** which were tested for the Diclofenac detection. UV-Vis spectroscopic analyses of the recognition reactions revealed a reversible sensing process which occurred by a *lock and key* mechanism in which the binding of the analyte was the result of the synergic interaction of the analyte with both the Rhodamine unit (electrostatic interactions) and the tetrapyrrolic platform (π-π and London dispersion forces). The binding of the analyte was mainly due to the Rhodamine unit and the tetrapyrrolic core only favoured the Diclofenac accommodation without forming specific bonds.

Future studies will be devoted to the exploitation of the investigated receptor as sensing material for the development of a chemical sensor. For this application, we will investigate the introduction of a spacer group on the *para* position of *meso*-aryl groups in order to anchor the chemosensor onto a surface by forming either covalent or non-covalent linkages.

Conflicts of interest

There are no conflicts to declare.

Notes and references

1 S. D. Richardson and T. A. Ternes, *Anal. Chem.*, 2018, **90**, 398-428.
2 T. Deblonde, C. Cossu-Leguille and P. Hartemann, *Int. J. Hyg. Environ. Health*, 2011, **214**, 442-448.
3 J. C. G. Sousa, A. R. Ribeiro, M. O. Barbosa, M. F. R. Pereira and A. M. T. Silva, *J. Hazard. Mater.*, 2018, **344**, 146-162.
4 Directive 2013/39/UE of the European Parliament and the Council of the 12 amending Directive 2000/60/EC and

2005/105/EC regards priority substances in the field of water policy, Official J. Eur. Union, 2013.
5 S. Schmidt, H. Hoffmann, L.-A. Garbe and R. J. Schneider, *J. Chromatogr. A*, 2018, **1538**, 112-116.
6 G. Daniele, M. Fieu, S. Joachim, A. Bado-Nilles, P. Baudoin, C. Turies, J.-M. Porcher, S. Andres and E. Vulliet, *Anal. Bioanal. Chem.*, 2016, **408**, 4435-4444.
7 P. C. Lindholm-Lehto, H. S. J. Ahkola, J. S. Knuutinen, J. Koistinen, K. Lahti, H. Vahtera and S. H. Herve, *Environ. Sci. Pollut. R.*, 2016, 1-12.
8 V. Osorio, M. Imbert-Bouchard, B. Zonja, J.-L. Abad, S. Pérez and D. Barceló, *J. Chromatogr. A*, 2014, **1347**, 63-71.
9 N. Hermes, K. S. Jewell, A. Wick and T. A. Ternes, *J. Chromatogr. A*, 2018, **1531**, 64-73.
10 C. E. D. Nazario and F. M. Lancas, *Food Anal. Method*, 2017, **10**, 2490-2496.
11 S. Motoc, F. Manea, A. Iacob, A. Martinez-Joaristi, J. Gascon, A. Pop and J. Schoonman, *Sensors*, 2016, **16**, 1719-1730.
12 G. P. Fard, E. Alipour and R. E. Ali Sabzi, *Anal. Methods*, 2016, **8**, 3966-3974.
13 G. Y. Aguilar-Lira, J. M. Gutiérrez-Salgado, A. Rojas-Hernández, J. A. Rodríguez-Ávila, M. E. Páez-Hernández and G. A. Álvarez-Romero, *J. Electroanal. Chem.*, 2017, **801**, 527-535.
14 F. Ahmed, K. Shah, I. Z. Awan and M. R. Shah, *Ecotoxicol. Environ. Saf.*, 2016, **129**, 103-108.
15 K. Shah, E. Hassan, F. Ahmed, I. Anis, M. Rabnawaz and M. R. Shah, *Ecotoxicol. Environ. Saf.*, 2017, **141**, 25-29.
16 N. Steinke, M. Rio, R. Wuchrer, C. Schuster, E. Ljasenko, D. Knopp, G. Gerlach and T. Härtling, *Sens. Actuators B Chem.*, 2018, **254**, 749-754.
17 J. Shi, M. Xu, Q. Tang, K. Zhao, A. Deng and J. Li, *Spectrochim. Acta A Mol. Biomol. Spectrosc.*, 2018, **191**, 1-7.
18 R. Paolesse, S. Nardis, D. Monti, M. Stefanelli and C. Di Natale, *Chem. Rev.*, 2017, **117**, 2517-2583.
19 Y. Ding, W.-H. Zhu and Y. Xie, *Chem. Rev.*, 2017, **117**, 2203-2256.
20 N. L. Bill, O. Trukhina, J. L. Sessler and T. Torres, *Chem. Commun.*, 2015, **51**, 7781-7794.
21 E. M. G. Santos, A. N. Araújo, C. M. C. M. Couto and M. C. B. S. M. Montenegro, *J. Pharm. Biomed. Anal.*, 2006, **42**, 535-542.
22 D. Vlascici, S. Pruneanu, L. Olenic, F. Pogacean, V. Ostafe, V. Chiriac, E. M. Pica, L. C. Bolundut, L. Nica and E. Fagadar-Cosma, *Sensors*, 2010, **10**, 8850-8864.
23 G. Pranitha and G. Venkateshwarlu, *World J. Pharm. Pharm. Sci.*, 2016, **5**, 2249-2260.
24 Z. Kormosh, I. Hunka, Y. Bazel, A. Laganovsky, I. Mazurenko and N. Kormosh, *Cent. Eur. J. Chem.*, 2007, **5**, 813-823.
25 R. Zhang, F. Yan, Y. Huang, D. Kong, Q. Ye, J. Xu and L. Chen, *RSC Advances*, 2016, **6**, 50732-50760.
26 O. Horváth, Z. Valicsek, M. A. Fodor, M. M. Major, M. Imran, G. Grampp and A. Wankmüller, *Coord. Chem. Rev.*, 2016, **325**, 59-66.
27 E. J. Ngen, L. Xiao, P. Rajaputra, X. Yan and Y. You, *Photochem. Photobiol.*, 2013, **89**, 841-848.
28 T. Mani, D. M. Niedzwiedzki and S. A. Vinogradov, *J. Phys. Chem. A*, 2012, **116**, 3598-3610.
29 E. J. Ngen, P. Rajaputra and Y. You, *Bioorg. Med. Chem.*, 2009, **17**, 6631-6640.
30 X. Sun, D. Li, G. Chen and J. Zhang, *Dyes Pigm.*, 2006, **71**, 118-122.
31 H. M. Titi, B. K. Tripuramallu and I. Goldberg, *CrystEngComm*, 2016, **18**, 3318-3339.
32 A. D'Urso, A. Di Mauro, A. Cunsolo, R. Purrello and M. E. Fragalà, *J. Phys. Chem. C*, 2013, **117**, 17659-17665.
33 M. Soylak, Y. E. Unsal, E. Yilmaz and M. Tuzen, *Food Chem. Toxicol.*, 2011, **49**, 1796-1799.
34 M. Gruden, S. Grubisic, A. G. Coutsolelos and S. R. Niketic, *J. Mol. Struct.*, 2001, **595**, 209-224.
35 W. Jentzen, X.-Z. Song and J. A. Shelnutt, *J. Phys. Chem. B*, 1997, **101**, 1684-1699.
36 W. Jentzen, J.-G. Ma and J. A. Shelnutt, *Biophys. J.*, 1998, **74**, 753-763.
37 R.F. Pasternack and P.J. Collings, *Science*, 1995, **269**, 935-939.

Journal Name

ARTICLE

Graphical Abstract

The synthesis of a porphyrin chemosensor is here reported as well as its sensing activity in detecting the emerging pollutant Diclofenac with an overall 1:1 binding constant of about 10^5 M^{-1}.

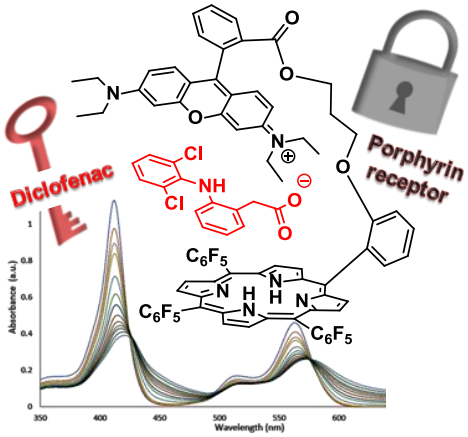

Electronic Supplementary Information

Sensing of Diclofenac by a Porphyrin-based Artificial Receptor

Daniela Intrieri,[a] Caterina Damiano,[a] Silvia Rizzato,[a] Roberto Paolesse,[b] Mariano Venanzi,[b] Donato Monti,*[b] Marco Savioli[b], Manuela Stefanelli[b] and Emma Gallo.*[a]

[a]*Department of Chemistry, University of Milan, Via C. Golgi 19, 20133 Milan (Italy). E-mail: emma.gallo@unimi.it.*

[b]*Department of Chemical Science and Technologies, University of Roma Tor Vergata, Via della Ricerca Scientifica, 00133 Rome (Italy). E-mail: dmonti@uniroma2.it*

1. General

Unless otherwise specified, all the reactions were carried out under a nitrogen atmosphere by employing standard Schlenk techniques and magnetic stirring. Dichloromethane, chloroform, *N,N*-dimethylformamide and pyrrole were distilled over CaH_2 and stored under nitrogen. Acetone was distilled over K_2CO_3 and stored under nitrogen. All the other starting materials and Zn(TPP) were commercial products which were used as received. 2-(3-Bromopropoxy)benzaldehyde[1] and sodium phenylacetate[2] were synthesized by methods reported in the literature or by using minor modifications of them. Solvents used for spectroscopy investigations were of Spectroscopic Grade of the highest degree of purity available and used as received. NMR spectra were recorded at room temperature on a Bruker Avance 400-DRX spectrometers, operating at 400 MHz for ^{1}H, at 100 MHz for ^{13}C and at 376 MHz for ^{19}F. Chemical shifts (ppm) are reported relative to TMS. The ^{1}H NMR signals of the compounds described in the following have been attributed by COSY and NOESY techniques. Assignments of the resonance in ^{13}C NMR were made using the APT pulse sequence and HSQC and HMBC techniques. UV/Vis spectra were recorded on an Agilent 8453E instrument. Elemental analyses and mass spectra were recorded in the analytical laboratories of Milan University. All spectroscopic studies were carried out at 298.0 (± 0.5) K (Julabo F25 Thermostat). Steady-state Fluorescence and Resonance Light Scattering Spectroscopy studies were carried out on Fluoromax 4 (Horiba Instruments). Time-resolved Fluorescence Spectroscopy studies were carried out on LifeSpoec–ps (Edimburg Instruments), equipped with a Hamamatsu Photonics K.K. laser. X-ray data collection was performed at 150 K using graphite-monochromated Mo Kα radiation (λ = 0.71073 Å) on a Bruker ApexII CCD area-detector diffractometer equipped with an Oxford Cryosystems N_2 gas blower. A ω-scan was performed within the Bragg limits of $1.3 < \theta < 25.0°$. Determination of the integrated intensities and unit cell refinements were performed using SAINT[3] and all absorption corrections were applied by using SADABS.[4] The structures were solved by direct methods (SIR2014)[5] and refined by full-matrix least squares on F^2 (SHELX 2014)[6] with the WINGX interface.[7]

2. Synthetic procedures

2.1. Synthesis of 1.

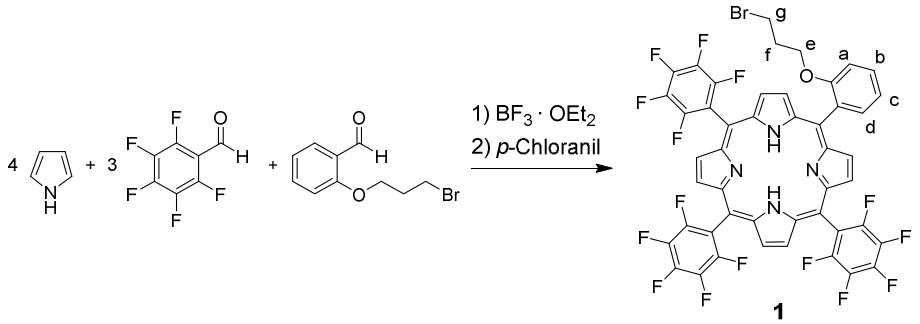

Freshly distilled pyrrole (173 µL, 2.50 mmol), pentafluorobenzaldehyde (231 µL, 1.87 mmol) and 2-(3-bromopropoxy)benzaldehyde (110 µL, 0.62 mmol) were dissolved in dry dichloromethane (250 mL) in a 500 mL two necks round-bottom flask. The reaction mixture was shielded from ambient light and $BF_3{\cdot}OEt_2$ (31 µL, 0.25 mmol) was added dropwise by a syringe. The obtained pale orange solution was stirred in the dark for 3 hours at room temperature and then tetrachloro-1,4-benzoquinone (*p*-chloranil) (0.615 g, 2.50 mmol) was added. The resulting solution was refluxed in air for 6 hours, the solvent evaporated to dryness under reduced pressure and the resulting black solid purified by flash column chromatography on silica gel (60 µm, eluent *n*-hexane/dichloromethane = 90:10) yielding **1** (20% yield) as a purple solid. Elemental Analysis calc. for $C_{47}H_{20}BrF_{15}N_4O$: C, 55.26; H, 1.97; N, 5.48; found: C, 55.66; H, 2.11; N, 5.31. UV-Vis, λ_{max} (MeOH)/nm (log ε_M): 410 (5.39), 506 (4.47), 536 (3.61), 582 (3.98), 643 (3.15). LR-MS (ESI): m/z ($C_{47}H_{20}BrF_{15}N_4O$ $[M+H]^+$) calcd. 1020.06; found 1021.2. ^{1}H NMR (400 MHz, $CDCl_3$, 298 K) δ: 8.97 (d, J = 4.7 Hz, 2H, $H_{\beta pyrr}$), 8.91 (s, 4H, $H_{\beta pyrr}$), 8.84 (d, J = 4.7 Hz, 2H, $H_{\beta pyrr}$), 8.08 (dd, J_o = 7.4 Hz, J_m = 1.5 Hz, 1H, H_d), 7.83 (t, J = 8.1 Hz, 1H, H_b), 7.44 (t, J = 7.6 Hz, 1H, H_c), 7.38 (d, J = 8.1 Hz, 1H, H_a), 4.10 (t, J = 5.4 Hz, 2H, H_e),

2.26 (t, J = 6.0 Hz, 2H, H_g), 1.46 (m, 2H, H_f), -2.81 (s, 2H, NH_{pyrr}). ^{13}C NMR (100 MHz, $CDCl_3$, 298 K) δ: 158.3, 147.8, 145.4, 143.4, 140.9, 138.8, 136.3, 135.6, 130.6, 129.8 (2 signals overlapped), 119.9, 119.4, 116.0, 117.7, 102.8, 101.9, 65.1, 31.3, 29.8. Six quaternary carbon atoms were not detected. ^{19}F NMR (376 MHz, $CDCl_3$, 298 K) δ: -136.9, -152.1, -162.0.

2.2. Synthesis of 2.

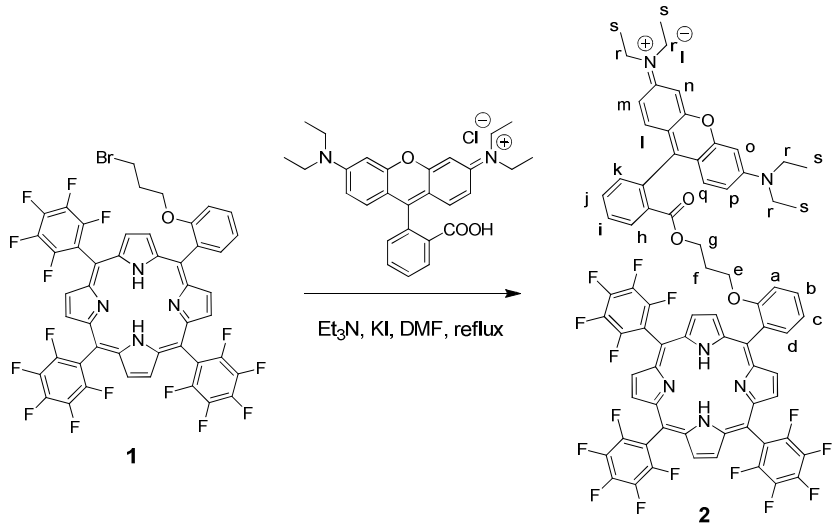

1 **2**

Rhodamine B (0.200 g, 0.418 mmol), triethylamine (58.0 μL, 0.418 mmol) and KI (0.069 g, 0.418 mmol) were added to a dry DMF (25 mL) solution of **1** (0.171 g, 0.167 mmol). The dark purple mixture was refluxed under stirring for 10 hours, then the solvent was evaporated to dryness under reduced pressure and the residue purified by flash column chromatography on silica gel (60 μm, eluent: gradient, from dichloromethane to 3% methanol in dichloromethane) yielding **2** (45% yield) as a dark purple solid (which resulted pink in solution). Elemental Analysis calc. for $C_{75}H_{50}F_{15}IN_6O_4$: C, 59.61; H, 3.34; N, 5.56; found: C, 59.93; H, 3.13; N, 5.83. UV-Vis, λ_{max} (MeOH)/nm (log ε_M): 412 (5.67), 512 (4.82), 559 (5.24), 638 (3.18). LR-MS (ESI): m/z ($C_{75}H_{50}F_{15}N_6O_4^+$ $[M]^+$) calcd. 1383.36; found 1383.6. ^{1}H NMR (400 MHz, $CDCl_3$, 298 K) δ: 8.87 (m, 6H, $H_{\beta pyrr}$), 8.73 (d, J = 4.3 Hz, 2H, $H_{\beta pyrr}$), 8.00 (dd, J_o = 7.4 Hz, J_m = 1.6 Hz, 1H, H_d), 7.78 (m, 2H, H_b and H_h), 7.63 (m, 1H, H_j), 7.40 (t, J = 7.4 Hz, 2H, H_c and H_i), 7.31 (m, 1H, H_a), 7.14 (m, 1H, H_k), 6.83 (d, J = 9.9 Hz, 2H, H_l and H_q), 6.64 (m, 4H, H_m, H_n, H_o and H_p), 3.87 (t, J = 5.5 Hz, 2H, H_e), 3.43 (m, 8H, H_r), 3.17 (t, J = 6.1 Hz, 2H, H_g), 1.13 (m, 14H, H_f and H_s), -2.84 (s, 2H, NH_{pyrr}). ^{13}C NMR (100 MHz, $CDCl_3$, 298 K) δ: 164.4, 158.6, 158.1, 157.5, 155.3, 147.8, 145.3, 143.4, 140.9, 138.8, 135.8, 133.2, 132.9, 131.3, 131.1, 131.0, 130.9, 130.1, 129.62, 129.56, 120.0, 119.4, 116.3, 114.2, 113.3, 112.0, 102.7, 96.3, 64.6, 61.9, 46.1, 43.5, 41.3, 36.0, 29.1 27.8, 12.5. ^{19}F NMR (376 MHz, $CDCl_3$, 298 K) δ: -137.0, -140.38, -140.89, -152.0, -161.8.

2.3. Synthesis of 3.

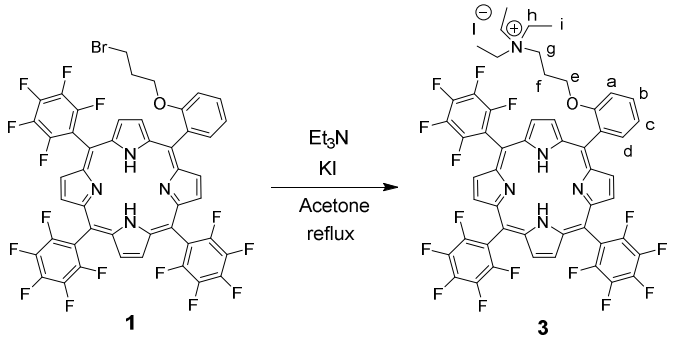

1 **3**

Triethylamine (0.172 mL, 1.24 mmol) and KI (0.207 g, 1.24 mmol) were added to a dry acetone (15 mL) solution of **1** (0.127 g, 0.124 mmol). The dark brown mixture was refluxed under stirring for 6 hours, then

the solvent evaporated to dryness under reduced pressure and the resulting solid purified by flash column chromatography on silica gel (60 μm, eluent: gradient, from dichloromethane to 3% methanol in dichloromethane) yielding **3** (55% yield) as a dark red solid. Elemental Analysis calc. for $C_{53}H_{35}F_{15}IN_5O$: C, 54.42; H, 3.02; N, 5.99; found: C, 54.23; H, 3.11; N, 6.06. UV-Vis, λ_{max} (CH_2Cl_2)/nm (log ε_M): 413 (5.49), 507 (4.28), 536 (3.47), 583 (3.80), 636 (3.14). λ_{max} (MeOH)/nm (log ε_M): 409 (5.49), 505 (4.27), 535 (3.39), 580 (3.76), 635 (2.96). LR-MS (ESI): m/z ($C_{53}H_{35}F_{15}N_5O^+$ $[M]^+$) calcd. 1042.26; found 1042.4. ^{1}H NMR (400 MHz, $CDCl_3$, 298 K) δ: 8.96 (m, , 6H, $H_{\beta pyrr}$), 8.89 (d, J = 4.5 Hz, 2H, $H_{\beta pyrr}$), 8.22 (dd, J_o = 7.6 Hz, J_m = 1.5 Hz, 1H, H_d), 7.86 (t, J = 8.0 Hz, 1H, H_b), 7.54 (t, J = 7.6 Hz, 1H, H_c), 7.34 (d, J = 8.0 Hz, 1H, H_a), 3.96 (t, J = 4.8 Hz, 2H, H_e), 1.29 (m, 2H, H_f), 0.97 (q, J = 6.9 Hz, 6H, H_h), 0.6 (m, 2H, H_g), -1.26 (t, J = 6.9 Hz, 9H, H_i), -2.94 (s, 2H, NH_{pyrr}). ^{13}C NMR (100 MHz, $CDCl_3$, 298 K) δ: 162.8, 158.5, 148.5, 145.4, 140.0, 136.4, 134.2, 131.7, 130.8, 121.5, 119.8, 114.5, 103.3, 65.8, 52.7, 51.5, 22.4, 5.2. Eight quaternary carbon atoms were not detected. ^{19}F NMR (376 MHz, $CDCl_3$, 298 K) δ: -137.8, -151.0, -161.0.

2.4. Synthesis of Zn(2).

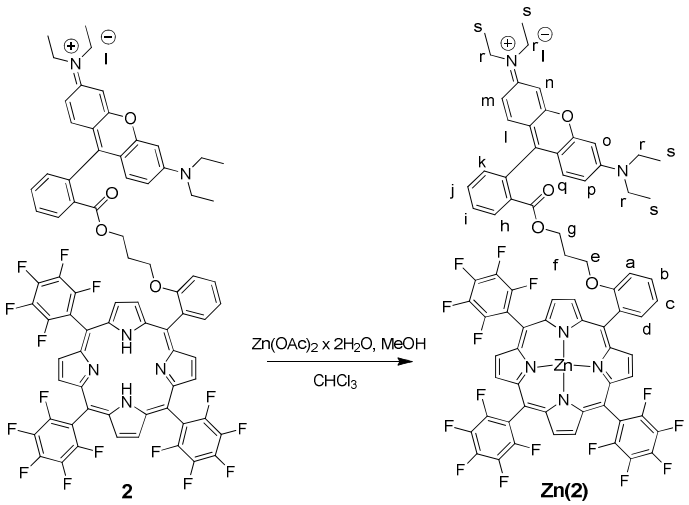

A dry CH_3OH (13.50 mL) solution of $Zn(OAc)_2 \cdot 2H_2O$ (72 mg, 0.33 mmol) was added to a $CHCl_3$ (6.50 mL) solution of **2** (49 mg, 0.033 mmol) in a 50 mL dried Schlenk. The mixture was refluxed under stirring for 2 hours, then the solvent was evaporated to dryness under reduced pressure and 15 mL of CH_2Cl_2 was added to the residue. The organic phase was washed with water (3 x 15 mL), dried over $NaSO_4$ and the filtrate was evaporated to dryness under reduced pressure yielding Zn(**2**) in a quantitative yield. Elemental Analysis: calc. for $C_{75}H_{48}F_{15}IN_6O_4Zn$: C, 62.23; H, 3.34; N, 5.81; found: C, 62.40; H, 3.71; N, 5.62. UV-Vis, λ_{max} (CH_2Cl_2)/nm (log ε_M): 419 (5.05), 560 (4.99). λ_{max} (MeOH)/nm (log ε_M): 418(5.01), 561(4.83). LR-MS (ESI): m/z ($C_{75}H_{48}F_{15}N_6O_4Zn^+$ $[M]^+$) calcd. 1445.28; found 1446.67. ^{1}H NMR (400 MHz, $CDCl_3$, 298 K): δ 8.91 (m, 6H, $H_{\beta pyrr}$), 8.75 (s, 2H, $H_{\beta pyrr}$), 8.14 (d, J = 6.7 Hz, 1H, H_h), 7.76 (t, J=7.6 Hz, 1H, H_j), 7.44 (br s, 2H, H_i and H_a), 7.26 (br s, H_k and H_c), 7.13 (br s, 1H, H_b), 6.88 (d, J=7.4 Hz, 1H, H_d), 6.53 (s, 2H, H_l and H_q), 6.41 (m, 4H, H_m, H_n, H_o and H_p), 3.48 (s, 2H, H_e), 3.38 (br s, 8H, H_r), 1.28 (solvent overlap H_g), 1.12 (s, 12H, H_s), 0.62 (s, 2H, H_f). ^{13}C NMR (100 MHz, $CDCl_3$, 298K): δ 158.8, 157.9, 157.3, 155.3, 151.3, 150.1, 149.8, 149.6, 148.3, 145.0, 135.1, 133.6, 132.7, 132.5, 132.4, 131.6, 131.2, 130.7, 130.4, 129.8, 129.7, 120.8, 114.0, 113.0, 103.1, 102.3, 96.4, 66.1, 61.8, 46.1, 29.8, 27.2, 12.6. eight quaternary carbon atoms were not detected. ^{19}F NMR (376 MHz, $CDCl_3$, 298 K): δ -136.7, -137.7, 140.3, 141.3, 152.4, -153.1, -162.3 to -163.0.

3. ^{1}H, ^{13}C and ^{19}F NMR spectra of reported compounds

Figure 1. ^{1}H NMR spectrum (400 MHz, $CDCl_3$, 298 K) of porphyrin **1**

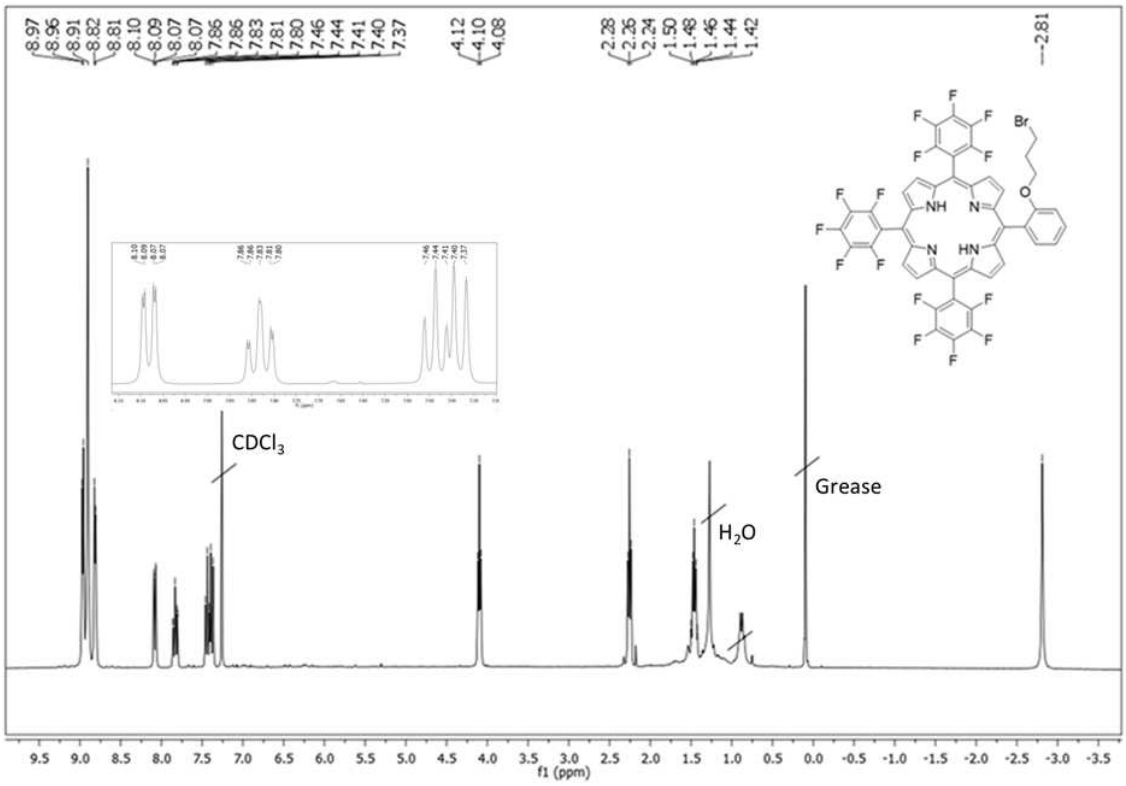

Figure 2. ^{13}C NMR spectrum (100 MHz, $CDCl_3$, 298 K) of porphyrin **1**

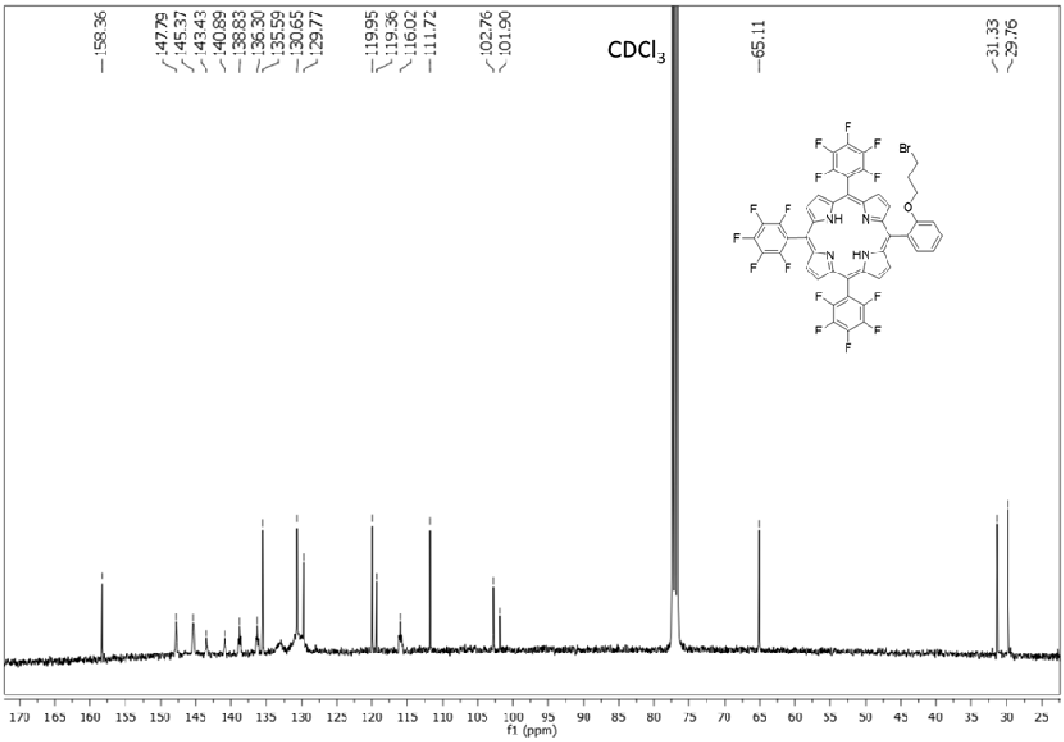

Figure 3. ^{19}F NMR spectrum (376 MHz, $CDCl_3$, 298 K) of porphyrin **1**

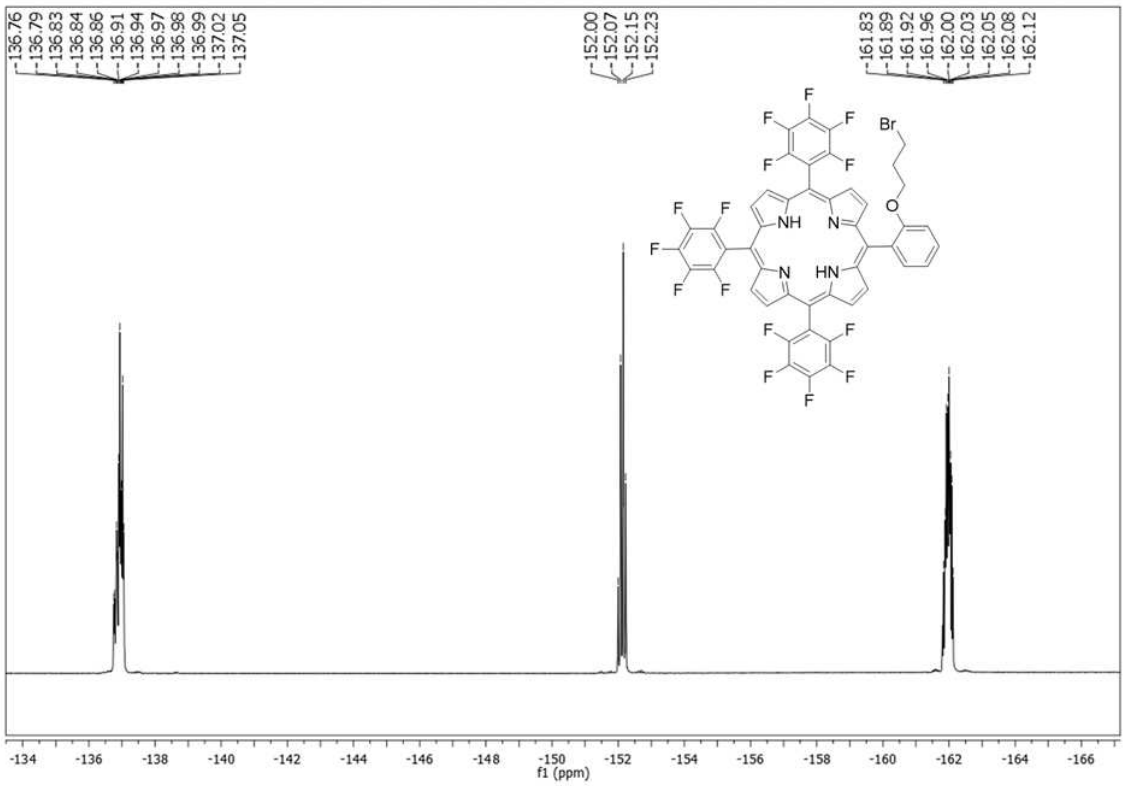

Figure 4. ^{1}H NMR spectrum (400 MHz, $CDCl_3$, 298 K) of porphyrin **2**

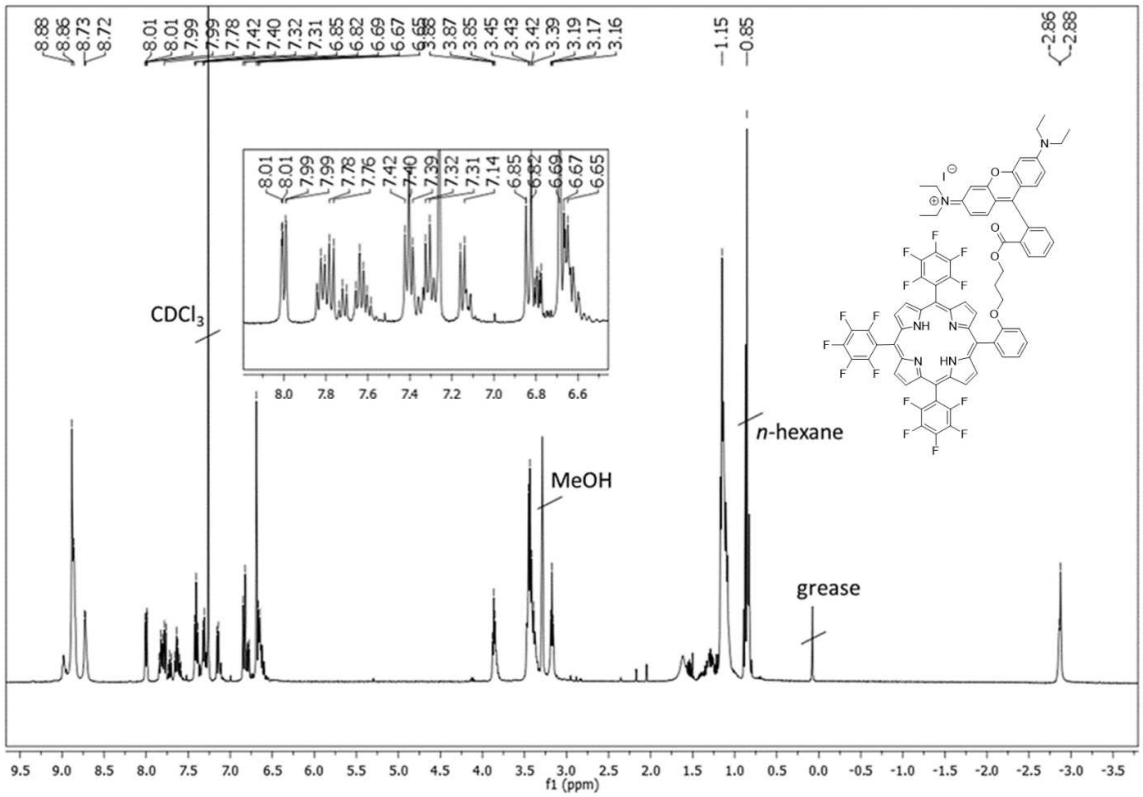

Figure 5. ^{13}C NMR spectrum (100 MHz, $CDCl_3$, 298 K) of porphyrin **2**

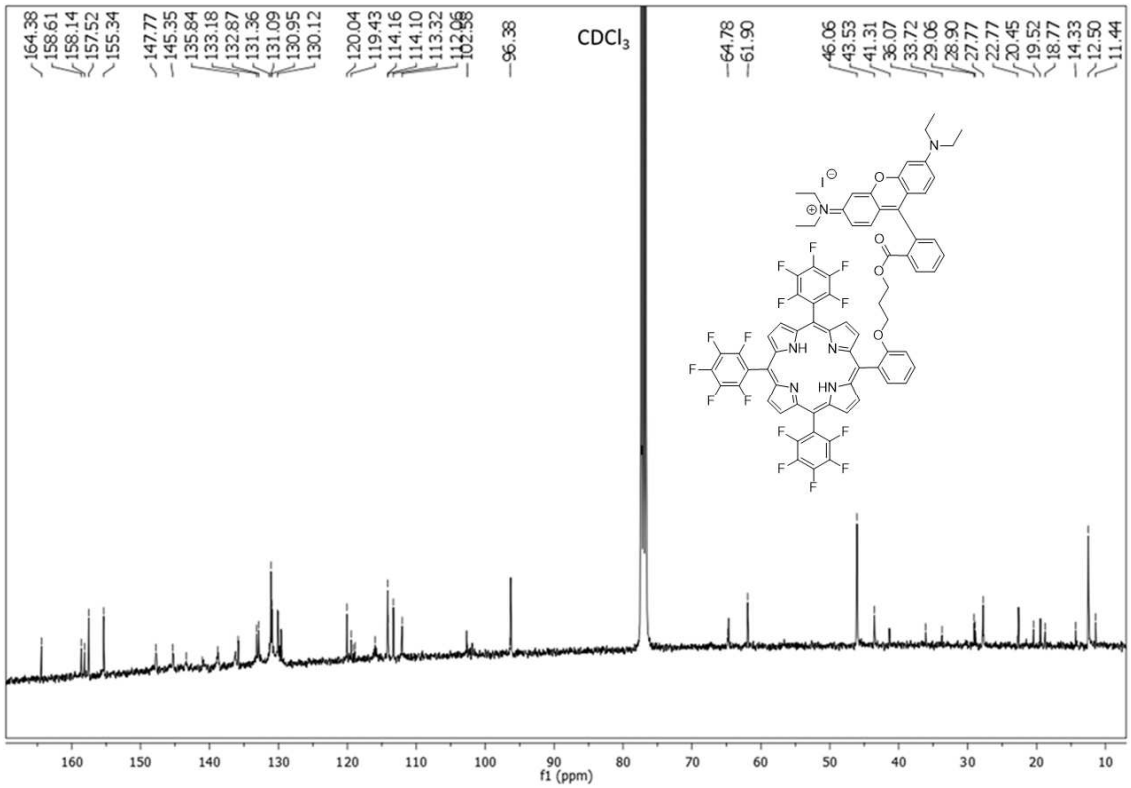

Figure 6. ^{19}F NMR spectrum (376 MHz, $CDCl_3$, 298 K) of porphyrin **2**

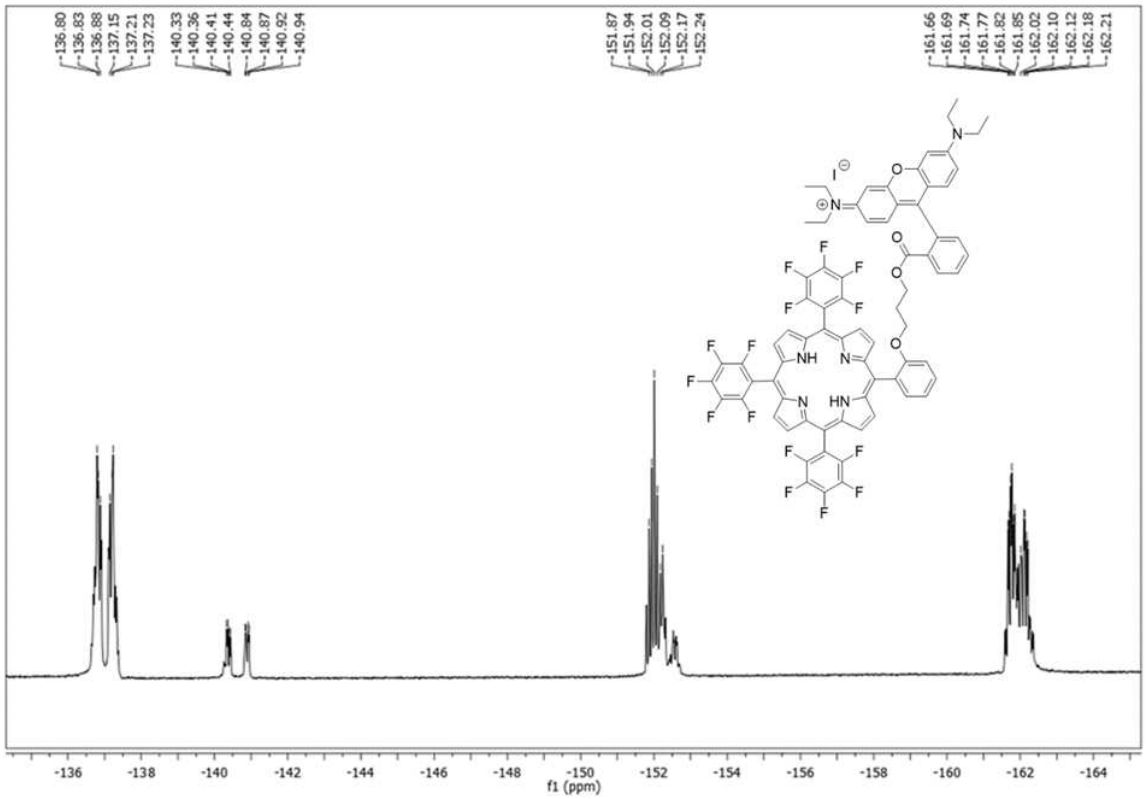

Figure 7. ^{1}H NMR spectrum (400 MHz, $CDCl_3$, 298 K) of porphyrin **3**

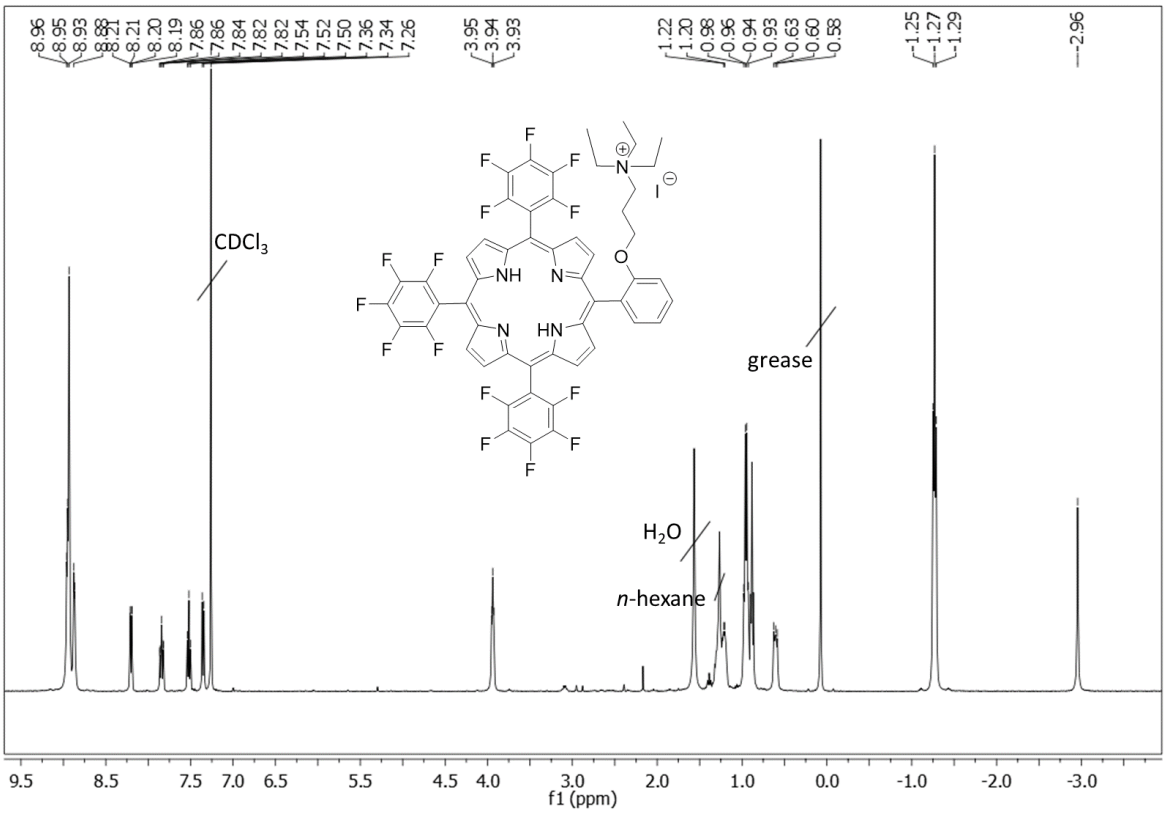

Figure 8. ^{13}C NMR spectrum (100 MHz, $CDCl_3$, 298 K) of porphyrin **3**

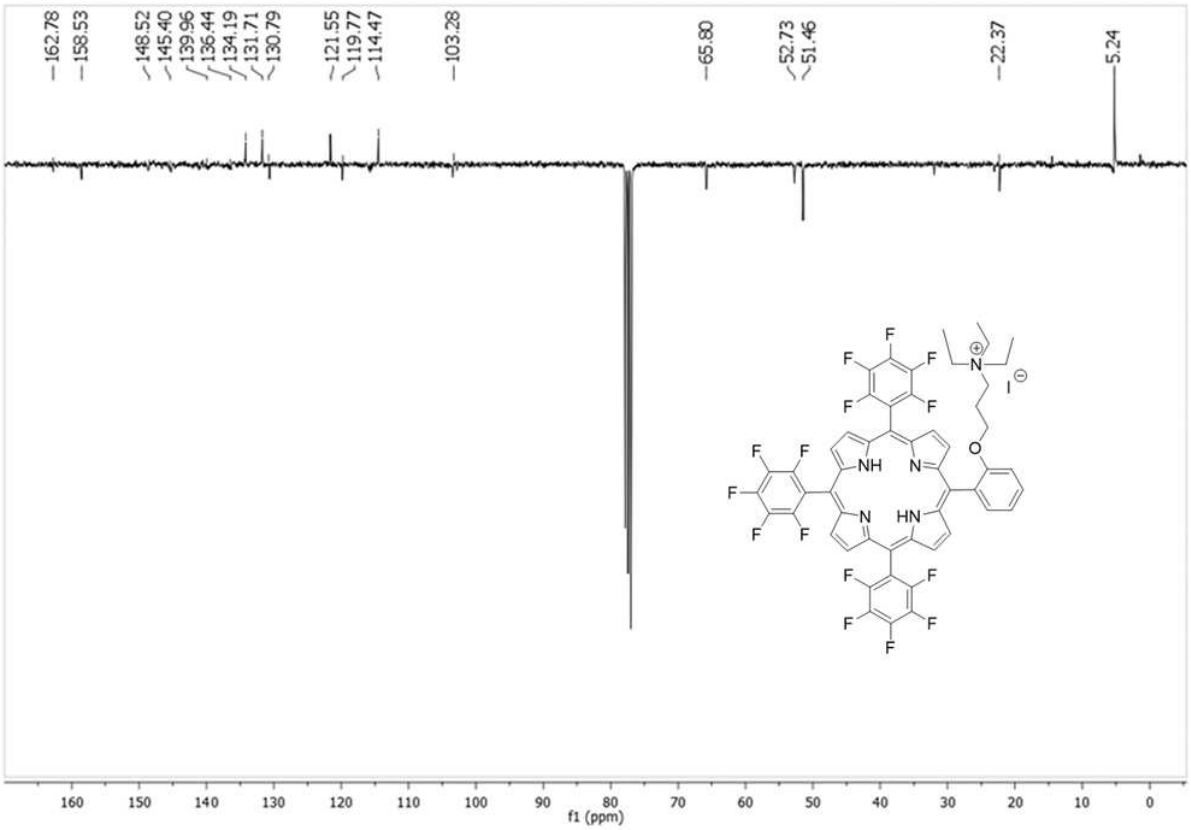

Figure 9. ^{19}F NMR spectrum (376 MHz, $CDCl_3$, 298 K) of porphyrin **3**

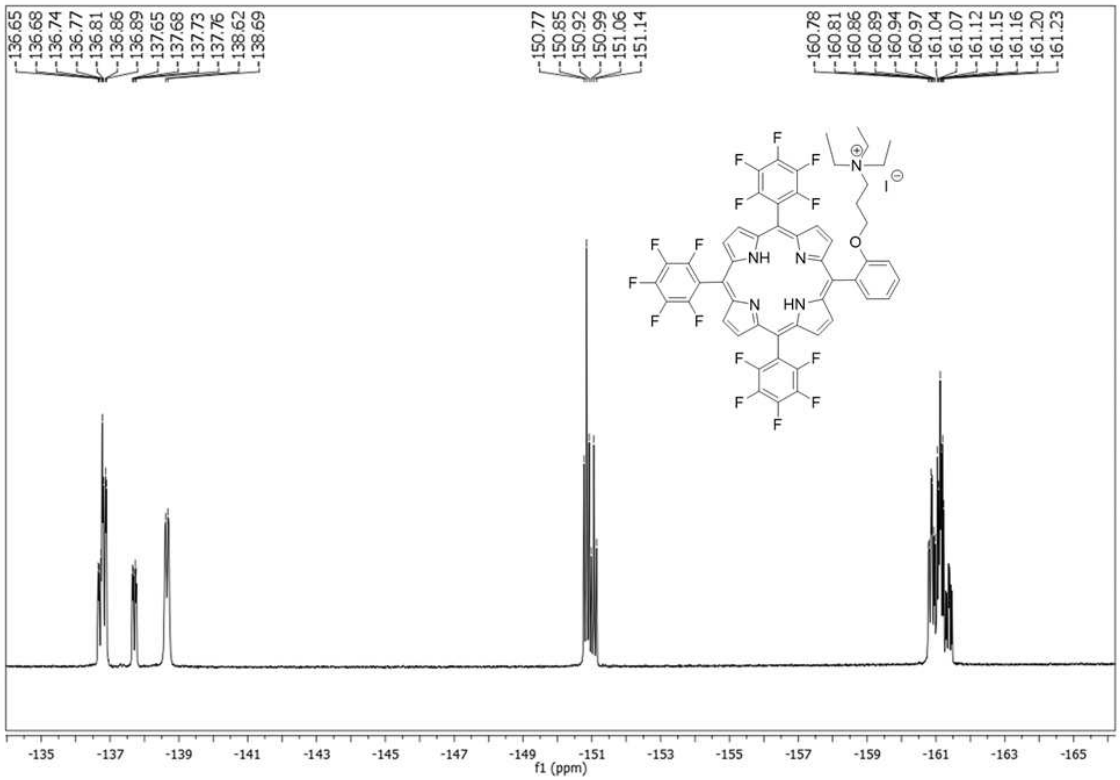

Figure 10. ^{1}H NMR spectrum (400 MHz, $CDCl_3$, 298 K) of porphyrin Zn(**2**)

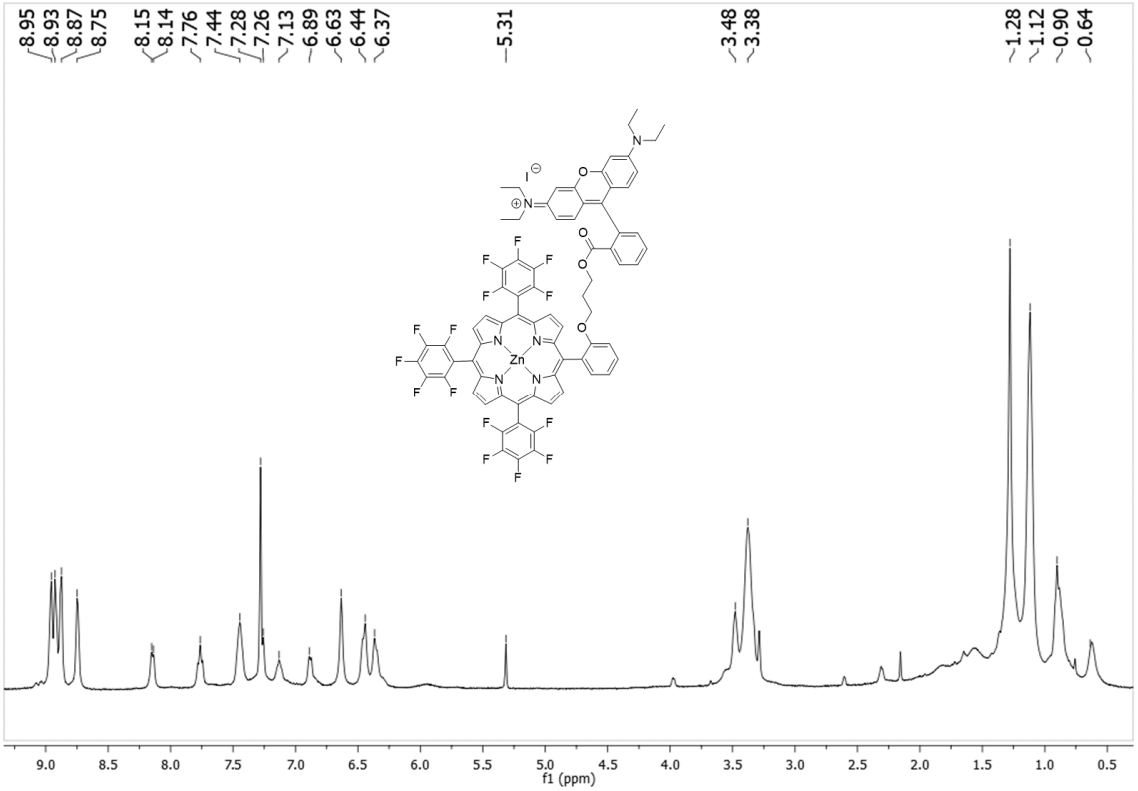

Figure 11. ^{13}C NMR spectrum (100 MHz, $CDCl_3$, 298 K) of porphyrin Zn(**2**)

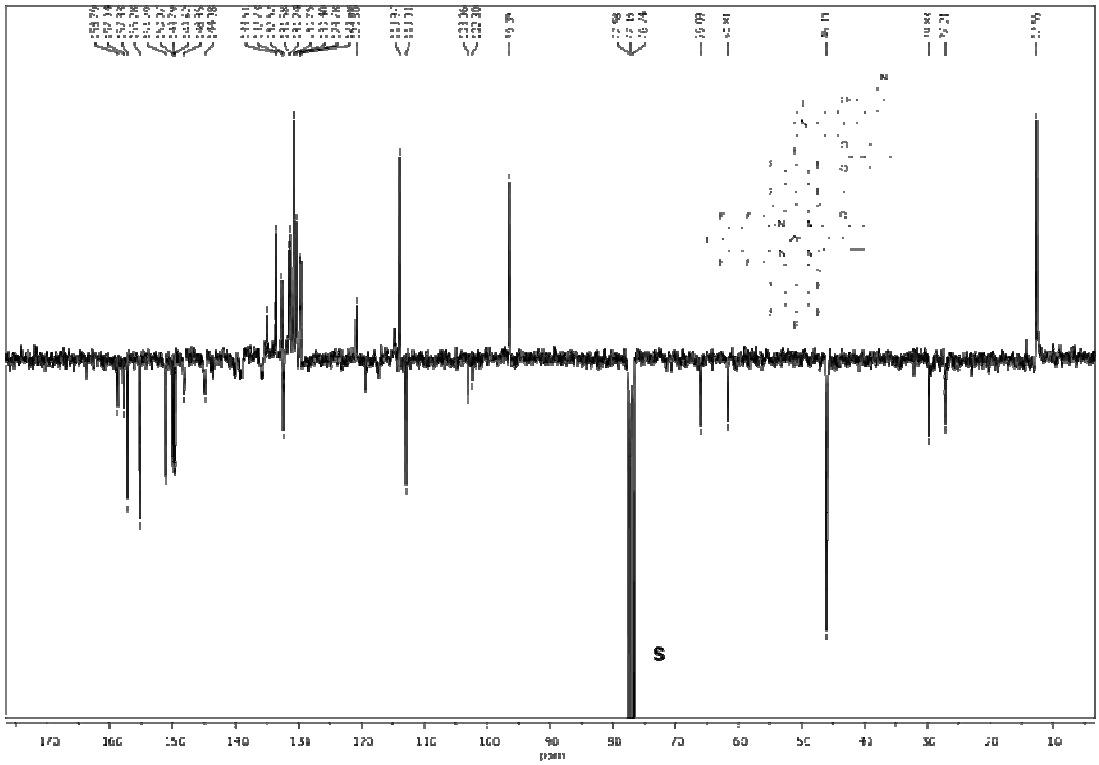

Figure 12. ^{19}F NMR spectrum (376 MHz, $CDCl_3$, 298 K) of porphyrin Zn(**2**)

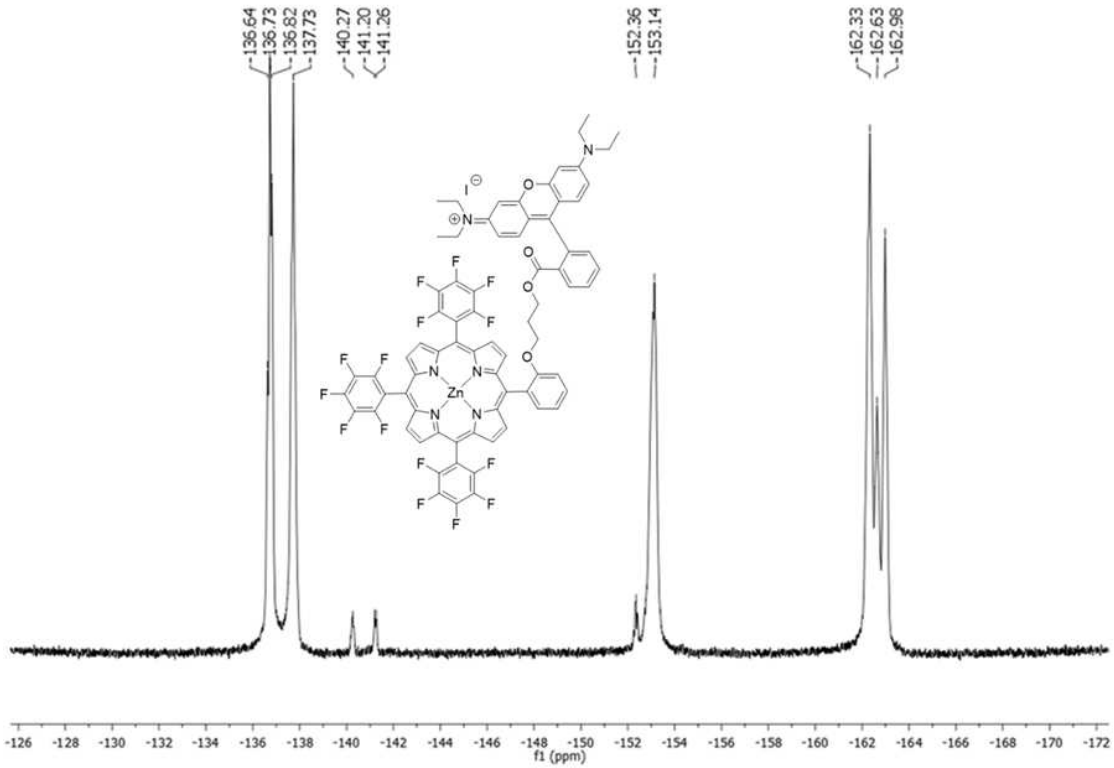

4. UV-Vis spectra

Figure 13. UV-vis spectra of **1**, **2**, **3**, Zn(**2**) and Rhodamine B in MeOH.

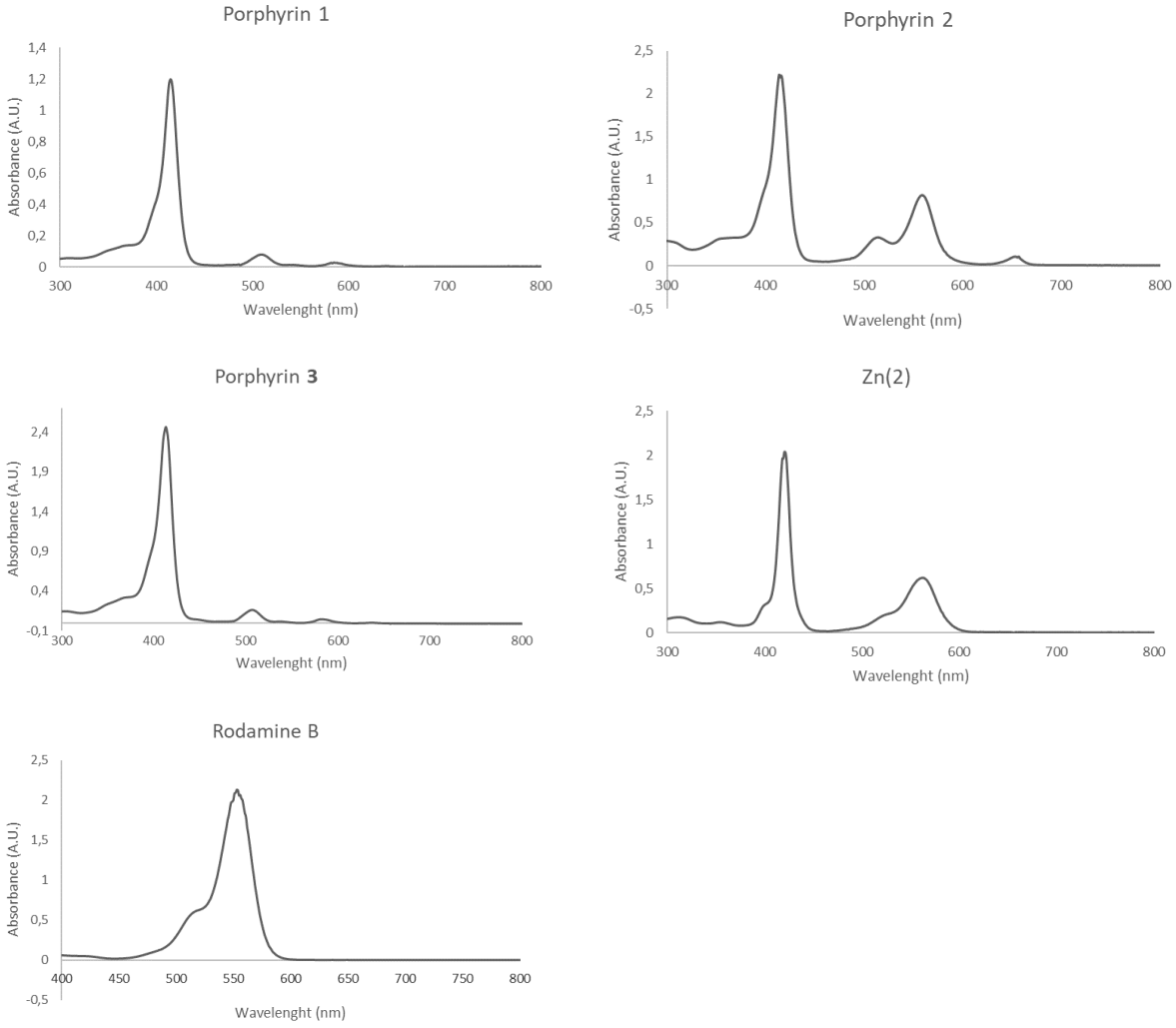

5. UV-Vis binding tests

Binding constant measurements were carried out on a Cary 100 Spectrophotometer at 298.0 (± 0.5) °C by adding consecutive aliquots of a (DCF)Na solution (1.00 mM) to 2.0 mL of 1:1 MeOH/H_2O (v:v) receptor (**2** or Zn(**2**)) solution (10.0 μM). The corresponding spectra was acquired after every (DCF)Na addition. The (DCF)Na solution was prepared by dissolving the required amount of salt into 10.0 mL of 10.0 μM porphyrin solution, in order to keep the concentration of the receptor to a constant value throughout the titration. The absorbance values at 419 nm were plotted against (DCF)Na concentration and acquired data fitted to Equation 1[8] for a 1:1 molecular complex formation by using a non-linear regression fit program (KaleidaGraph ® 4.1 Synergy Software). Experiments were performed in duplicate and obtained results showed a very good reproducibility. The same procedure was followed in the presence of sodium phenylacetate, sodium salicylate, L tyrosine sodium salt, sodium sarcosinate, L-alanine sodium salt as well as for Fluorescence and Resonance Light Scattering (RLS) studies.

Equation 1

$$\frac{A_0 - A}{A - A_\infty} = \frac{[S]_t + [L]_n + 1/K_{binding} - \sqrt{([S]_t + [L]_n + 1/K_{binding})^2 - 4[S]_t[L]_n}}{2[S]_t}$$

Figure 14. UV-vis binding test with porphyrin **2**

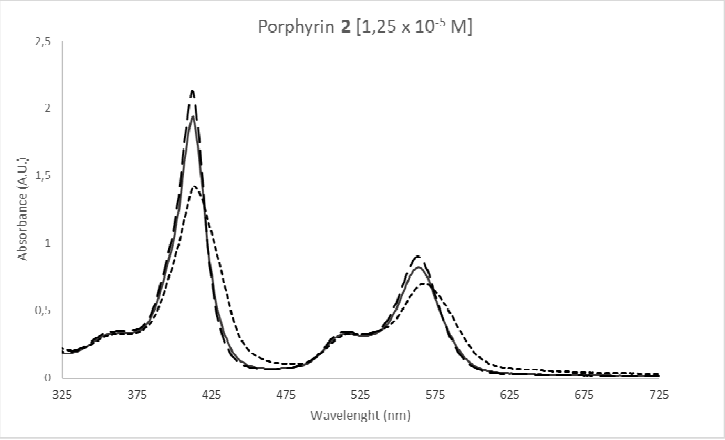

Figure 15. UV-vis binding test with porphyrin Zn(**2**)

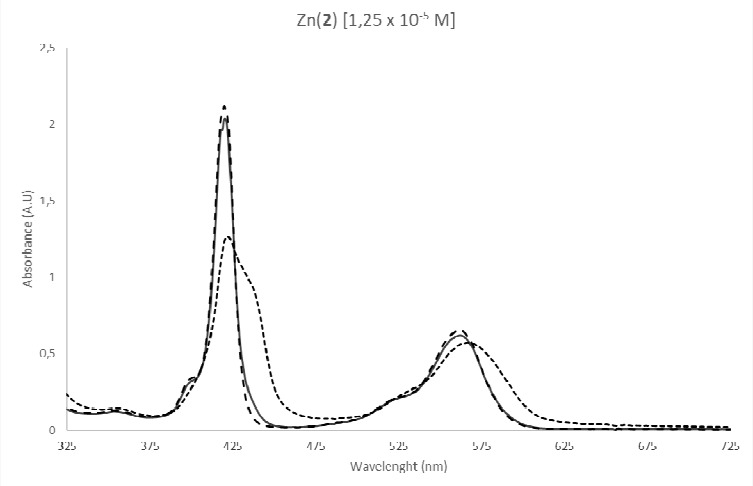

Figure 16. UV-Vis spectral pattern variation of **2** (10 μM; MeOH/H_2O 1:1 v:v) upon addition of (DCF)Na and equimolar amount of sodium salicylate (SalONa).

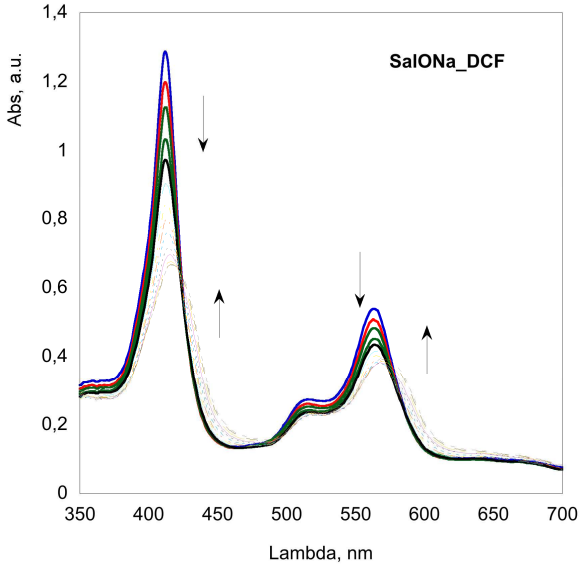

Figure 17. Non-linear regression fit, and calculated binding constant value (Langmuir type equation, see above) for the **2@DCF** formation in the presence of equimolar amount of sodium salicylate.

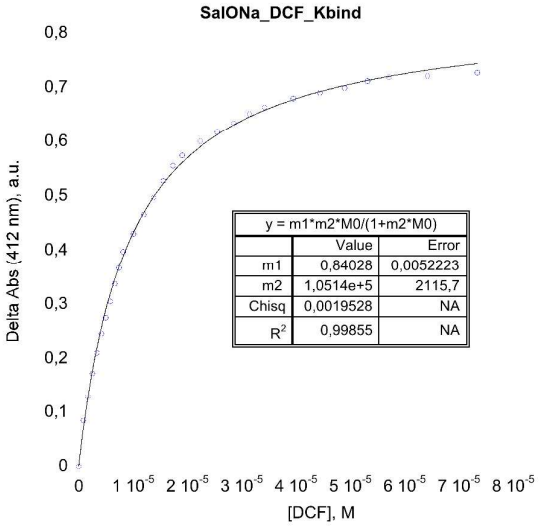

6. Fluorescence experiments

Figure 18. Fluorescence emission spectrum of **2** at λ_{exc} = 412 nm.

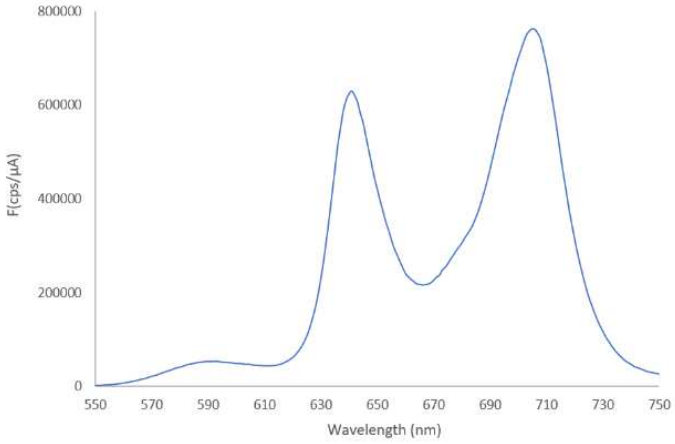

Figure 19. Fluorescence excitation spectrum of **2** at λ_{em}=590 nm (Rhodamine emission)

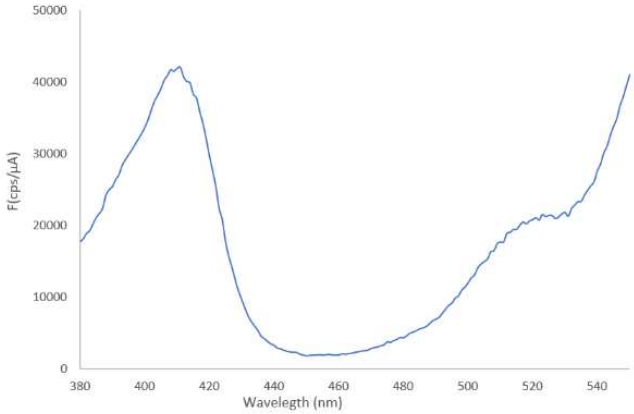

Figure 20. Fluorescence excitation spectrum of **2** at λ_{em}=705 nm (Porphyrin emission)

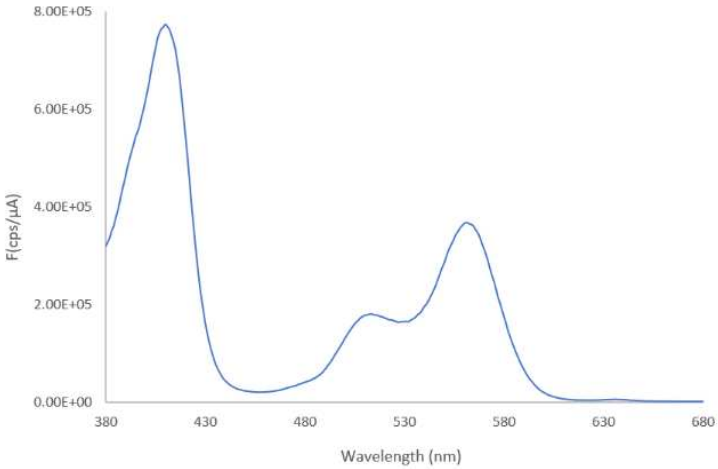

Figure 21. Fluorescence emission spectra of **2** for increasing concentrations of DCF. **A**: λ_{ex}=412 nm (Porphyrin absorption); **B**: λ_{ex}=555 nm (Rhodamine preferential absorption).

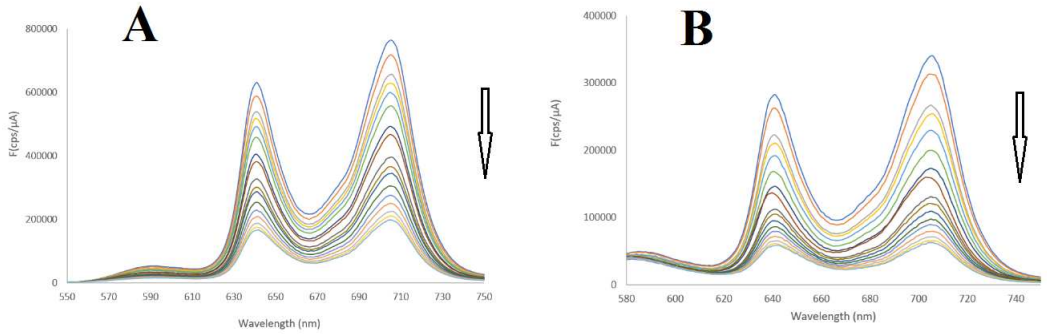

Figure 22. **2**/DCF binding isotherm from fluorescence intensities of **2** for different (DCF)Na concentrations. The analogous of Equation 1 was applied.

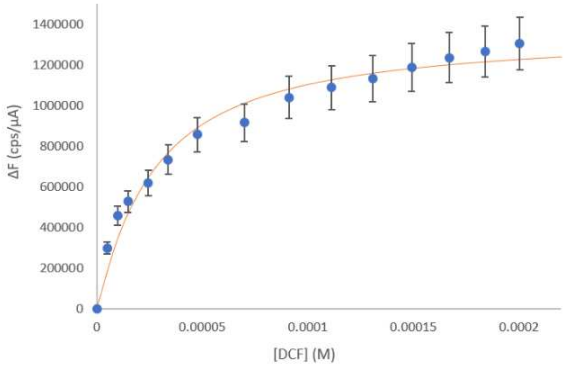

Figure 23. Fluorescence time decays of **2** for different **2**/DCF concentration ratios (λ_{ex}=342 nm; λ_{em}=645 nm).

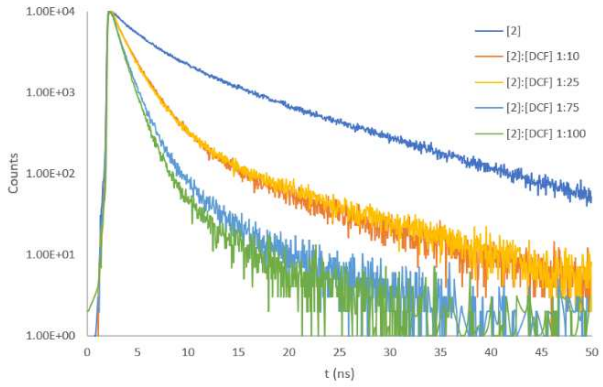

Table 1. Time decay parameters of **2** (porphyrin emission) for different **2**/DCF concentration ratios (λ_{ex}=342 nm; λ_{em}=645 nm).

[2]:[DCF]	τ_1 (ns)	α_1	τ_2 (ns)	α_2	τ_3 (ns)	α_3	<τ> (ns)	χ^2
1:0	11.6	0.38	3.45	0.46	1.0	0.17	6.3	1.303
1:10	10.2	0.02	2.2	0.52	0.95	0.46	1.8	1.154
1:25	10.0	0.03	2.1	0.48	0.88	0.49	1.7	1.031
1:75	6.1	0.01	1.5	0.41	0.72	0.58	1.1	1.052
1:100	5.0	0.01	1.2	0.50	0.64	0.49	1.0	0.913

7. X-ray single-crystal structure determination.

Crystal data for **3** are reported in Table 2. All hydrogen atoms of porphyrin molecule, except the H atoms of methyl groups, were located from the difference Fourier map and refined freely with isotropic displacement *parameters*. Methyl hydrogens and H-atoms of the guest molecule (*n*-hexane) were placed in geometrically calculated positions and included in the refinement using a riding model in conjunction with a $U_{iso}(H) = 1.2 U_{eq}(CH_2, CH)$ or $1.5U_{eq}(CH_3)$ constraint. All non-hydrogen atoms were *refined with* full occupancy and *anisotropic displacement parameters* except for hexane carbon atoms. ISOR instruction was used for F2 atom as otherwise it went non-positive definite. The solvate hexane molecule was find to be disordered and refined isotropically over two positions using a suitable model (49.7, 50.1%). Geometry constraints (SADI) were used to keep reasonable bond distances.

Table 2. Crystal data and structure refinement for **3**.

Chemical formula	$[C_{53}H_{35}F_{15}N_5O]I\cdot 0.5(C_6H_{14})$
Empirical formula	$C_{56}\ H_{42}\ F_{15}\ I\ N_5\ O$
Formula weight ($g\cdot mol^{-1}$)	1212.85
Temperature (K)	150(2)
Wavelength (Å)	0.71073
Crystal system	Triclinic
Space group	*P* -1
a / Å	11.465(3)
b / Å	15.353(4)
c / Å	16.170(5)
α (deg)	103.382(3)
β (deg)	90.662(3)
γ (deg)	106.684(3)
V / $Å^3$	14687(2)
Z	12
$D_{calc.}$ ($g\cdot cm^{-3}$)	1.524
μ (mm^{-1})	0.704
θ range for data collection (deg)	1.3 to 25.0
Index ranges	-13<=h<=13, -18<=k<=18, -19<=l<=19
Reflections collected	23475
Independent reflections	9334 [R(int) = 0.0383]
Completeness to theta	99.9 %
Data/restraints/parameters	9334 / 21 / 775
F(000)	1218
Goodness-of-fit on F^2	1.039
Final *R* indices [I>2sigma(I)]	$R_1 = 0.0580$, w$R_2 = 0.1461$
R indices (all data)	$R_1 = 0.0855$, w$R_2 = 0.1719$
$\Delta\rho$ max,min ($e\cdot Å^{-3}$)	2.432 and -0.775

Table 3. Selected bond lengths [Å] and angles [°] for **3**.

N(1)-C(1)	1.365(6)	N(1)-C(4)-C(5)	125.7(5)
N(1)-C(4)	1.365(7)	N(1)-C(4)-C(3)	109.6(5)
N(2)-C(6)	1.362(7)	C(5)-C(4)-C(3)	124.6(5)
N(2)-C(9)	1.363(7)	C(4)-C(5)-C(6)	126.8(5)
N(3)-C(14)	1.364(6)	C(4)-C(5)-C(21)	117.4(5)
N(3)-C(11)	1.370(6)	C(6)-C(5)-C(21)	115.6(5)
N(4)-C(16)	1.364(7)	N(2)-C(6)-C(5)	125.5(5)
N(4)-C(19)	1.372(6)	N(2)-C(6)-C(7)	107.5(5)
C(1)-C(20)	1.401(7)	C(5)-C(6)-C(7)	126.9(5)
C(1)-C(2)	1.443(8)	C(8)-C(7)-C(6)	108.0(5)
C(2)-C(3)	1.330(8)	C(7)-C(8)-C(9)	107.8(5)
C(3)-C(4)	1.445(8)	N(2)-C(9)-C(10)	126.6(4)
C(4)-C(5)	1.383(8)	N(2)-C(9)-C(8)	107.2(5)
C(5)-C(6)	1.396(8)	C(10)-C(9)-C(8)	126.2(5)
C(5)-C(21)	1.504(7)	C(9)-C(10)-C(11)	124.7(5)
C(6)-C(7)	1.421(8)	C(9)-C(10)-C(27)	117.5(4)
C(7)-C(8)	1.349(8)	C(11)-C(10)-C(27)	117.5(5)
C(8)-C(9)	1.428(7)	N(3)-C(11)-C(10)	126.0(5)
C(9)-C(10)	1.396(7)	N(3)-C(11)-C(12)	109.8(4)
C(10)-C(11)	1.398(7)	C(10)-C(11)-C(12)	124.1(5)
C(10)-C(27)	1.489(7)	C(13)-C(12)-C(11)	107.3(5)
C(11)-C(12)	1.442(8)	C(12)-C(13)-C(14)	106.7(5)
C(12)-C(13)	1.340(8)	N(3)-C(14)-C(15)	125.2(5)
C(13)-C(14)	1.446(7)	N(3)-C(14)-C(13)	110.1(4)
C(14)-C(15)	1.398(7)	C(15)-C(14)-C(13)	124.6(5)
C(15)-C(16)	1.392(7)	C(16)-C(15)-C(14)	126.9(5)
C(15)-C(33)	1.499(7)	C(16)-C(15)-C(33)	116.5(4)
C(16)-C(17)	1.430(7)	C(14)-C(15)-C(33)	116.6(5)
C(17)-C(18)	1.347(8)	N(4)-C(16)-C(15)	125.3(5)
C(18)-C(19)	1.433(7)	N(4)-C(16)-C(17)	108.0(4)
C(19)-C(20)	1.391(7)	C(15)-C(16)-C(17)	126.7(5)
C(20)-C(39)	1.497(7)	C(18)-C(17)-C(16)	107.6(5)
C(32)-O(1)	1.377(7)	C(17)-C(18)-C(19)	108.2(5)
N(1S)-C(3B)	1.505(8)	N(4)-C(19)-C(20)	125.8(4)
N(1S)-C(4B)	1.507(8)	N(4)-C(19)-C(18)	107.3(4)
N(1S)-C(8B)	1.508(7)	C(20)-C(19)-C(18)	126.9(5)
N(1S)-C(6B)	1.522(7)	C(19)-C(20)-C(1)	126.1(5)
O(1)-C(1B)	1.425(9)	C(19)-C(20)-C(39)	116.8(4)
C(1B)-C(2B)	1.521(9)	C(1)-C(20)-C(39)	117.1(5)
C(2B)-C(3B)	1.522(9)	O(1)-C(32)-C(31)	119.7(5)
C(4B)-C(5B)	1.521(9)	O(1)-C(32)-C(27)	119.6(5)
C(6B)-C(7B)	1.505(10)	C(3B)-N(1S)-C(4B)	111.5(5)
C(8B)-C(9B)	1.525(9)	C(3B)-N(1S)-C(8B)	106.3(4)
		C(4B)-N(1S)-C(8B)	111.6(5)
		C(3B)-N(1S)-C(6B)	110.3(5)
C(1)-N(1)-C(4)	105.8(4)	C(4B)-N(1S)-C(6B)	106.3(4)
C(6)-N(2)-C(9)	109.4(4)	C(8B)-N(1S)-C(6B)	110.8(5)
C(14)-N(3)-C(11)	106.0(4)	C(32)-O(1)-C(1B)	116.0(5)
C(16)-N(4)-C(19)	108.9(4)	O(1)-C(1B)-C(2B)	106.9(6)
N(1)-C(1)-C(20)	125.2(5)	C(1B)-C(2B)-C(3B)	109.0(5)
N(1)-C(1)-C(2)	110.5(4)	N(1S)-C(3B)-C(2B)	115.3(5)
C(20)-C(1)-C(2)	124.3(5)	N(1S)-C(4B)-C(5B)	114.5(5)
C(3)-C(2)-C(1)	106.5(5)	C(7B)-C(6B)-N(1S)	114.2(5)
C(2)-C(3)-C(4)	107.6(5)	N(1S)-C(8B)-C(9B)	115.3(5)

Table 4. Hydrogen-bond geometry for **3** (Å, °)

Donor- H···Acceptor	*D* - H	H···A	*D*···A	*D* - H···A
N2-H2N···N1	0.70(9)	2.48(9)	2.913(7)	123(9)
N2-H2N···N3	0.70(9)	2.43(9)	2.897(7)	126(8)
N4-H4N···N1	0.75(9)	2.49(9)	2.895(7)	116(8)
N4-H4N···N3	0.75(9)	2.36(8)	2.905(6)	131(8)

8. Conformational analysis.

The porphyrin **3** adopts a "close" conformation in which the amino-alkyl side arm is folded toward the core of the macrocycle, with the terminal methyl groups of the pendant triethylammonium moiety pointing toward the pyrrole rings (I, II, IV). The lateral displacement of the side arm from the porphyrin centroid is generated by a gauche/anti/anti/anti(N)/anti conformation sequence along the main chain.

The porphyrin core is quasi-planar with an average deviation of the macrocycle atoms from their least squares plane (Δ24, Table 5) of only 0.065 Å. The larger deviations are associated with the *meso*-carbon (C_m) C10 (0.106(5) Å) bonded to the para substituted aryl group and with the C_β of the neighbouring pyrrole rings (-0.089(6)-0.172(6) Å). Likewise, the C_α-C_m-C_α angle between the α-pyrrolic and *meso* carbons varies only slightly (Table 5) with the smallest value and the bigger deviation at *meso*-C10 position again (124.7(5)°).

The overall slightly distortion results essentially in a *saddle* shaped conformation characterized by an alternating displacement of the pyrrole rings N(I), (III) and (IV) below and above the mean plane (Figure 24).[9] A closer look of the out-of-plane distortion pattern suggests a small contribute from *wave* conformation involving the pyrrolic unit N(II) (toward which the side arm of porphyrin is bent).[10] The minor deformation from planarity of porphyrin macrocycle and the different role of the pyrrolic units is also reflected by the values of the dihedral angle between the pyrrole rings and the N_4-core mean plane (Table 5).

All the conformational data seem indicate that the small distortions observed for the macrocycle are essentially due to the presence and orientation of the "long" alkyl chain on the para position of a *meso*-aryl group. Despite the asymmetric substituent arrangement, the inner cavity shape composed by the four N atoms is square-like as indicated by the core elongation factor (Ξ = 0.013 Å) and by the distances between the neighbouring N-N atoms (2.895(7) – 2.913(7) Å). The N-H groups are involved in bifurcated N-H···(N,N) intramolecular hydrogen bonds (Table 4) and result only slightly tilted out of the plane of macrocycle.

Table 5. Selected conformational parameters for **3** (deviations and distances in Å, angles in °)

Core size ⊗[a]	2.053	C_α-C_{15}-C_α	126.9(5)
Core elongation Ξ[b]	0.013	C_α-C_{20}-C_α	126.1(5)
Δ24[c]	0.065	*cis* C_α-N···N-C_α[g]	4.2
N1···N2	2.913(7)	*trans* C_α-N···N-C_α	177.1
N2···N3	2.897(7)	φ_{pyr}N1[h]	1.89
N3···N4	2.905(6)	φ_{pyr}N2	7.24
N4···N1	2.895(7)	φ_{pyr}N3	3.18
δC_m[d]	0.074	φ_{pyr}N4	0.93
δC_α[e]	0.051	φ_{ar}C5[i]	87.05
δC_β[f]	0.102	φ_{ar}C10	87.87
C_α-C_5-C_α	126.8(5)	φ_{ar}C15	82.98
C_α-C_{10}-C_α	124.7(5)	φ_{ar}C20	81.15

C_m (*meso* carbon) = 5, 10, 15, 20; C_β (*β-pyrrole* position) = 2, 3, 7, 8, 12, 13, 17, 18; C_α (*α-pyrrole* position) = 1, 4, 6, 9, 11, 14, 16, 19. [a]The core size is defined as the geometrical centre of the four nitrogen atoms. [b]The core elongation parameter is defined as the difference between the vector lengths (|N1-N2|+|N3-N4|)/2 - (|N2-N3|+|N1-N4|)/2. [c]Deviation of the 24 macrocycle atoms from their least squares plane. [d]Average deviation of the C_m carbon atoms from the 4N plane. [e]Average deviation of the C_α atoms from the 4N plane. [f]Average deviation of the C_β atoms from the 4N plane. [g]Cis C_α –N–N– C_α dihedral angles.[11] [h]Pyrrole tilt angle with the 4N plane. [i]Phenyl tilt angle against the 4N plane.

Figure 24. Linear display of the skeletal deviations (in units of 0.001 Å) of the macrocycle atoms from the mean porphyrin plane (of 24 atom).[10] The *x* axis is not to scale.

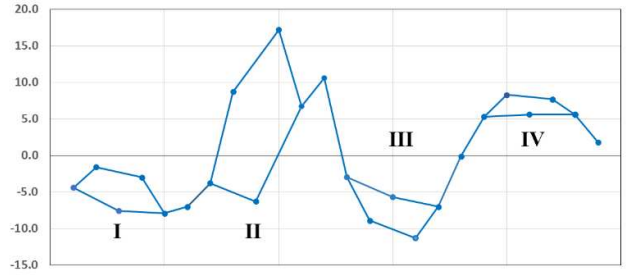

References

[1] T. A. D. Pinto, R. Hrdina, G. Kirsch, A. M. F. Oliveira-Campos, L. M. Rodrigues and A. P. Esteves, ARKIVOC 2012, **6**, 185-193

[2]H. G. Brittain, *Cryst. Growth Des*., 2010, **10**, 1990-2003

[3] Bruker, *SAINT+*, 2007, Bruker AXS Inc., Madison, Wisconsin, USA.

[4] Bruker, APEX II, 2009, Bruker AXS Inc., Madison, Wisconsin, USA.

[5] M. C. Burla, R. Caliandro, M. Camalli, B. Carrozzini, G. L. Cascarano, L. De Caro, C. Giacovazzo, G. Polidori and R. Spagna, *J. Appl. Crystallogr.*, 2005, **38**, 381-388.

[6] G. M. Sheldrick, *Acta Crystallogr. Sect. C Struct. Chem.*, 2015, **71**, 3-8.

[7] L. J. Farrugia, *J. Appl. Crystallogr.*, 2012, **45**, 849-854.

[8] K. A. Connors: *Binding constants — the measurement of molecular complex stability*, John Wiley & Sons, New York 1987, 91, 1398-1398.

[9] M. Gruden, S. Grubišić, A. G. Coutsolelos and S. R. Niketić, *J. Mol. Struct.*, 2001, **595**, 209–224.

[10] a) W. Jentzen, X.-Z. Song and J. A. Shelnutt, *J. Phys. Chem. B*, 1997, **101**, 1684-1699; b) W. Jentzen, J.-G. Ma and J. A. Shelnutt, *Biophys. J.*, 1998, **74**, 753-763.

[11] A. Fidalgo-Marijuan, G. Barandika, B. Bazán, M.-K. Urtiaga and M. I. Arriortua, *CrystEngComm*, 2013, **15**, 4181.

Electronic Supplementary Information

Sensing of Diclofenac by a Porphyrin-based Artificial Receptor

Daniela Intrieri,[a] Caterina Damiano,[a] Silvia Rizzato,[a] Roberto Paolesse,[b] Mariano Venanzi,[b] Donato Monti,*[b] Marco Savioli[b], Manuela Stefanelli[b] and Emma Gallo.*[a]

[a]*Department of Chemistry, University of Milan, Via C. Golgi 19, 20133 Milan (Italy). E-mail: emma.gallo@unimi.it.*

[b]*Department of Chemical Science and Technologies, University of Roma Tor Vergata, Via della Ricerca Scientifica, 00133 Rome (Italy). E-mail: dmonti@uniroma2.it*

1. General

Unless otherwise specified, all the reactions were carried out under a nitrogen atmosphere by employing standard Schlenk techniques and magnetic stirring. Dichloromethane, chloroform, *N*,*N*-dimethylformamide and pyrrole were distilled over CaH_2 and stored under nitrogen. Acetone was distilled over K_2CO_3 and stored under nitrogen. All the other starting materials and Zn(TPP) were commercial products which were used as received. 2-(3-Bromopropoxy)benzaldehyde[1] and sodium phenylacetate[2] were synthesized by methods reported in the literature or by using minor modifications of them. Solvents used for spectroscopy investigations were of Spectroscopic Grade of the highest degree of purity available and used as received. NMR spectra were recorded at room temperature on a Bruker Avance 400-DRX spectrometers, operating at 400 MHz for ^{1}H, at 100 MHz for ^{13}C and at 376 MHz for ^{19}F. Chemical shifts (ppm) are reported relative to TMS. The ^{1}H NMR signals of the compounds described in the following have been attributed by COSY and NOESY techniques. Assignments of the resonance in ^{13}C NMR were made using the APT pulse sequence and HSQC and HMBC techniques. UV/Vis spectra were recorded on an Agilent 8453E instrument. Elemental analyses and mass spectra were recorded in the analytical laboratories of Milan University. All spectroscopic studies were carried out at 298.0 (± 0.5) K (Julabo F25 Thermostat). Steady-state Fluorescence and Resonance Light Scattering Spectroscopy studies were carried out on Fluoromax 4 (Horiba Instruments). Time-resolved Fluorescence Spectroscopy studies were carried out on LifeSpoec–ps (Edimburg Instruments), equipped with a Hamamatsu Photonics K.K. laser. X-ray data collection was performed at 150 K using graphite-monochromated Mo Kα radiation (λ = 0.71073 Å) on a Bruker ApexII CCD area-detector diffractometer equipped with an Oxford Cryosystems N_2 gas blower. A ω-scan was performed within the Bragg limits of $1.3 < \theta < 25.0°$. Determination of the integrated intensities and unit cell refinements were performed using SAINT[3] and all absorption corrections were applied by using SADABS.[4] The structures were solved by direct methods (SIR2014)[5] and refined by full-matrix least squares on F^2 (SHELX 2014)[6] with the WINGX interface.[7]

2. Synthetic procedures

2.1. Synthesis of 1.

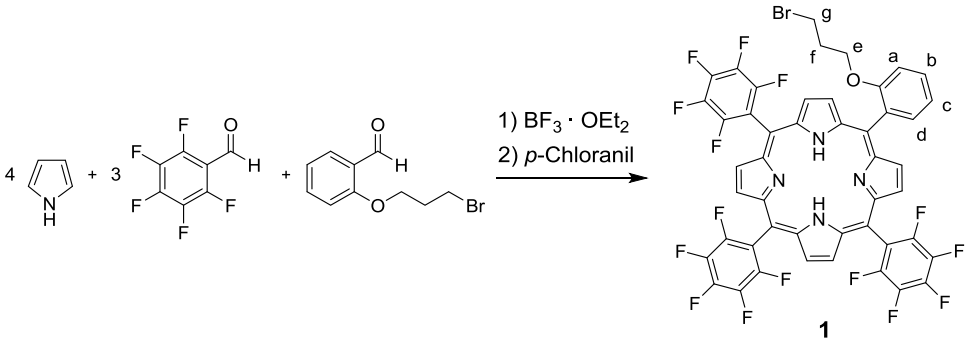

Freshly distilled pyrrole (173 μL, 2.50 mmol), pentafluorobenzaldehyde (231 μL, 1.87 mmol) and 2-(3-bromopropoxy)benzaldehyde (110 μL, 0.62 mmol) were dissolved in dry dichloromethane (250 mL) in a 500 mL two necks round-bottom flask. The reaction mixture was shielded from ambient light and $BF_3{\cdot}OEt_2$ (31 μL, 0.25 mmol) was added dropwise by a syringe. The obtained pale orange solution was stirred in the dark for 3 hours at room temperature and then tetrachloro-1,4-benzoquinone (*p*-chloranil) (0.615 g, 2.50 mmol) was added. The resulting solution was refluxed in air for 6 hours, the solvent evaporated to dryness under reduced pressure and the resulting black solid purified by flash column chromatography on silica gel (60 μm, eluent *n*-hexane/dichloromethane = 90:10) yielding **1** (20% yield) as a purple solid. Elemental Analysis calc. for $C_{47}H_{20}BrF_{15}N_4O$: C, 55.26; H, 1.97; N, 5.48; found: C, 55.66; H, 2.11; N, 5.31. UV-Vis, λ_{max} (MeOH)/nm (log ε_M): 410 (5.39), 506 (4.47), 536 (3.61), 582 (3.98), 643 (3.15). LR-MS (ESI): m/z ($C_{47}H_{20}BrF_{15}N_4O$ $[M+H]^+$) calcd. 1020.06; found 1021.2. ^{1}H NMR (400 MHz, $CDCl_3$, 298 K) δ: 8.97 (d, J = 4.7 Hz, 2H, $H_{\beta pyrr}$), 8.91 (s, 4H, $H_{\beta pyrr}$), 8.84 (d, J = 4.7 Hz, 2H, $H_{\beta pyrr}$), 8.08 (dd, J_o = 7.4 Hz, J_m = 1.5 Hz, 1H, H_d), 7.83 (t, J = 8.1 Hz, 1H, H_b), 7.44 (t, J = 7.6 Hz, 1H, H_c), 7.38 (d, J = 8.1 Hz, 1H, H_a), 4.10 (t, J = 5.4 Hz, 2H, H_e),

2.26 (t, J = 6.0 Hz, 2H, H_g), 1.46 (m, 2H, H_f), -2.81 (s, 2H, NH_{pyrr}). ^{13}C NMR (100 MHz, $CDCl_3$, 298 K) δ: 158.3, 147.8, 145.4, 143.4, 140.9, 138.8, 136.3, 135.6, 130.6, 129.8 (2 signals overlapped), 119.9, 119.4, 116.0, 117.7, 102.8, 101.9, 65.1, 31.3, 29.8. Six quaternary carbon atoms were not detected. ^{19}F NMR (376 MHz, $CDCl_3$, 298 K) δ: -136.9, -152.1, -162.0.

2.2. Synthesis of 2.

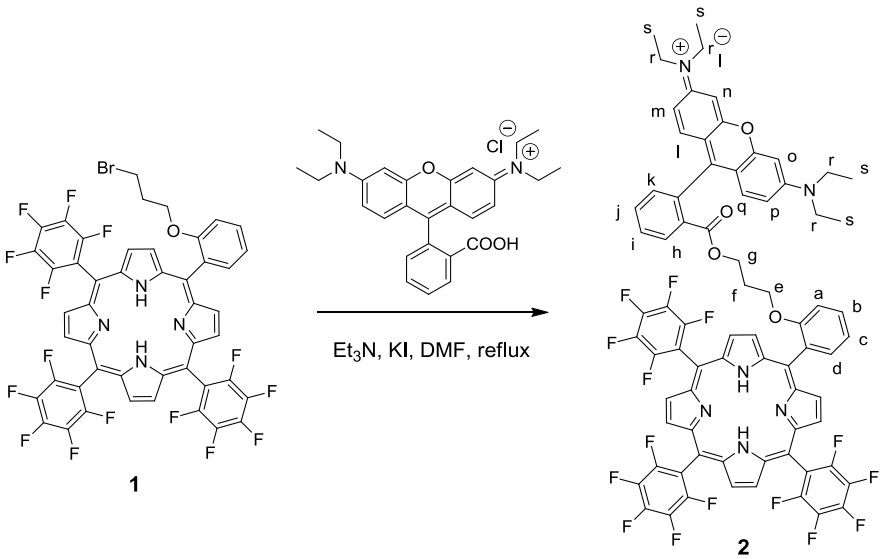

1 **2**

Rhodamine B (0.200 g, 0.418 mmol), triethylamine (58.0 μL, 0.418 mmol) and KI (0.069 g, 0.418 mmol) were added to a dry DMF (25 mL) solution of **1** (0.171 g, 0.167 mmol). The dark purple mixture was refluxed under stirring for 10 hours, then the solvent was evaporated to dryness under reduced pressure and the residue purified by flash column chromatography on silica gel (60 μm, eluent: gradient, from dichloromethane to 3% methanol in dichloromethane) yielding **2** (45% yield) as a dark purple solid (which resulted pink in solution). Elemental Analysis calc. for $C_{75}H_{50}F_{15}IN_6O_4$: C, 59.61; H, 3.34; N, 5.56; found: C, 59.93; H, 3.13; N, 5.83. UV-Vis, λ_{max} (MeOH)/nm (log ε_M): 412 (5.67), 512 (4.82), 559 (5.24), 638 (3.18). LR-MS (ESI): m/z ($C_{75}H_{50}F_{15}N_6O_4^+$ $[M]^+$) calcd. 1383.36; found 1383.6. ^{1}H NMR (400 MHz, $CDCl_3$, 298 K) δ: 8.87 (m, 6H, $H_{\beta pyrr}$), 8.73 (d, J = 4.3 Hz, 2H, $H_{\beta pyrr}$), 8.00 (dd, J_o = 7.4 Hz, J_m = 1.6 Hz, 1H, H_d), 7.78 (m, 2H, H_b and H_h), 7.63 (m, 1H, H_j), 7.40 (t, J = 7.4 Hz, 2H, H_c and H_i), 7.31 (m, 1H, H_a), 7.14 (m, 1H, H_k), 6.83 (d, J = 9.9 Hz, 2H, H_l and H_q), 6.64 (m, 4H, H_m, H_n, H_o and H_p), 3.87 (t, J = 5.5 Hz, 2H, H_e), 3.43 (m, 8H, H_r), 3.17 (t, J = 6.1 Hz, 2H, H_g), 1.13 (m, 14H, H_f and H_s), -2.84 (s, 2H, NH_{pyrr}). ^{13}C NMR (100 MHz, $CDCl_3$, 298 K) δ: 164.4, 158.6, 158.1, 157.5, 155.3, 147.8, 145.3, 143.4, 140.9, 138.8, 135.8, 133.2, 132.9, 131.3, 131.1, 131.0, 130.9, 130.1, 129.62, 129.56, 120.0, 119.4, 116.3, 114.2, 113.3, 112.0, 102.7, 96.3, 64.6, 61.9, 46.1, 43.5, 41.3, 36.0, 29.1 27.8, 12.5. ^{19}F NMR (376 MHz, $CDCl_3$, 298 K) δ: -137.0, -140.38, -140.89, -152.0, -161.8.

2.3. Synthesis of 3.

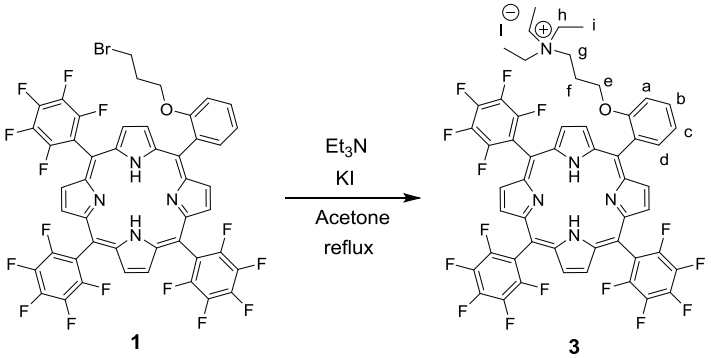

1 **3**

Triethylamine (0.172 mL, 1.24 mmol) and KI (0.207 g, 1.24 mmol) were added to a dry acetone (15 mL) solution of **1** (0.127 g, 0.124 mmol). The dark brown mixture was refluxed under stirring for 6 hours, then

the solvent evaporated to dryness under reduced pressure and the resulting solid purified by flash column chromatography on silica gel (60 μm, eluent: gradient, from dichloromethane to 3% methanol in dichloromethane) yielding **3** (55% yield) as a dark red solid. Elemental Analysis calc. for $C_{53}H_{35}F_{15}IN_5O$: C, 54.42; H, 3.02; N, 5.99; found: C, 54.23; H, 3.11; N, 6.06. UV-Vis, λ_{max} (CH_2Cl_2)/nm (log ε_M): 413 (5.49), 507 (4.28), 536 (3.47), 583 (3.80), 636 (3.14). λ_{max} (MeOH)/nm (log ε_M): 409 (5.49), 505 (4.27), 535 (3.39), 580 (3.76), 635 (2.96). LR-MS (ESI): m/z ($C_{53}H_{35}F_{15}N_5O^+$ $[M]^+$) calcd. 1042.26; found 1042.4. ^{1}H NMR (400 MHz, $CDCl_3$, 298 K) δ: 8.96 (m, , 6H, $H_{\beta pyrr}$), 8.89 (d, J = 4.5 Hz, 2H, $H_{\beta pyrr}$), 8.22 (dd, J_o = 7.6 Hz, J_m = 1.5 Hz, 1H, H_d), 7.86 (t, J = 8.0 Hz, 1H, H_b), 7.54 (t, J = 7.6 Hz, 1H, H_c), 7.34 (d, J = 8.0 Hz, 1H, H_a), 3.96 (t, J = 4.8 Hz, 2H, H_e), 1.29 (m, 2H, H_f), 0.97 (q, J = 6.9 Hz, 6H, H_h), 0.6 (m, 2H, H_g), -1.26 (t, J = 6.9 Hz, 9H, H_i), -2.94 (s, 2H, NH_{pyrr}). ^{13}C NMR (100 MHz, $CDCl_3$, 298 K) δ: 162.8, 158.5, 148.5, 145.4, 140.0, 136.4, 134.2, 131.7, 130.8, 121.5, 119.8, 114.5, 103.3, 65.8, 52.7, 51.5, 22.4, 5.2. Eight quaternary carbon atoms were not detected. ^{19}F NMR (376 MHz, $CDCl_3$, 298 K) δ: -137.8, -151.0, -161.0.

2.4. Synthesis of Zn(2).

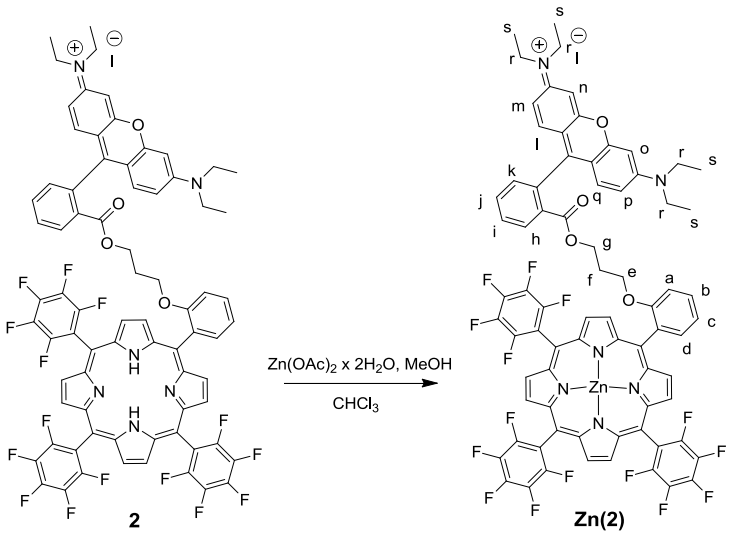

A dry CH_3OH (13.50 mL) solution of $Zn(OAc)_2 \cdot 2H_2O$ (72 mg, 0.33 mmol) was added to a $CHCl_3$ (6.50 mL) solution of **2** (49 mg, 0.033 mmol) in a 50 mL dried Schlenk. The mixture was refluxed under stirring for 2 hours, then the solvent was evaporated to dryness under reduced pressure and 15 mL of CH_2Cl_2 was added to the residue. The organic phase was washed with water (3 x 15 mL), dried over $NaSO_4$ and the filtrate was evaporated to dryness under reduced pressure yielding Zn(**2**) in a quantitative yield. Elemental Analysis: calc. for $C_{75}H_{48}F_{15}IN_6O_4Zn$: C, 62.23; H, 3.34; N, 5.81; found: C, 62.40; H, 3.71; N, 5.62. UV-Vis, λ_{max} (CH_2Cl_2)/nm (log ε_M): 419 (5.05), 560 (4.99). λ_{max} (MeOH)/nm (log ε_M): 418(5.01), 561(4.83). LR-MS (ESI): m/z ($C_{75}H_{48}F_{15}N_6O_4Zn^+$ $[M]^+$) calcd. 1445.28; found 1446.67. ^{1}H NMR (400 MHz, $CDCl_3$, 298 K): δ 8.91 (m, 6H, $H_{\beta pyrr}$), 8.75 (s, 2H, $H_{\beta pyrr}$), 8.14 (d, J = 6.7 Hz, 1H, H_h), 7.76 (t, J=7.6 Hz, 1H, H_j), 7.44 (br s, 2H, H_i and H_a), 7.26 (br s, H_k and H_c), 7.13 (br s, 1H, H_b), 6.88 (d, J=7.4 Hz, 1H, H_d), 6.53 (s, 2H, H_l and H_q), 6.41 (m, 4H, H_m, H_n, H_o and H_p), 3.48 (s, 2H, H_e), 3.38 (br s, 8H, H_r), 1.28 (solvent overlap H_g), 1.12 (s, 12H, H_s), 0.62 (s, 2H, H_f). ^{13}C NMR (100 MHz, $CDCl_3$, 298K): δ 158.8, 157.9, 157.3, 155.3, 151.3, 150.1, 149.8, 149.6, 148.3, 145.0, 135.1, 133.6, 132.7, 132.5, 132.4, 131.6, 131.2, 130.7, 130.4, 129.8, 129.7, 120.8, 114.0, 113.0, 103.1, 102.3, 96.4, 66.1, 61.8, 46.1, 29.8, 27.2, 12.6. eight quaternary carbon atoms were not detected. ^{19}F NMR (376 MHz, $CDCl_3$, 298 K): δ -136.7, -137.7, 140.3, 141.3, 152.4, -153.1, -162.3 to -163.0.

3. ^{1}H, ^{13}C and ^{19}F NMR spectra of reported compounds

Figure 1. ^{1}H NMR spectrum (400 MHz, $CDCl_3$, 298 K) of porphyrin **1**

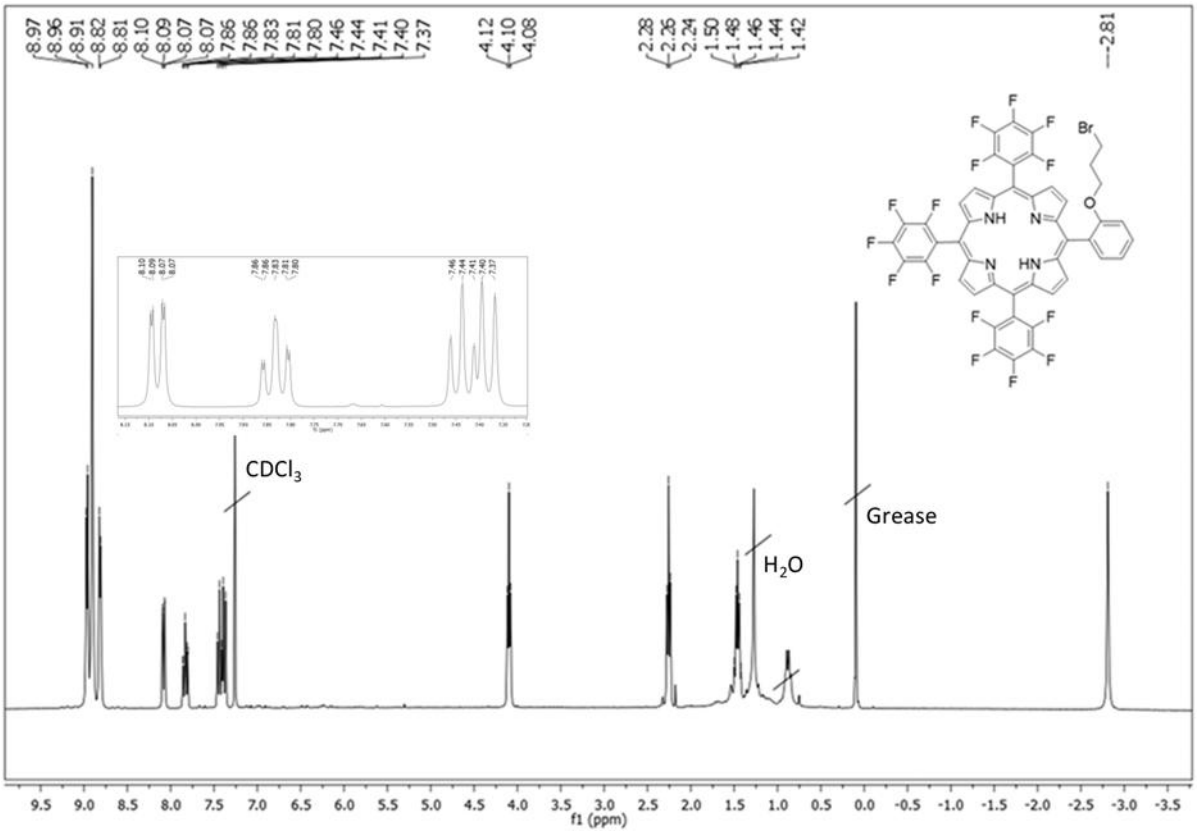

Figure 2. ^{13}C NMR spectrum (100 MHz, $CDCl_3$, 298 K) of porphyrin **1**

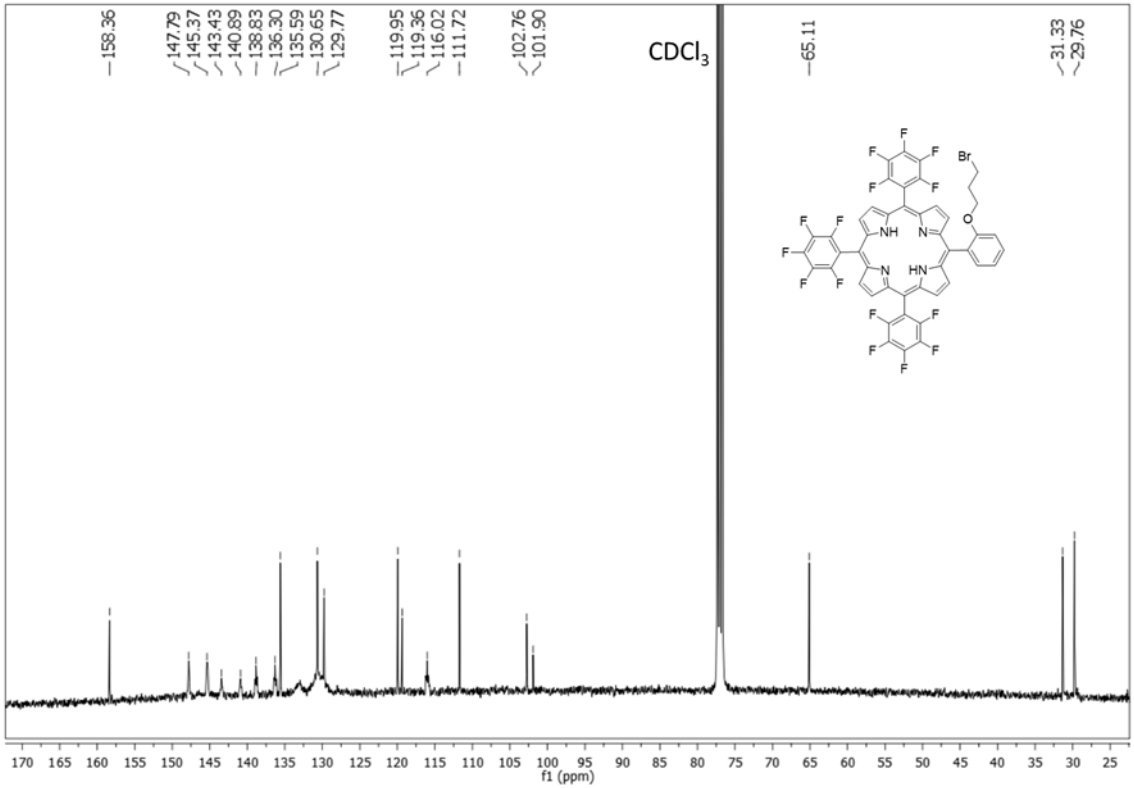

Figure 3. ^{19}F NMR spectrum (376 MHz, $CDCl_3$, 298 K) of porphyrin **1**

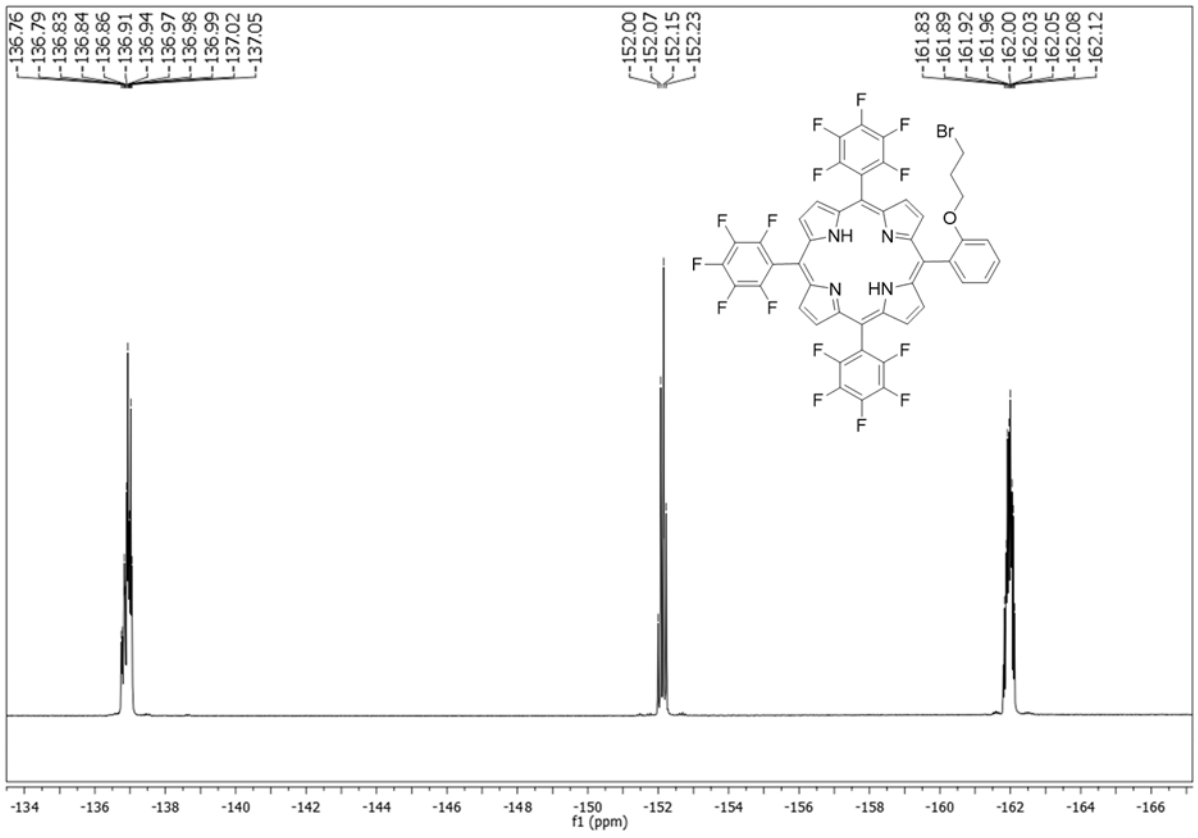

Figure 4. ^{1}H NMR spectrum (400 MHz, $CDCl_3$, 298 K) of porphyrin **2**

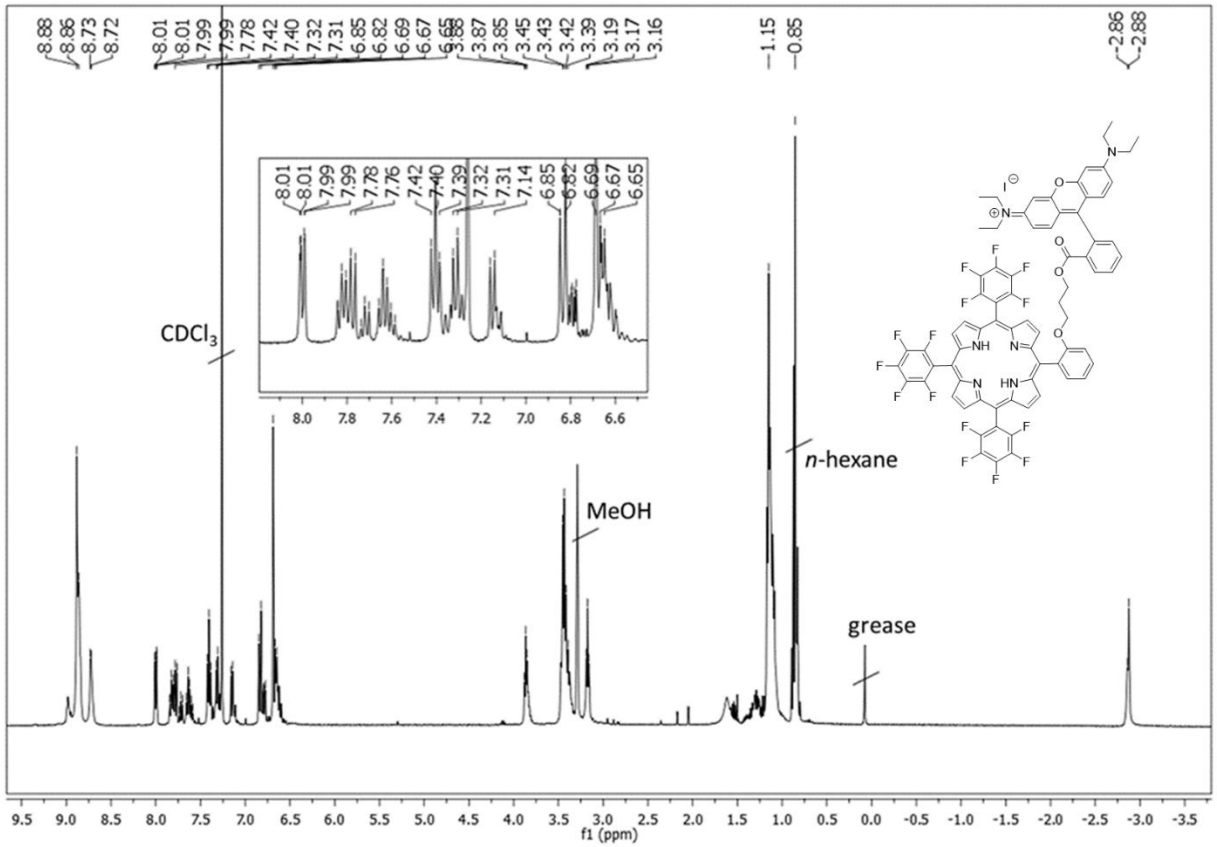

Figure 5. ^{13}C NMR spectrum (100 MHz, $CDCl_3$, 298 K) of porphyrin **2**

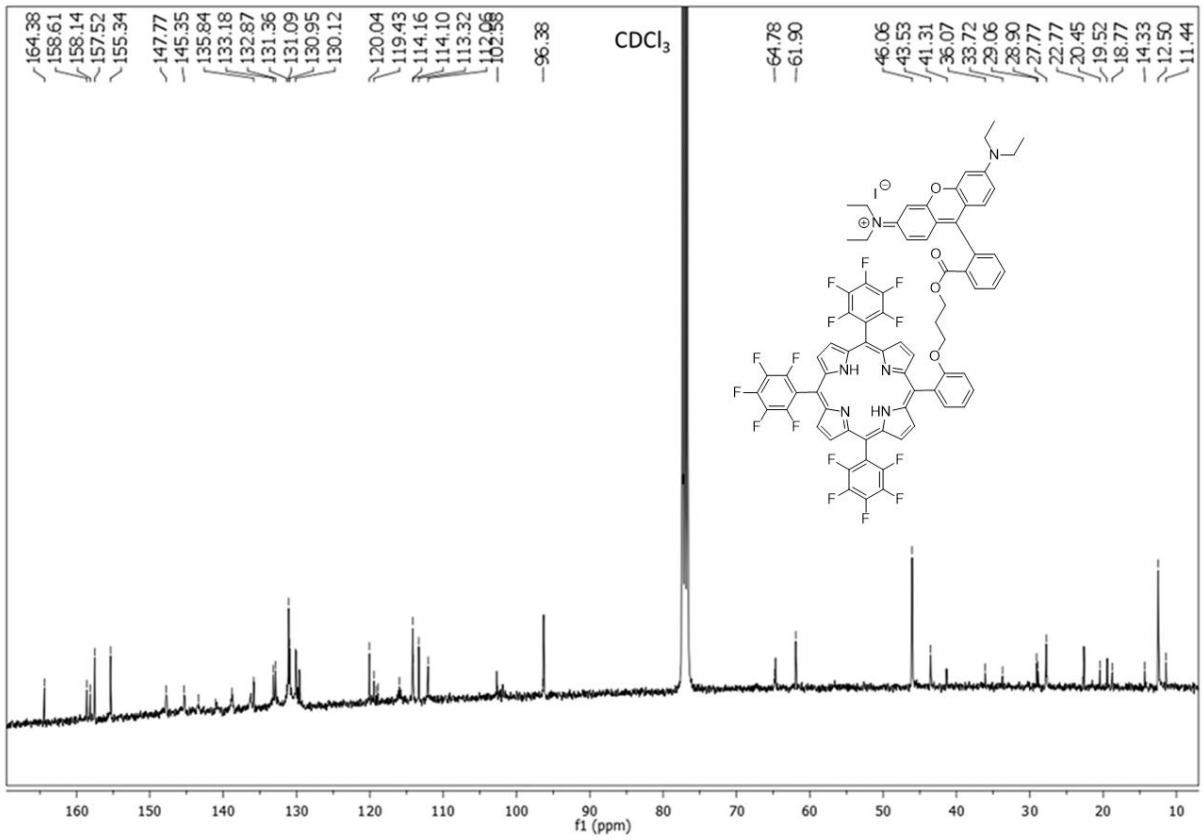

Figure 6. ^{19}F NMR spectrum (376 MHz, $CDCl_3$, 298 K) of porphyrin **2**

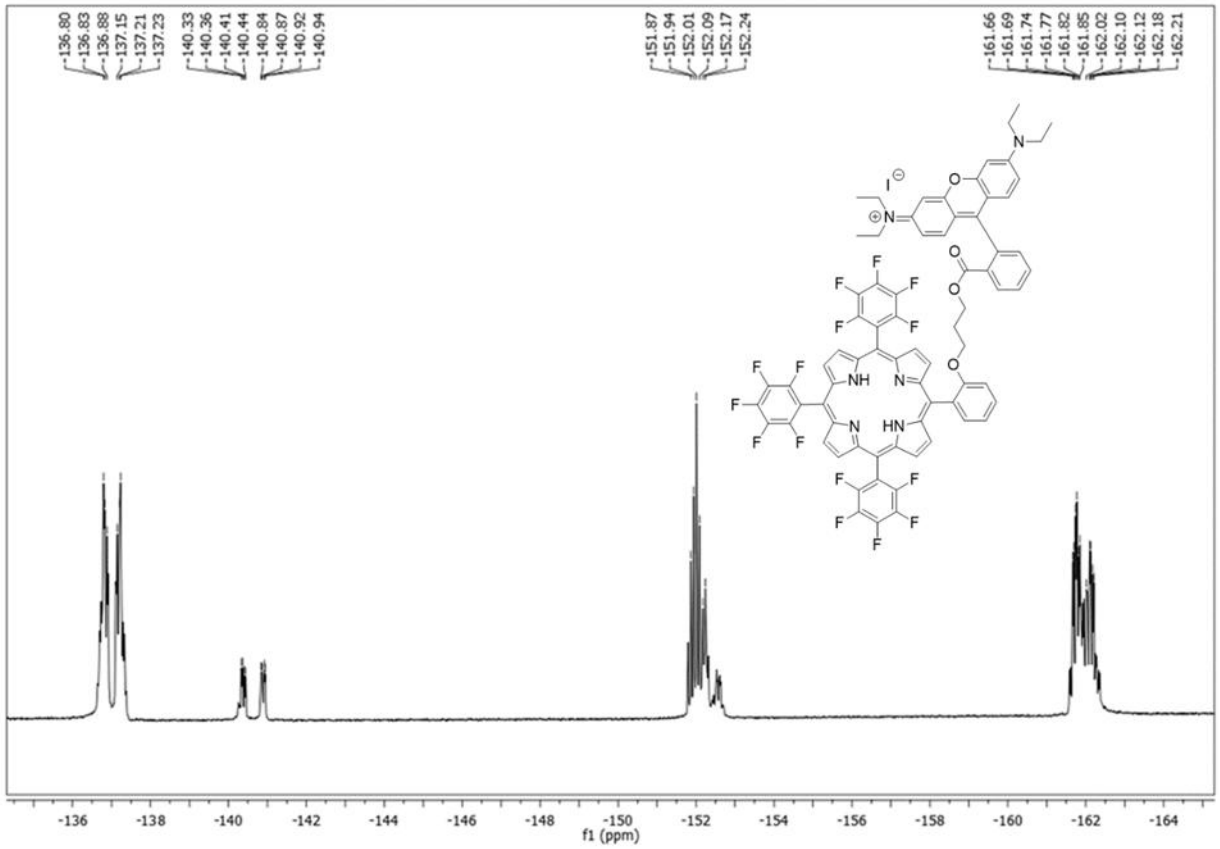

Figure 7. ^{1}H NMR spectrum (400 MHz, $CDCl_3$, 298 K) of porphyrin **3**

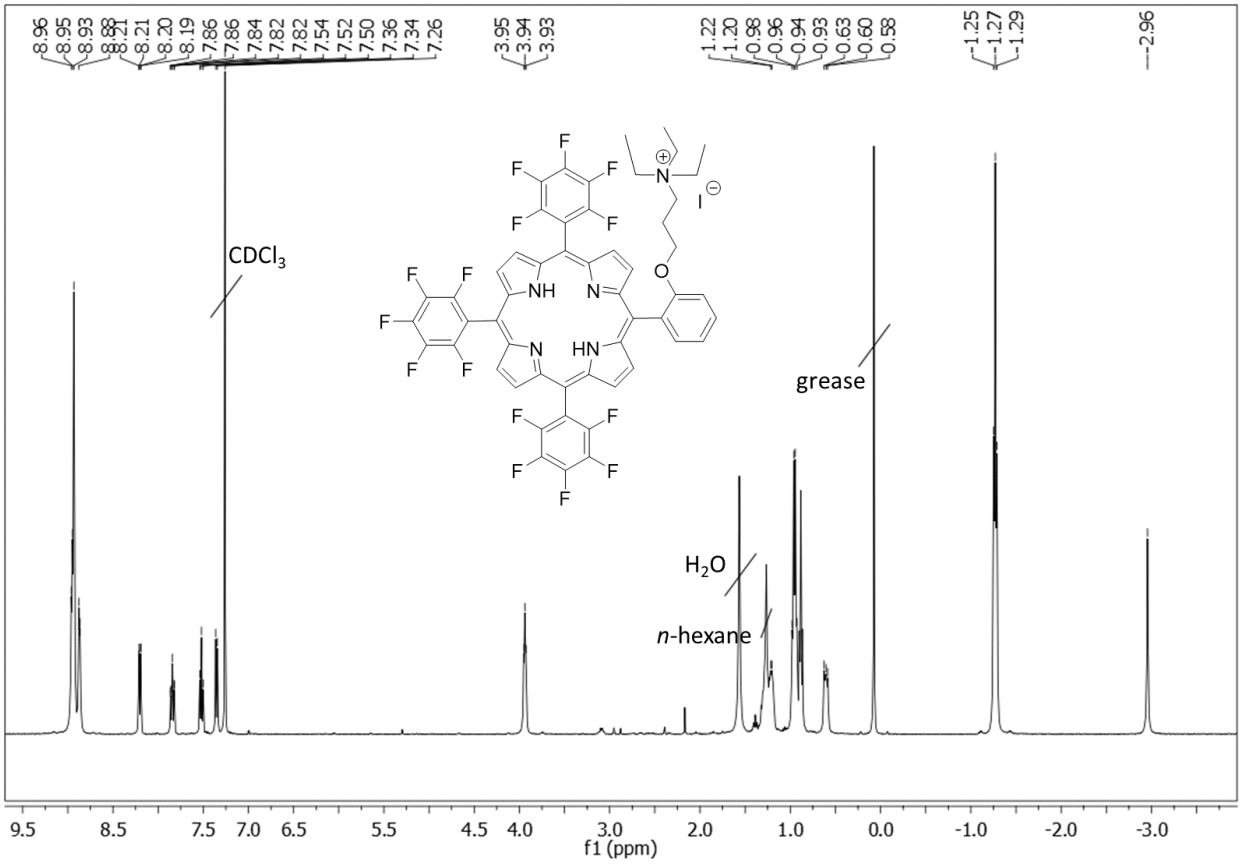

Figure 8. ^{13}C NMR spectrum (100 MHz, $CDCl_3$, 298 K) of porphyrin **3**

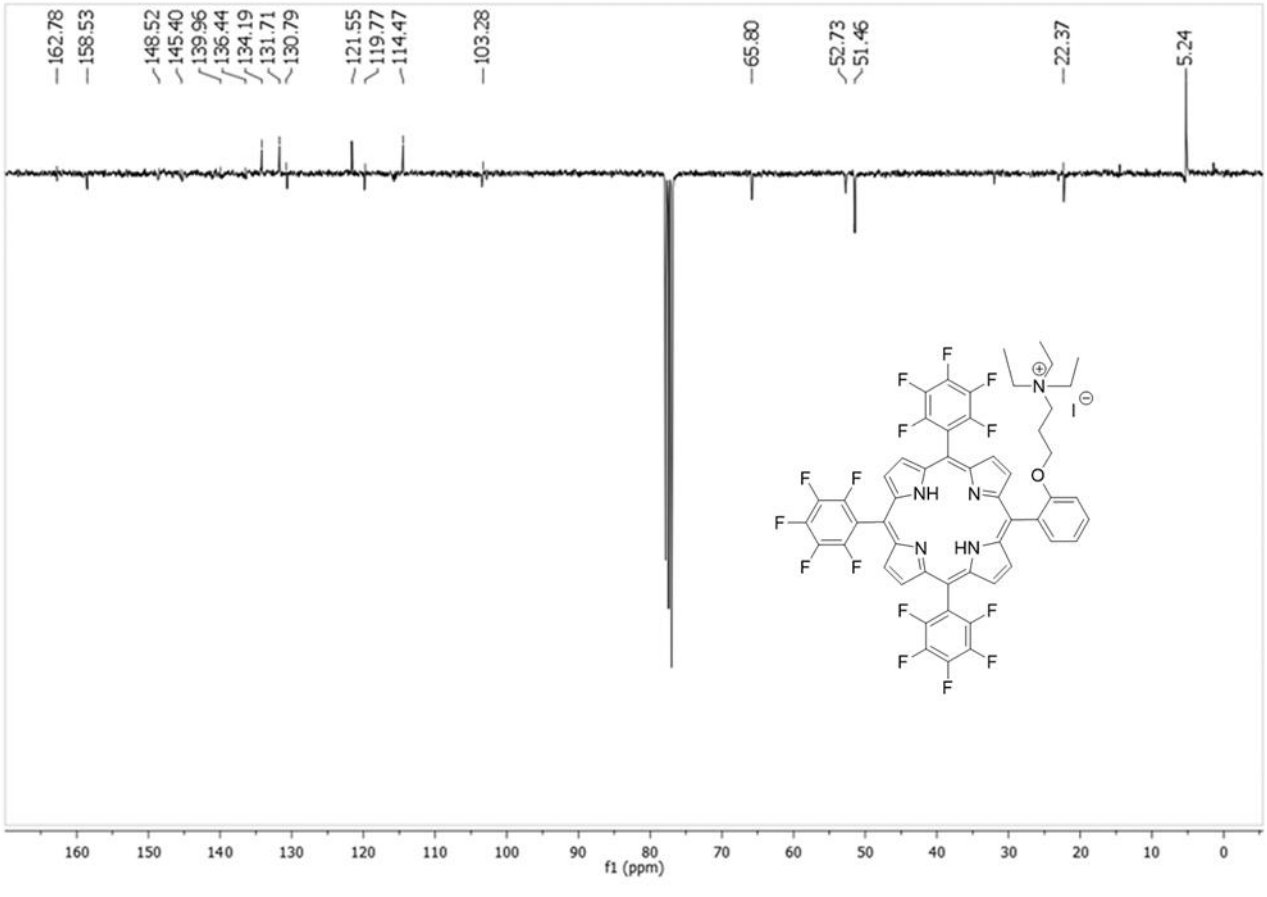

Figure 9. ^{19}F NMR spectrum (376 MHz, $CDCl_3$, 298 K) of porphyrin **3**

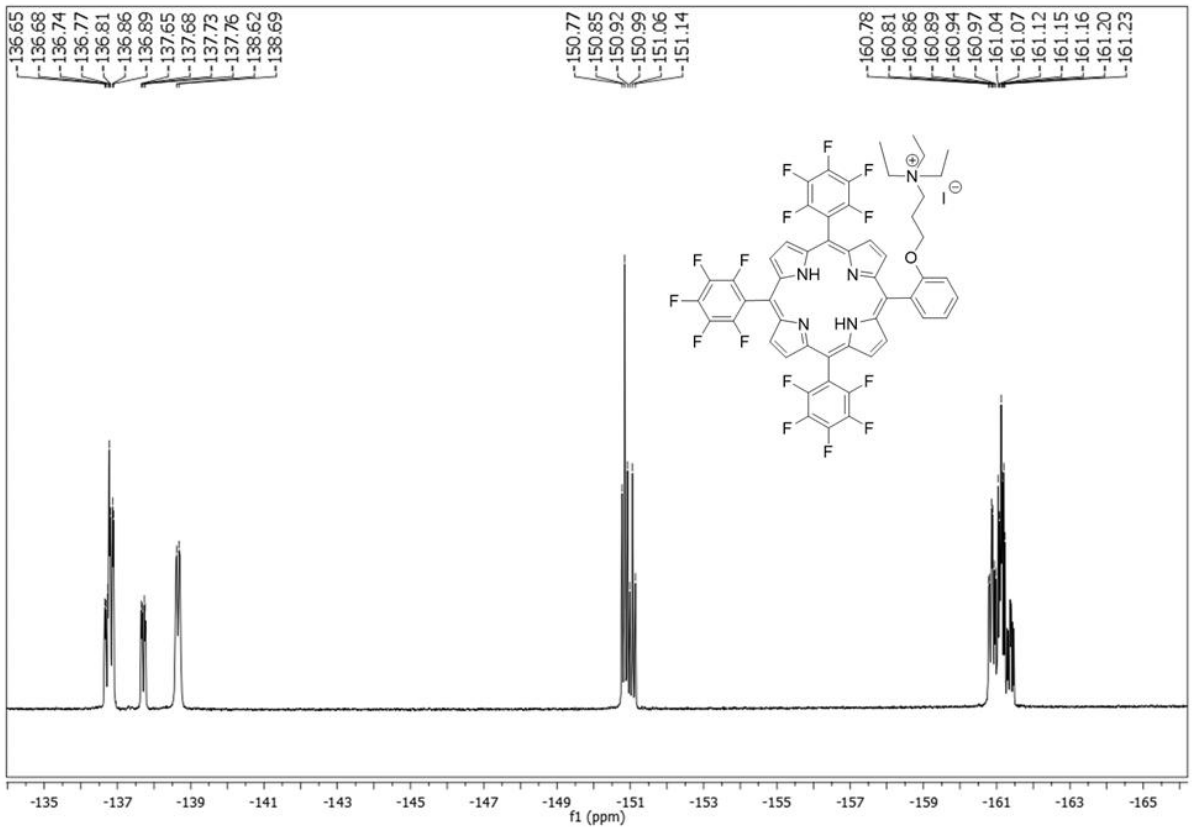

Figure 10. ^{1}H NMR spectrum (400 MHz, $CDCl_3$, 298 K) of porphyrin Zn(**2**)

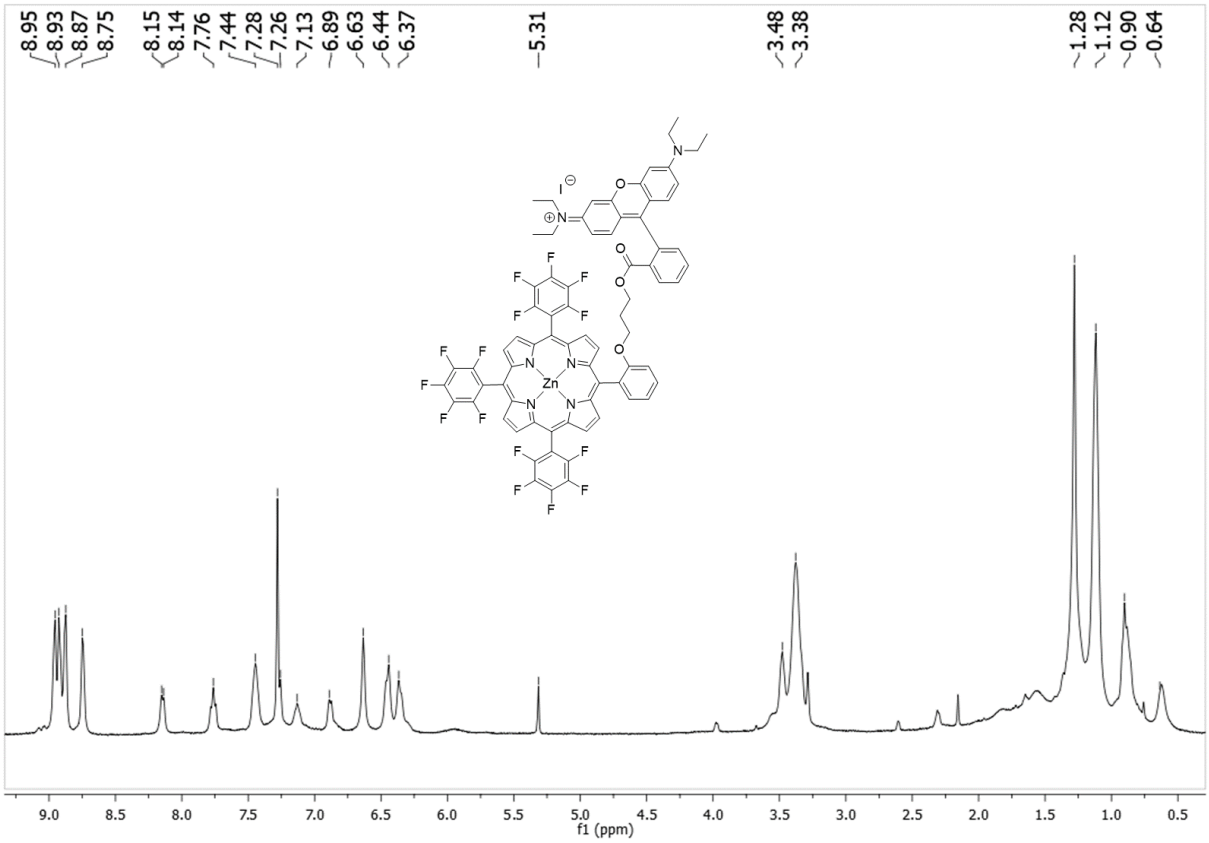

Figure 11. ^{13}C NMR spectrum (100 MHz, $CDCl_3$, 298 K) of porphyrin Zn(**2**)

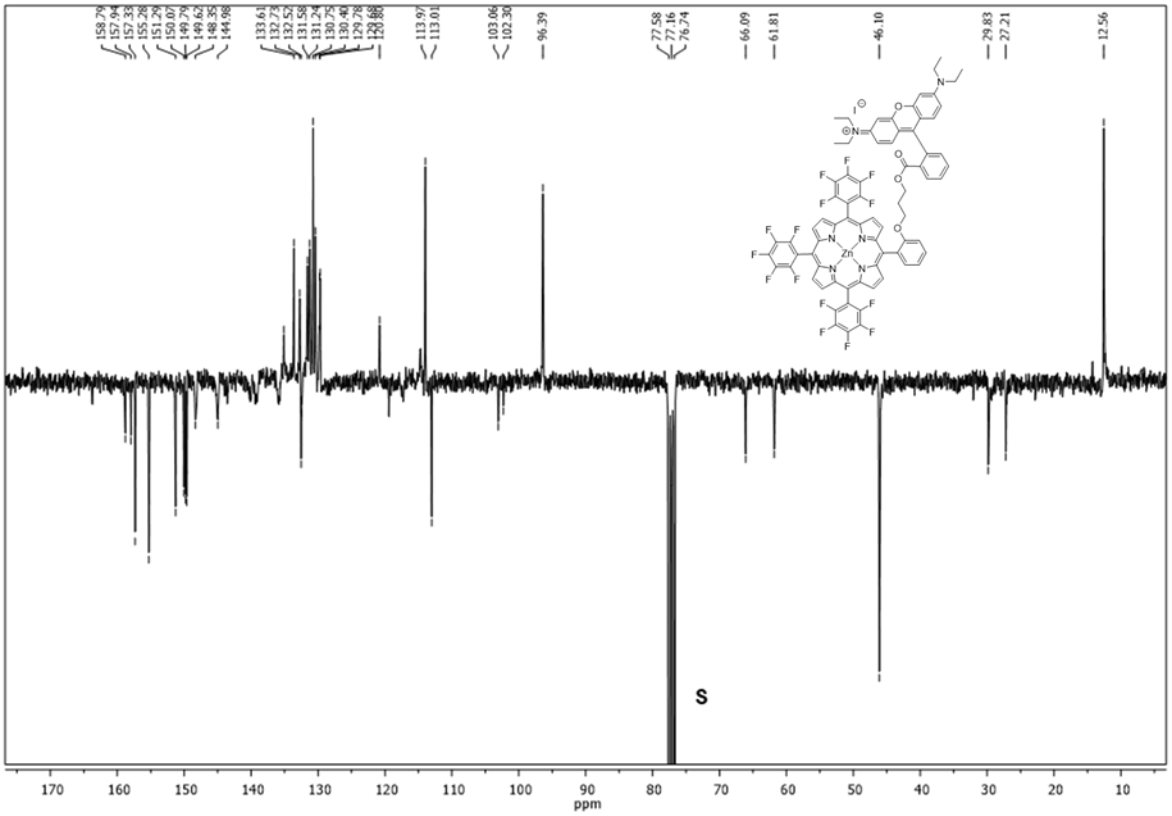

Figure 12. ^{19}F NMR spectrum (376 MHz, $CDCl_3$, 298 K) of porphyrin Zn(**2**)

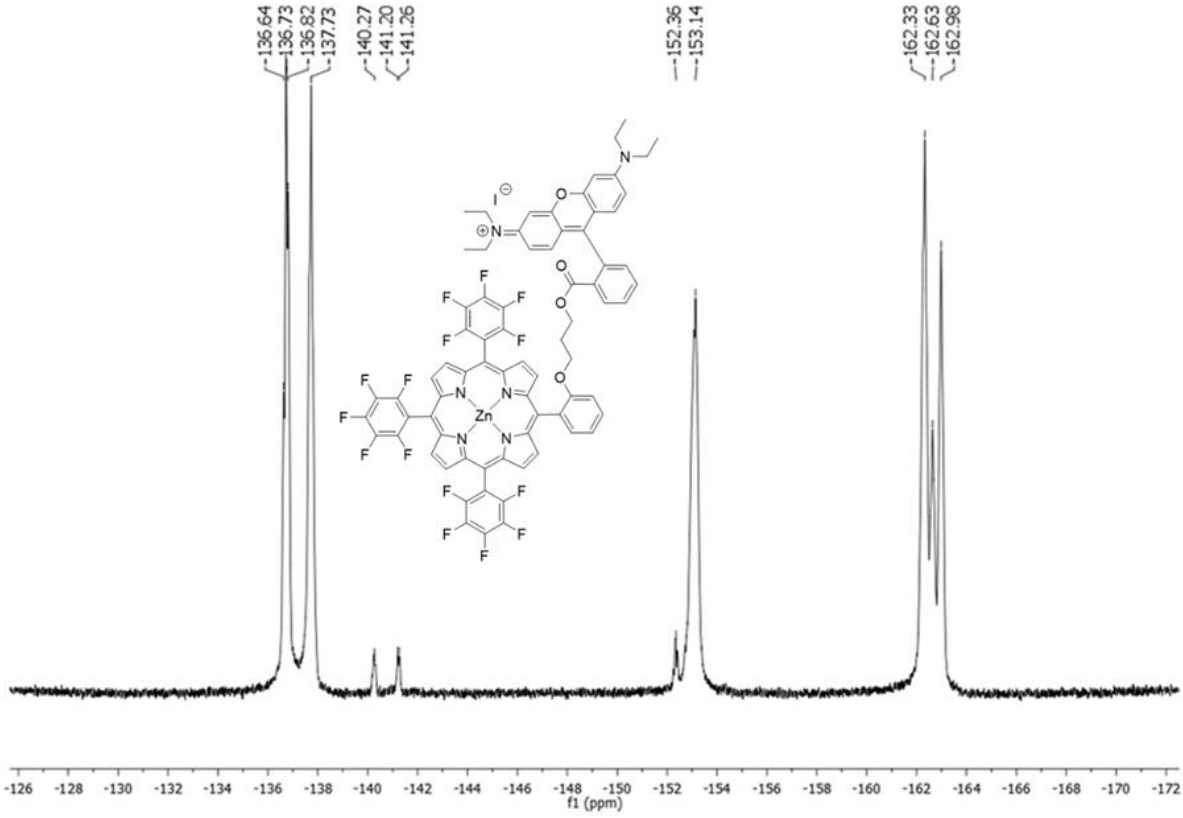

4. UV-Vis spectra

Figure 13. UV-vis spectra of **1**, **2**, **3**, Zn(**2**) and Rhodamine B in MeOH.

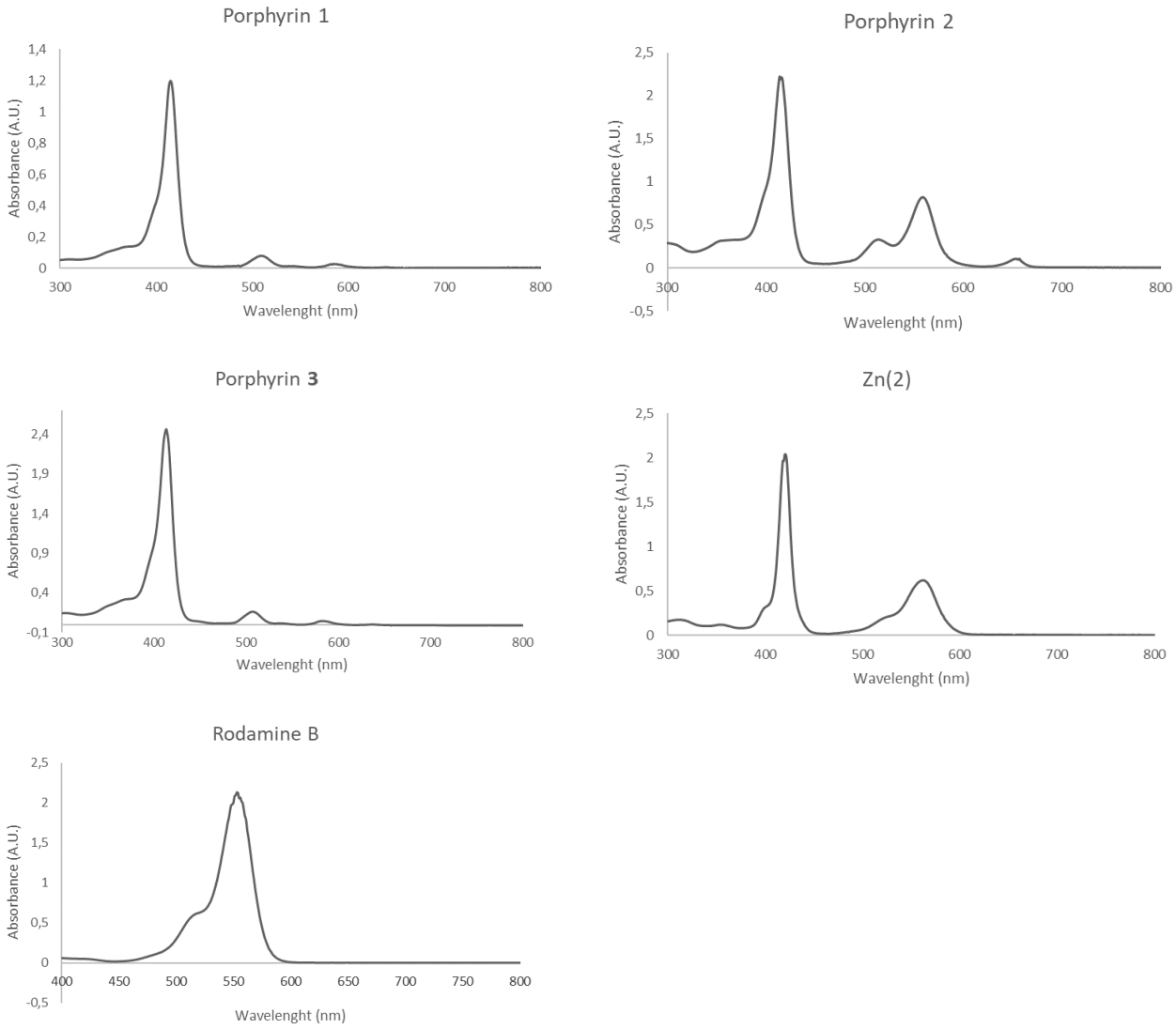

5. UV-Vis binding tests

Binding constant measurements were carried out on a Cary 100 Spectrophotometer at 298.0 (± 0.5) °C by adding consecutive aliquots of a (DCF)Na solution (1.00 mM) to 2.0 mL of 1:1 MeOH/H_2O (v:v) receptor (**2** or Zn(**2**)) solution (10.0 μM). The corresponding spectra was acquired after every (DCF)Na addition. The (DCF)Na solution was prepared by dissolving the required amount of salt into 10.0 mL of 10.0 μM porphyrin solution, in order to keep the concentration of the receptor to a constant value throughout the titration. The absorbance values at 419 nm were plotted against (DCF)Na concentration and acquired data fitted to Equation 1[8] for a 1:1 molecular complex formation by using a non-linear regression fit program (KaleidaGraph ® 4.1 Synergy Software). Experiments were performed in duplicate and obtained results showed a very good reproducibility. The same procedure was followed in the presence of sodium phenylacetate, sodium salicylate, L tyrosine sodium salt, sodium sarcosinate, L-alanine sodium salt as well as for Fluorescence and Resonance Light Scattering (RLS) studies.

Equation 1

$$\frac{A_0 - A}{A - A_\infty} = \frac{[S]_t + [L]_a + 1/K_{binding} - \sqrt{\left([S]_t + [L]_a + 1/K_{binding}\right)^2 - 4[S]_t[L]_a}}{2[S]_t}$$

Figure 14. UV-vis binding test with porphyrin **2**

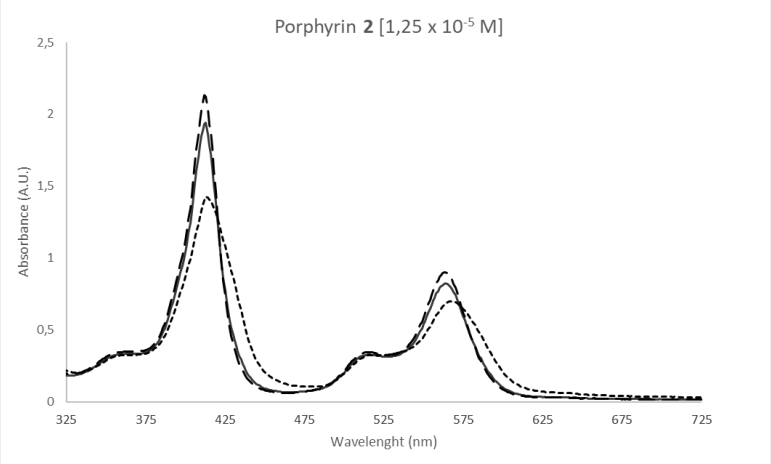

Figure 15. UV-vis binding test with porphyrin Zn(**2**)

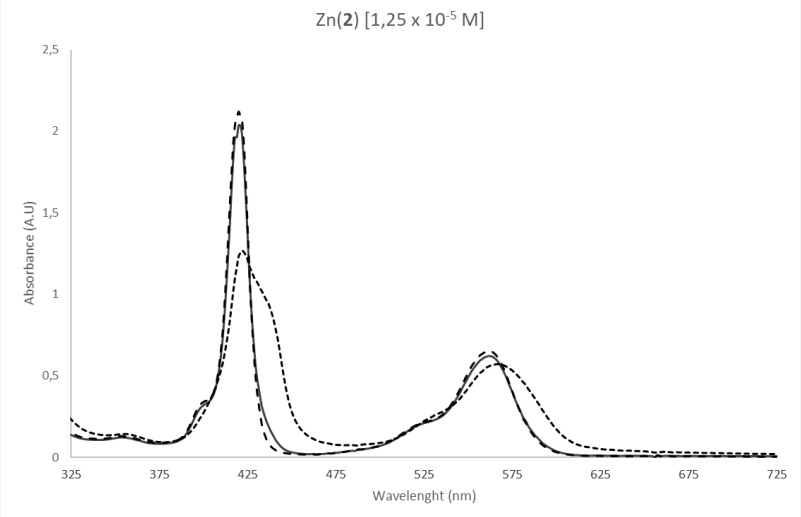

Figure 16. UV-Vis spectral pattern variation of **2** (10 μM; MeOH/H_2O 1:1 v:v) upon addition of (DCF)Na and equimolar amount of sodium salicylate (SalONa).

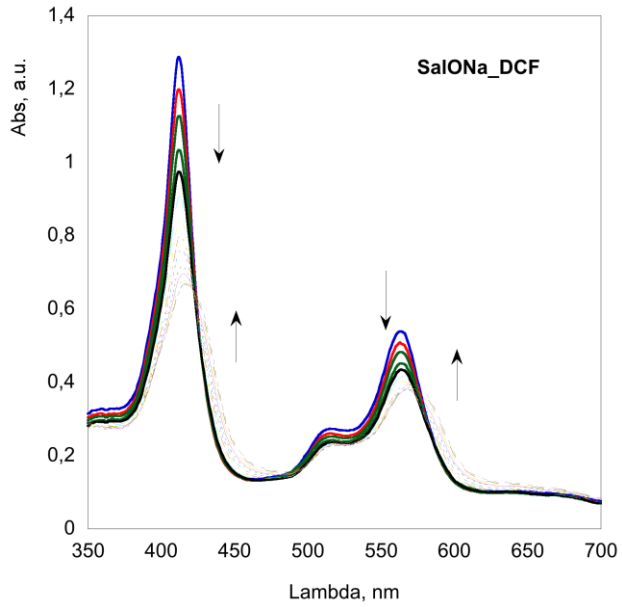

Figure 17. Non-linear regression fit, and calculated binding constant value (Langmuir type equation, see above) for the **2@DCF** formation in the presence of equimolar amount of sodium salicylate.

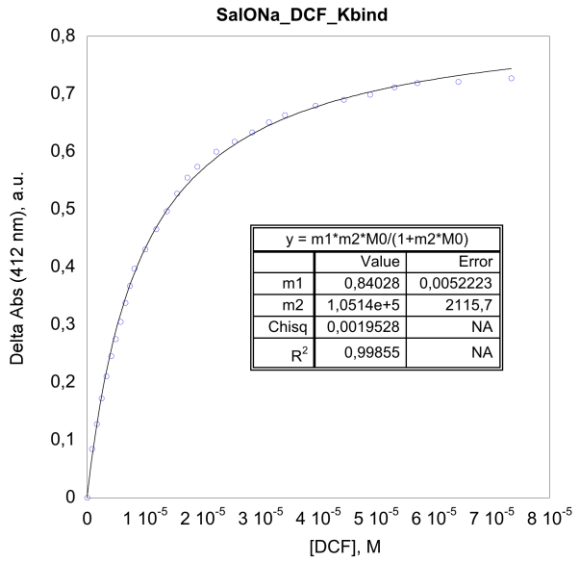

6. Fluorescence experiments

Figure 18. Fluorescence emission spectrum of **2** at λ_{exc} = 412 nm.

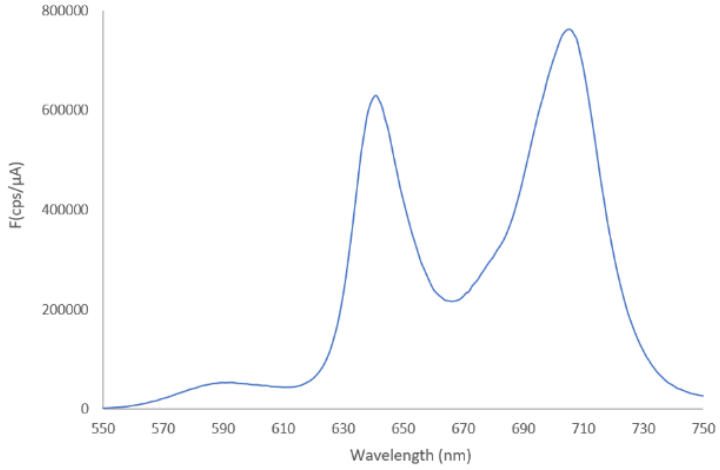

Figure 19. Fluorescence excitation spectrum of **2** at λ_{em}=590 nm (Rhodamine emission)

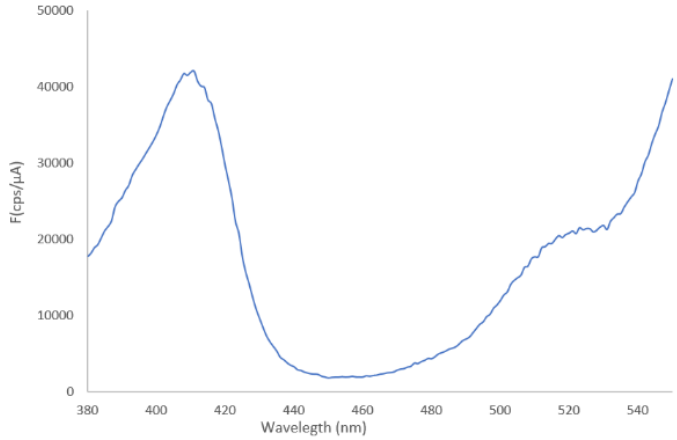

Figure 20. Fluorescence excitation spectrum of **2** at λ_{em}=705 nm (Porphyrin emission)

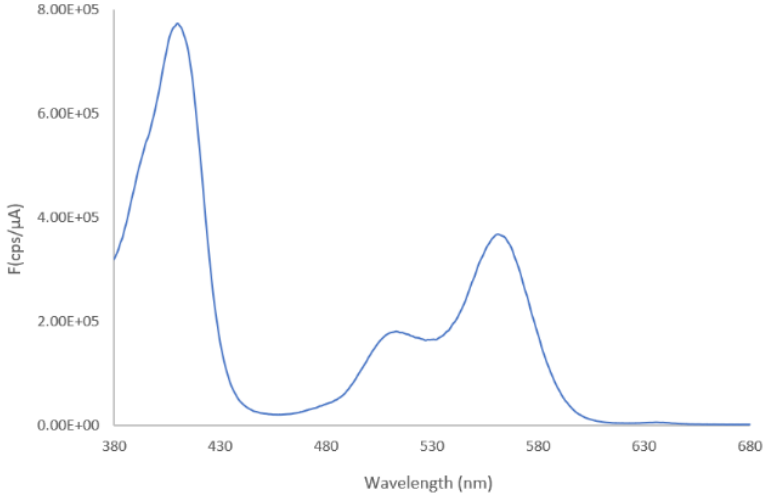

Figure 21. Fluorescence emission spectra of **2** for increasing concentrations of DCF. **A**: λ_{ex}=412 nm (Porphyrin absorption); **B**: λ_{ex}=555 nm (Rhodamine preferential absorption).

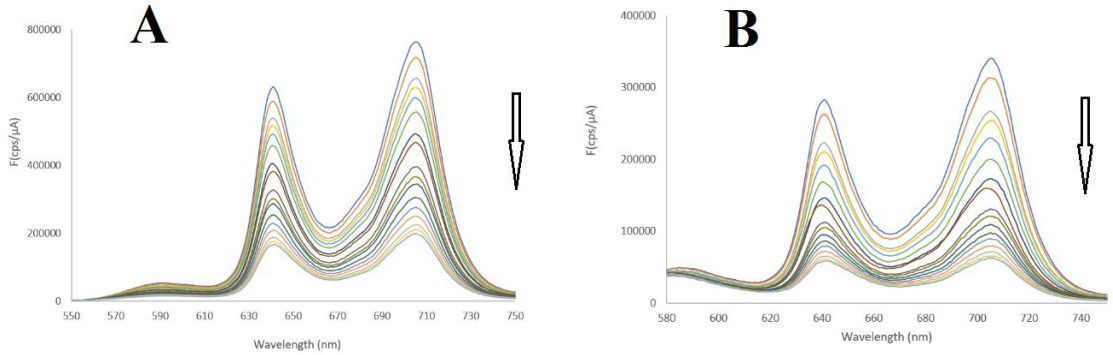

Figure 22. **2**/DCF binding isotherm from fluorescence intensities of **2** for different (DCF)Na concentrations. The analogous of Equation 1 was applied.

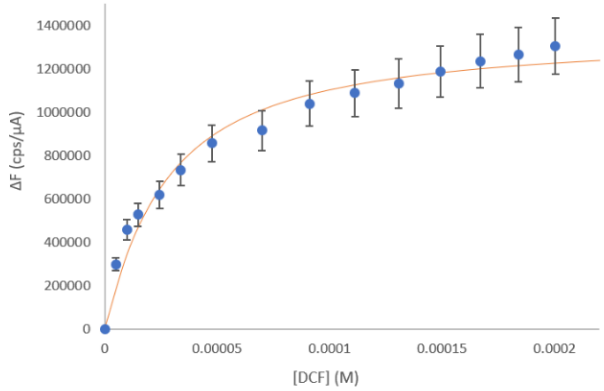

Figure 23. Fluorescence time decays of **2** for different **2**/DCF concentration ratios (λ_{ex}=342 nm; λ_{em}=645 nm).

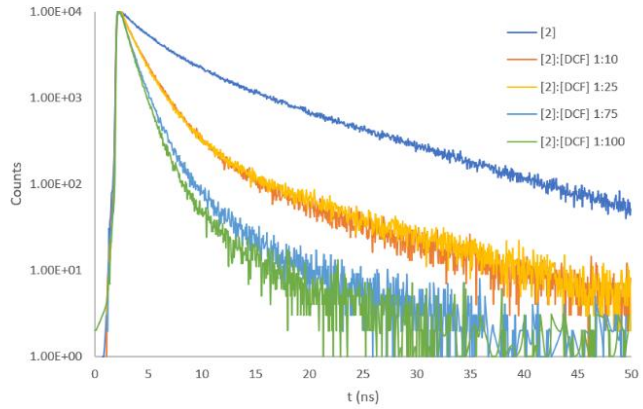

Table 1. Time decay parameters of **2** (porphyrin emission) for different **2**/DCF concentration ratios (λ_{ex}=342 nm; λ_{em}=645 nm).

[2]:[DCF]	τ_1 (ns)	α_1	τ_2 (ns)	α_2	τ_3 (ns)	α_3	$\langle\tau\rangle$ (ns)	χ^2
1:0	11.6	0.38	3.45	0.46	1.0	0.17	6.3	1.303
1:10	10.2	0.02	2.2	0.52	0.95	0.46	1.8	1.154
1:25	10.0	0.03	2.1	0.48	0.88	0.49	1.7	1.031
1:75	6.1	0.01	1.5	0.41	0.72	0.58	1.1	1.052
1:100	5.0	0.01	1.2	0.50	0.64	0.49	1.0	0.913

7. X-ray single-crystal structure determination.

Crystal data for **3** are reported in Table 2. All hydrogen atoms of porphyrin molecule, except the H atoms of methyl groups, were located from the difference Fourier map and refined freely with isotropic displacement *parameters*. Methyl hydrogens and H-atoms of the guest molecule (*n*-hexane) were placed in geometrically calculated positions and included in the refinement using a riding model in conjunction with a $U_{iso}(H) = 1.2 U_{eq}(CH_2, CH)$ or $1.5U_{eq}(CH_3)$ constraint. All non-hydrogen atoms were *refined with* full occupancy and *anisotropic displacement parameters* except for hexane carbon atoms. ISOR instruction was used for F2 atom as otherwise it went non-positive definite. The solvate hexane molecule was find to be disordered and refined isotropically over two positions using a suitable model (49.7, 50.1%). Geometry constraints (SADI) were used to keep reasonable bond distances.

Table 2. Crystal data and structure refinement for **3**.

Chemical formula	$[C_{53}H_{35}F_{15}N_5O]I\cdot 0.5(C_6H_{14})$
Empirical formula	$C_{56}\ H_{42}\ F_{15}\ I\ N_5\ O$
Formula weight ($g\cdot mol^{-1}$)	1212.85
Temperature (K)	150(2)
Wavelength (Å)	0.71073
Crystal system	Triclinic
Space group	*P* -1
a / Å	11.465(3)
b / Å	15.353(4)
c / Å	16.170(5)
α (deg)	103.382(3)
β (deg)	90.662(3)
γ (deg)	106.684(3)
V / $Å^3$	14687(2)
Z	12
$D_{calc.}$ ($g\cdot cm^{-3}$)	1.524
μ (mm^{-1})	0.704
θ range for data collection (deg)	1.3 to 25.0
Index ranges	-13<=h<=13, -18<=k<=18, -19<=l<=19
Reflections collected	23475
Independent reflections	9334 [R(int) = 0.0383]
Completeness to theta	99.9 %
Data/restraints/parameters	9334 / 21 / 775
F(000)	1218
Goodness-of-fit on F^2	1.039
Final *R* indices [I>2sigma(I)]	R_1 = 0.0580, wR_2 = 0.1461
R indices (all data)	R_1 = 0.0855, wR_2 = 0.1719
$\Delta\rho$ max,min ($e\cdot Å^{-3}$)	2.432 and -0.775

Table 3. Selected bond lengths [Å] and angles [°] for **3**.

N(1)-C(1)	1.365(6)	N(1)-C(4)-C(5)	125.7(5)
N(1)-C(4)	1.365(7)	N(1)-C(4)-C(3)	109.6(5)
N(2)-C(6)	1.362(7)	C(5)-C(4)-C(3)	124.6(5)
N(2)-C(9)	1.363(7)	C(4)-C(5)-C(6)	126.8(5)
N(3)-C(14)	1.364(6)	C(4)-C(5)-C(21)	117.4(5)
N(3)-C(11)	1.370(6)	C(6)-C(5)-C(21)	115.6(5)
N(4)-C(16)	1.364(7)	N(2)-C(6)-C(5)	125.5(5)
N(4)-C(19)	1.372(6)	N(2)-C(6)-C(7)	107.5(5)
C(1)-C(20)	1.401(7)	C(5)-C(6)-C(7)	126.9(5)
C(1)-C(2)	1.443(8)	C(8)-C(7)-C(6)	108.0(5)
C(2)-C(3)	1.330(8)	C(7)-C(8)-C(9)	107.8(5)
C(3)-C(4)	1.445(8)	N(2)-C(9)-C(10)	126.6(4)
C(4)-C(5)	1.383(8)	N(2)-C(9)-C(8)	107.2(5)
C(5)-C(6)	1.396(8)	C(10)-C(9)-C(8)	126.2(5)
C(5)-C(21)	1.504(7)	C(9)-C(10)-C(11)	124.7(5)
C(6)-C(7)	1.421(8)	C(9)-C(10)-C(27)	117.5(4)
C(7)-C(8)	1.349(8)	C(11)-C(10)-C(27)	117.5(5)
C(8)-C(9)	1.428(7)	N(3)-C(11)-C(10)	126.0(5)
C(9)-C(10)	1.396(7)	N(3)-C(11)-C(12)	109.8(4)
C(10)-C(11)	1.398(7)	C(10)-C(11)-C(12)	124.1(5)
C(10)-C(27)	1.489(7)	C(13)-C(12)-C(11)	107.3(5)
C(11)-C(12)	1.442(8)	C(12)-C(13)-C(14)	106.7(5)
C(12)-C(13)	1.340(8)	N(3)-C(14)-C(15)	125.2(5)
C(13)-C(14)	1.446(7)	N(3)-C(14)-C(13)	110.1(4)
C(14)-C(15)	1.398(7)	C(15)-C(14)-C(13)	124.6(5)
C(15)-C(16)	1.392(7)	C(16)-C(15)-C(14)	126.9(5)
C(15)-C(33)	1.499(7)	C(16)-C(15)-C(33)	116.5(4)
C(16)-C(17)	1.430(7)	C(14)-C(15)-C(33)	116.6(5)
C(17)-C(18)	1.347(8)	N(4)-C(16)-C(15)	125.3(5)
C(18)-C(19)	1.433(7)	N(4)-C(16)-C(17)	108.0(4)
C(19)-C(20)	1.391(7)	C(15)-C(16)-C(17)	126.7(5)
C(20)-C(39)	1.497(7)	C(18)-C(17)-C(16)	107.6(5)
C(32)-O(1)	1.377(7)	C(17)-C(18)-C(19)	108.2(5)
N(1S)-C(3B)	1.505(8)	N(4)-C(19)-C(20)	125.8(4)
N(1S)-C(4B)	1.507(8)	N(4)-C(19)-C(18)	107.3(4)
N(1S)-C(8B)	1.508(7)	C(20)-C(19)-C(18)	126.9(5)
N(1S)-C(6B)	1.522(7)	C(19)-C(20)-C(1)	126.1(5)
O(1)-C(1B)	1.425(9)	C(19)-C(20)-C(39)	116.8(4)
C(1B)-C(2B)	1.521(9)	C(1)-C(20)-C(39)	117.1(5)
C(2B)-C(3B)	1.522(9)	O(1)-C(32)-C(31)	119.7(5)
C(4B)-C(5B)	1.521(9)	O(1)-C(32)-C(27)	119.6(5)
C(6B)-C(7B)	1.505(10)	C(3B)-N(1S)-C(4B)	111.5(5)
C(8B)-C(9B)	1.525(9)	C(3B)-N(1S)-C(8B)	106.3(4)
		C(4B)-N(1S)-C(8B)	111.6(5)
		C(3B)-N(1S)-C(6B)	110.3(5)
C(1)-N(1)-C(4)	105.8(4)	C(4B)-N(1S)-C(6B)	106.3(4)
C(6)-N(2)-C(9)	109.4(4)	C(8B)-N(1S)-C(6B)	110.8(5)
C(14)-N(3)-C(11)	106.0(4)	C(32)-O(1)-C(1B)	116.0(5)
C(16)-N(4)-C(19)	108.9(4)	O(1)-C(1B)-C(2B)	106.9(6)
N(1)-C(1)-C(20)	125.2(5)	C(1B)-C(2B)-C(3B)	109.0(5)
N(1)-C(1)-C(2)	110.5(4)	N(1S)-C(3B)-C(2B)	115.3(5)
C(20)-C(1)-C(2)	124.3(5)	N(1S)-C(4B)-C(5B)	114.5(5)
C(3)-C(2)-C(1)	106.5(5)	C(7B)-C(6B)-N(1S)	114.2(5)
C(2)-C(3)-C(4)	107.6(5)	N(1S)-C(8B)-C(9B)	115.3(5)

Table 4. Hydrogen-bond geometry for **3** (Å, °)

Donor- H···Acceptor	*D* - H	H···A	*D*···A	*D* - H···A
N2-H2N···N1	0.70(9)	2.48(9)	2.913(7)	123(9)
N2-H2N···N3	0.70(9)	2.43(9)	2.897(7)	126(8)
N4-H4N···N1	0.75(9)	2.49(9)	2.895(7)	116(8)
N4-H4N···N3	0.75(9)	2.36(8)	2.905(6)	131(8)

8. Conformational analysis.

The porphyrin **3** adopts a "close" conformation in which the amino-alkyl side arm is folded toward the core of the macrocycle, with the terminal methyl groups of the pendant triethylammonium moiety pointing toward the pyrrole rings (I, II, IV). The lateral displacement of the side arm from the porphyrin centroid is generated by a gauche/anti/anti/anti(N)/anti conformation sequence along the main chain.

The porphyrin core is quasi-planar with an average deviation of the macrocycle atoms from their least squares plane (Δ24, Table 5) of only 0.065 Å. The larger deviations are associated with the *meso*-carbon (C_m) C10 (0.106(5) Å) bonded to the para substituted aryl group and with the C_β of the neighbouring pyrrole rings (-0.089(6)-0.172(6) Å). Likewise, the C_α-C_m-C_α angle between the α-pyrrolic and *meso* carbons varies only slightly (Table 5) with the smallest value and the bigger deviation at *meso*-C10 position again (124.7(5)°).

The overall slightly distortion results essentially in a *saddle* shaped conformation characterized by an alternating displacement of the pyrrole rings N(I), (III) and (IV) below and above the mean plane (Figure 24).[9] A closer look of the out-of-plane distortion pattern suggests a small contribute from *wave* conformation involving the pyrrolic unit N(II) (toward which the side arm of porphyrin is bent).[10] The minor deformation from planarity of porphyrin macrocycle and the different role of the pyrrolic units is also reflected by the values of the dihedral angle between the pyrrole rings and the N_4-core mean plane (Table 5).

All the conformational data seem indicate that the small distortions observed for the macrocycle are essentially due to the presence and orientation of the "long" alkyl chain on the para position of a *meso*-aryl group. Despite the asymmetric substituent arrangement, the inner cavity shape composed by the four N atoms is square-like as indicated by the core elongation factor (Ξ = 0.013 Å) and by the distances between the neighbouring N-N atoms (2.895(7) – 2.913(7) Å). The N-H groups are involved in bifurcated N-H···(N,N) intramolecular hydrogen bonds (Table 4) and result only slightly tilted out of the plane of macrocycle.

Table 5. Selected conformational parameters for **3** (deviations and distances in Å, angles in °)

Core size ⊗[a]	2.053	C_α-C_{15}-C_α	126.9(5)
Core elongation Ξ[b]	0.013	C_α-C_{20}-C_α	126.1(5)
Δ24[c]	0.065	*cis* C_α-N···N-C_α[g]	4.2
N1···N2	2.913(7)	*trans* C_α-N···N-C_α	177.1
N2···N3	2.897(7)	φ_{pyr} N1[h]	1.89
N3···N4	2.905(6)	φ_{pyr} N2	7.24
N4···N1	2.895(7)	φ_{pyr} N3	3.18
δC_m[d]	0.074	φ_{pyr} N4	0.93
δC_α[e]	0.051	φ_{ar} C5[i]	87.05
δC_β[f]	0.102	φ_{ar} C10	87.87
C_α-C_5-C_α	126.8(5)	φ_{ar} C15	82.98
C_α-C_{10}-C_α	124.7(5)	φ_{ar} C20	81.15

C_m (*meso* carbon) = 5, 10, 15, 20; C_β (*β-pyrrole* position) = 2, 3, 7, 8, 12, 13, 17, 18; C_α (*α-pyrrole* position) = 1, 4, 6, 9, 11, 14, 16, 19. [a]The core size is defined as the geometrical centre of the four nitrogen atoms. [b]The core elongation parameter is defined as the difference between the vector lengths (|N1-N2|+|N3-N4|)/2 - (|N2-N3|+|N1-N4|)/2. [c]Deviation of the 24 macrocycle atoms from their least squares plane. [d]Average deviation of the C_m carbon atoms from the 4N plane. [e]Average deviation of the C_α atoms from the 4N plane. [f]Average deviation of the C_β atoms from the 4N plane. [g]Cis C_α –N–N– C_α dihedral angles.[11] [h]Pyrrole tilt angle with the 4N plane. [i]Phenyl tilt angle against the 4N plane.

Figure 24. Linear display of the skeletal deviations (in units of 0.001 Å) of the macrocycle atoms from the mean porphyrin plane (of 24 atom).[10] The *x* axis is not to scale.

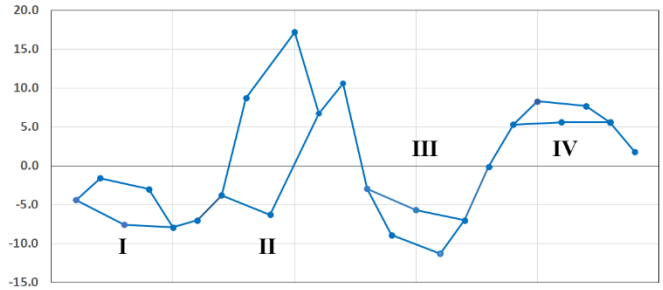

References

[1] T. A. D. Pinto, R. Hrdina, G. Kirsch, A. M. F. Oliveira-Campos, L. M. Rodrigues and A. P. Esteves, ARKIVOC 2012, **6**, 185-193

[2]H. G. Brittain, *Cryst. Growth Des.*, 2010, **10**, 1990-2003

[3] Bruker, *SAINT+*, 2007, Bruker AXS Inc., Madison, Wisconsin, USA.

[4] Bruker, APEX II, 2009, Bruker AXS Inc., Madison, Wisconsin, USA.

[5] M. C. Burla, R. Caliandro, M. Camalli, B. Carrozzini, G. L. Cascarano, L. De Caro, C. Giacovazzo, G. Polidori and R. Spagna, *J. Appl. Crystallogr.*, 2005, **38**, 381-388.

[6] G. M. Sheldrick, *Acta Crystallogr. Sect. C Struct. Chem.*, 2015, **71**, 3-8.

[7] L. J. Farrugia, *J. Appl. Crystallogr.*, 2012, **45**, 849-854.

[8] K. A. Connors: *Binding constants — the measurement of molecular complex stability*, John Wiley & Sons, New York 1987, 91, 1398-1398.

[9] M. Gruden, S. Grubišić, A. G. Coutsolelos and S. R. Niketić, *J. Mol. Struct.*, 2001, **595**, 209–224.

[10] a) W. Jentzen, X.-Z. Song and J. A. Shelnutt, *J. Phys. Chem. B*, 1997, **101**, 1684-1699; b) W. Jentzen, J.-G. Ma and J. A. Shelnutt, *Biophys. J.*, 1998, **74**, 753-763.

[11] A. Fidalgo-Marijuan, G. Barandika, B. Bazán, M.-K. Urtiaga and M. I. Arriortua, *CrystEngComm*, 2013, **15**, 4181.

Journal Name

ARTICLE

Sensing of Diclofenac by a Porphyrin-based Artificial Receptor

Daniela Intrieri,[a] Caterina Damiano,[a] Silvia Rizzato,[a] Roberto Paolesse,[b] Mariano Venanzi,[b] Donato Monti,*[b] Marco Savioli,[b] Manuela Stefanelli[b] and Emma Gallo.*[a]

Graphical Abstract

The synthesis of a porphyrin chemosensor is reported as well as its activity in detecting Diclofenac with an overall 1:1 $K_{binding} \cong 10^5$.

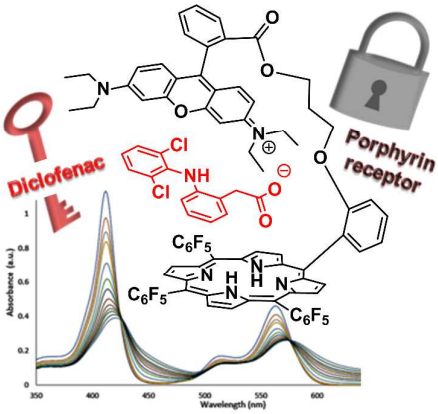

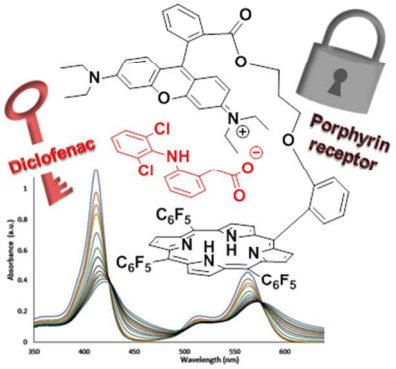

254x190mm (96 x 96 DPI)

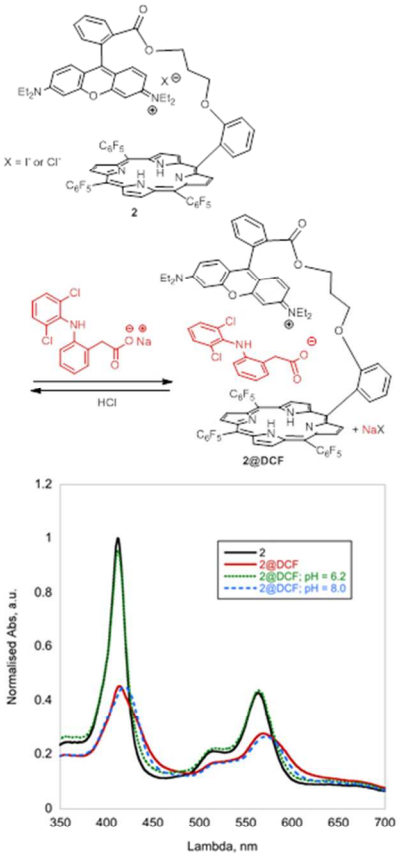

Figure 2. UV-Vis spectra showing the reversible formation of 2@DCF adduct.

190x254mm (96 x 96 DPI)

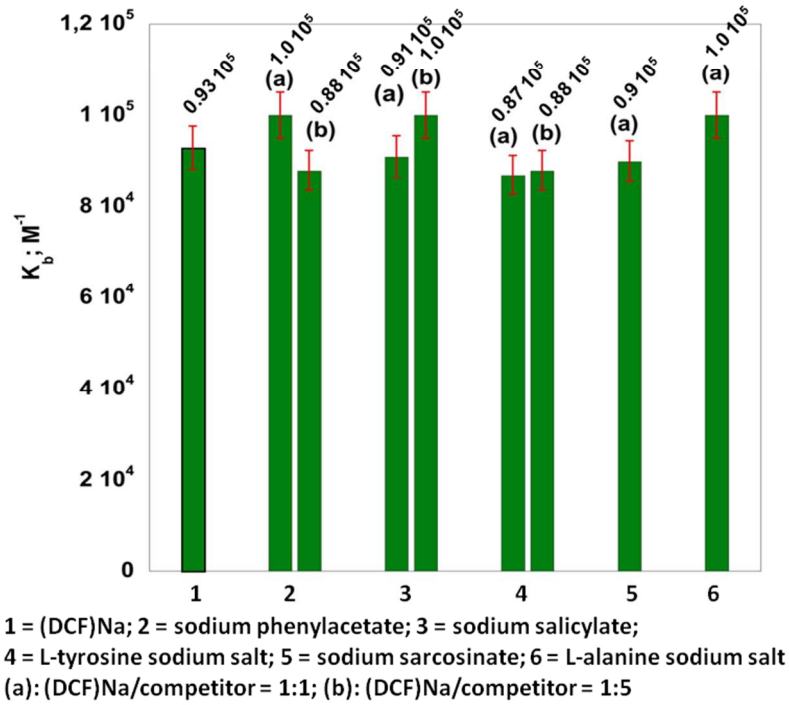

Figure 6. Binding constant values for the formation of 2@DCF adduct in the presence of interfering sodium salts. (a): 1:1 molar ratio, (b): 1:5 molar ratio (error bars 5%).

254x190mm (96 x 96 DPI)